Investigating the role of ascorbic acid and its transporters in medulloblastoma

Manon Jones BSc

Thesis submitted to the University of Nottingham for the degree of Master of Research

September 2024

Abstract

Medulloblastoma is a highly malignant paediatric brain tumour, accounting for 20% of cases. Current treatment achieves a 70% 5-year-survival rate but can result in long-term neurological side effects. Treatment is further complicated by the disease's heterogeneity, comprising four molecular subgroups: Group 3, Group 4, SHH and WNT. Novel therapeutic strategies are urgently needed to improve outcomes while addressing both treatment toxicity and the diverse molecular landscape. Adjuvant therapies that enhance treatment efficacy could reduce therapeutic doses and minimise side effects. A unique feature of the SHH subgroup is a collagen-rich extracellular matrix (ECM) shell, which is associated with improved survival, possibly by limiting tumour growth and invasiveness. This makes it a potential target for therapeutic manipulation in SHH tumours. Ascorbic acid (Vitamin C) plays a critical role as a co-factor in collagen production and could influence the collagen-rich ECM shell encapsulating SHH tumours. In addition, at high doses, ascorbic acid generates reactive oxygen species (ROS) via the Fenton reaction, leading to enhanced oxidative stress. Therefore, high-dose ascorbic acid could be a compelling candidate as an adjuvant treatment of SHH tumours, by promoting a tumour-restrictive microenvironment and increasing oxidative stress to enhance current treatment efficacy.

This thesis investigated the expression of ascorbic acid transporter genes in medulloblastoma patients, with a focus on SHH tumours. Analysis identified GLUT10 and SVCT2 as potential players in medulloblastoma biology, with differential expression linked to survival outcomes in SHH patients. These transporters were also significantly correlated with genes involved in antioxidant activity and collagen metabolism, including those contributing to the ECM shell in SHH tumours. To explore the functional effects of ascorbic acid, SHH spheroids, a 3D cell culture model that mimics tumour architecture, were treated with increasing concentrations of ascorbic acid. Physiological concentrations promoted spheroid growth, while high-dose ascorbic acid, when combined with the chemotherapeutic agent cisplatin, reduced spheroid size, suggesting an enhancement of cisplatin's anti-proliferative effects. To investigate the underlying mechanism, acute ROS production in spheroids was measured following treatment. Pre-treatment with physiological ascorbic acid protected SHH spheroids from cisplatin-induced oxidative stress, whereas high-dose ascorbic acid exacerbated ROS production in pre-stressed spheroids. These findings suggest that high-dose ascorbic acid could enhance ROS generation achieved by a chemotherapeutic alone. Future research should further explore the potential synergy between ascorbic acid and cisplatin, as well as determine whether ascorbic acid-mediated spheroid growth is due to increased collagen deposition. This would help establish high-dose ascorbic acid as a potential adjuvant therapy in SHH medulloblastoma.

Acknowledgements

I am incredibly proud of the work I have done to produce this thesis. Little did I know when I frantically attempted to write a worthwhile undergraduate dissertation it would lead to the opportunities that I have been afforded in my MRes, for which I am extremely grateful.

I could not have completed this work without the wonderful people that supported me through this year. I would firstly like to thank my two fantastic supervisors. Ian if I didn't know four years ago how lucky I was to be lumped with you as a personal tutor I sure do now. You are a bounty of knowledge, dry wit and kindness. Beth, you continually inspired me and drove my eagerness to produce meaningful science, if in part to get an encouraging nod from you. Thank you both for your incredible support and guidance.

Of course, I would like to thank everyone in the lab but first and foremost Deb. Thank you for your unparalleled help and guidance, you really were my first point of call for anything lab related or not. Thank you to Sakura, Norah, Imogen and Susie you were all absolutely lush and made doing the same western blot for the 10th time at least a little enjoyable. Thank you to Ian Ward for all your help and knowledge with immunohistochemistry, you and Denise both contributed to my sanity during that time. Thank you to extended lab members Alistair, Joe, Asifa, Izzie, Hannah and Connor you baked lovely goods and had even better advice.

Lastly, thank you to my family and friends you guys are my rocks, and I am very lucky to have such a solid support network behind me.

Table of Contents

List of Common Abbreviations

Sonic Hedgehog	**SHH**	Wingless	**WNT**
Ascorbic acid	**AA**	Dehydroascorbic acid	**DHA**
Reactive oxygen species	**ROS**	Hydrogen peroxide	**H_2O_2**
Hydroxyl radical	**OH^-**	Iron	**Fe^{3+}/Fe^{2+}**
Lysyl oxidase	**LOX**	Metalloproteinase	**MMP**
Glutathione	**GSH**	Glutathione-reductase	**GSR**
Sodium-dependent vitamin C transporter	**SVCT**	Solute carrier family 23	**SLC23**
Glucose transporter	**GLUT**	Solute carrier family 2	**SLC2**
Endoplasmic reticulum	**ER**	Extracellular matrix	**ECM**
Epithelial-mesenchymal transition	**EMT**	Tissue inhibitor of metalloproteinase	**TIMP**
2' 7'-dichlorodihydrofluorescein diacetate	**DCFH-DA**	2',7'-dichlorofluorescein	**DCF**
Analysis of variance	**ANOVA**	Ultra-low attachment	**ULA**
Inhibitory concentration	**IC**	Arterial Tortuosity Syndrome	**ATS**

1. Introduction

1.1. Overview of medulloblastoma

Medulloblastoma is a highly malignant brain tumour that accounts for 20% of paediatric brain tumours and 10% of all paediatric cancer deaths (Medulloblastoma.org; Northcott et al. 2019). Classified as a Grade IV tumour by the World Health Organization (WHO), medulloblastoma is primarily located in the cerebellum (infratentorial region). It typically arises from the cerebellar vermis and can protrude into the fourth ventricle, although a smaller proportion can develop in the cerebellar hemispheres, especially in older children and adults (Pfizer and Clifford, 2009; Millard and De Braganca, 2016; Figure 1.1) . The disease predominantly affects children aged 3-8 years old, with approximately 50 cases diagnosed in the UK annually (Cancer Research UK).
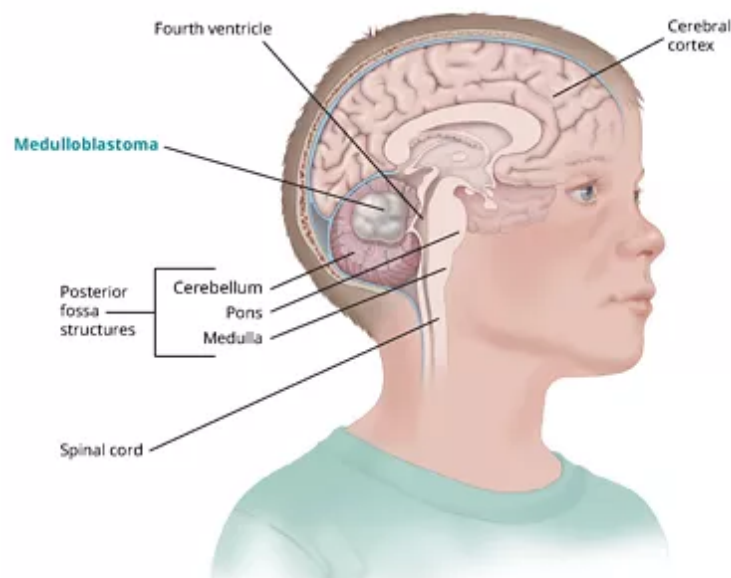
Figure 1.1. Medulloblastoma location within the brain. Medulloblastoma is found in the infratentorial region of the brain in the cerebellum of the posterior fossa adjacent to the fourth ventricle. *Image obtained from stjude.org*

1.1.1. Diagnosis, Treatment and Prognosis

Presenting symptoms include headaches, nausea, ataxia and behavioural changes, largely resulting from increased intracranial pressure and cerebellar dysfunction (Millard and De Braganca, 2016). Unfortunately, these symptoms are non-specific, leading to possible diagnostic delays. Diagnosis is achieved through imaging techniques such as CT (Computed Tomography) and MRI (Magnetic Resonance Imaging) of the brain and total spine (Massimino et al., 2016). Cerebrospinal fluid (CSF) cytology is often used in adjuvant to assess metastasis (Massimino et al., 2016).

1.1.2. Medulloblastoma classification

The 2007 WHO central nervous system (CNS) tumour classification initially classified tumours based solely on their histology (Louis et al., 2007). Advancements lead to the integration of molecular parameters with histology in the 2016 WHO CNS classification (Louis et al., 2016).

1.1.2.1. Histological classification of medulloblastoma

Histological classification of medulloblastoma includes four major variants: classic, desmoplastic/nodular (D/N), medulloblastoma with extensive nodularity (MBEN), and large cell/anaplastic (LC/A) (Louis et al., 2007; Figure 1.2.). Approximately 65% of medulloblastomas are classified as classic, characterised by small to medium hyperchromatic nuclei and minimal cytoplasm (Milliard and Braganca, 2015). About 25% are of the desmoplastic subtype, consisting of reticulin-free nodules surrounded by proliferating cells producing a reticulin-rich extracellular matrix (Polkinghorn and Tarbell, 2007). The MBEN subtype, found almost exclusively in infants, makes up 5% of cases and has an expanded lobular architecture with prominent reticulin-free zones (Orr et al., 2020). The LC/A subtype, also accounts for 5%, is the most undifferentiated and shows poor prognosis compared to classic medulloblastomas (Millard and Braganca, 2015), whilst desmoplastic and MBEN variants have better outcomes
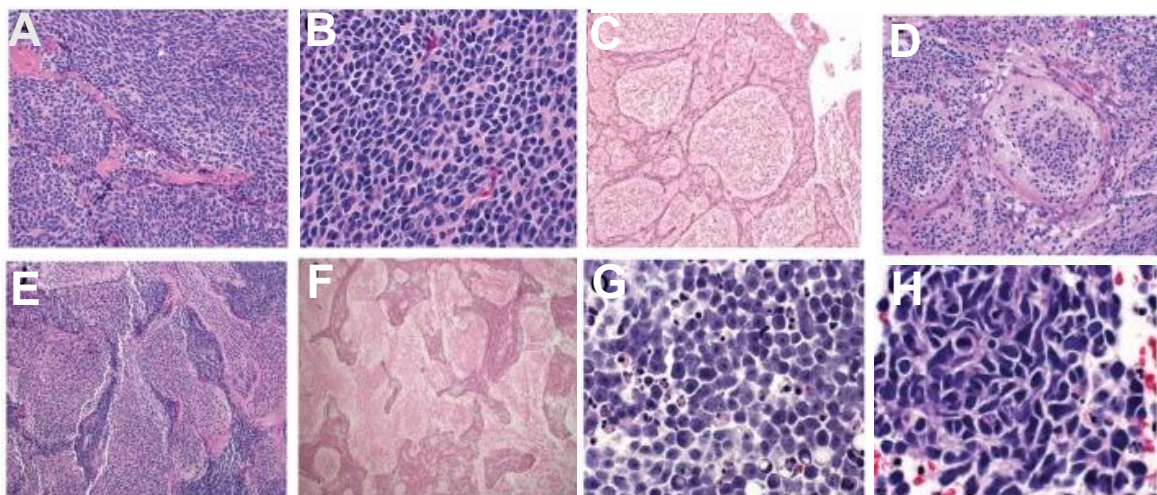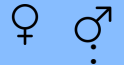
Figure 1.2. Histological images of the histological variants of medulloblastoma. A and B) Classical histology shown by small cells with round nuclei. **C and D)** Desmoplastic/nodular histology shown by nodules of neurocytic cells surrounded by internodular areas. **E and F)** Medulloblastoma with extensive nodularity shown by larger extended nodules surrounded by smaller internodular areas. **G and H)** Large cell / anaplastic histology shown by large cells with prominent nuclei and cell moulding. *Image adapted from Orr, 2020.*

1.1.2.2. Molecular classification of medulloblastoma

Four distinct molecular subgroups of medulloblastoma have been defined: Wingless (WNT), Sonic Hedgehog (SHH), Group 3, and Group 4, each also associated with differences in their demographics, clinical, genetic and cytogenetic features (Taylor et al., 2012; Louis et al., 2016; Table 1.1). Subsequent research also identified inherent intra-subgroup heterogeneity such that 12 subtypes within the medulloblastoma subgroups were characterised: These are WNT α and β, SHH α, β, γ and δ, Group 3 α, β and γ, and Group 4 α, β and γ (Cavalli et al., 2017; Figure 1.3.)

Table 1.1. – Medulloblastoma Molecular Subgroups. *References: Taylor et al., 2012; Northcott et al., 2012; Northcott et al., 2019*

WNT

10%

>90% 5-year Survival

<5% Met at Diagnosis

Located in lower rhombic lip and brainstem

Classic Histology

Local and Metastatic

Genetics

CTNB1, *TP53*, and *APC* mutations
WNT pathway activation
Monosomy 6

SHH

30%

75% 5-year Survival

20% Met at Diagnosis

Cerebellar hemisphere

Classic, LC/A, D/N, and MBEN histology

Local Relapse

Genetics

PTCH1, SMO, and *SUFU* somatic mutations
MYCN, GLI1, and *GLI2* amplications
HOX gene family amplication
SHH pathway activation

Group 3

25%

<60% 5-year Survival

40-50% Met at Diagnosis

Fourth ventricle touching the brainstem

Classic and LC/A histology

Metastatic

Genetics

MYC and *OTX2* amplification
SMARCA4 mutation
I17q isochoromosome
Chromosome 5q, 9q, 10q, 11, 16q and 17p loss

Group 4

35%

75% 5-year Survival

35-40% Met at Diagnosis

Centrally in the fourth ventricle

Classic and LC/A histology

Metastatic

Genetics

MYCN and *SNCAIP* amplification
BRCA2, KCNA1, and *KDM* family mutations
I17q isochoromosome
Chromosome 8p, 10q and 17p loss

Infant (0-3); Child (6-17); Adult (18+); Female; Male; **Met** metastatic
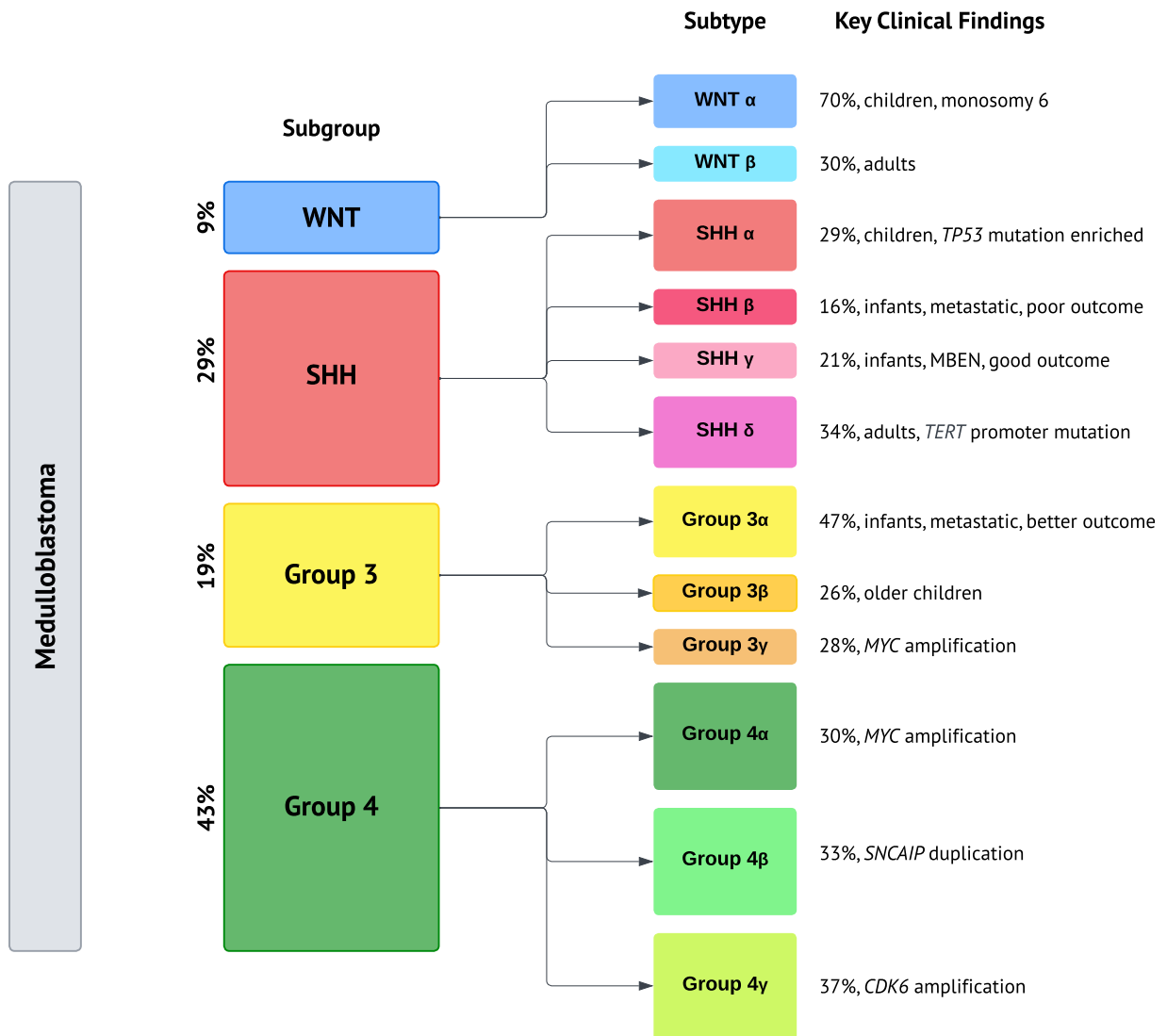
Figure 1.3 Medulloblastoma subgroups and their subtypes. The WNT subgroup (blue), SHH subgroup (red), Group 3 (yellow), and Group 4 (green). Adapted from Cavalli et al., 2017.

1.1.2.2.1. *WNT subgroup*

WNT medulloblastoma is the best-characterised subgroup, yet only accounts for about 10% of cases (Gibson et al., 2010; Kool et al., 2012). It predominantly affects older children, with a peak incidence at 10–12 years old, and has an excellent prognosis, with a 5-year survival rate exceeding 90% (Cavalli et al., 2017). Tumours in this subgroup are located in the midline of the brain, occupying the fourth ventricle and often present with classic histology (Gibson et al., 2010; Taylor et al., 2012).

The molecular mechanism of WNT tumours is underpinned by the activation of the WNT pathway, principally attributed to activating somatic mutations of *CTNB1* (Catenin Beta 1) that then accumulates in the nucleus (~86% of WNT patients) (Thompson et al., 2006; Northcott et al., 2012). WNT activation pathway has roles in the regulation of cellular processes such as proliferation, differentiation, migration, and apoptosis.

WNT medulloblastomas can be divided into two subtypes: WNT-α (70%), consisting primarily of children, and WNT-β (30%), consisting primarily of older children and adults (Cavalli et al., 2017).

1.1.2.2.2.   SHH subgroup

The SHH subgroup accounts for about 30% of medulloblastoma cases and has an overall 5-year survival rate of 75% (Kool et al., 2012). It has a bimodal age distribution, affecting both infants and adolescents over 16, and an equal gender incidence ratio (Kool et al., 2014) (Table 1.1). SHH tumours are primarily located in the cerebellar hemispheres and cells commonly have a nodular/desmoplastic histology (Gibson et al., 2010). The 5-year survival rate varies with age and histological subtype, infants with desmoplastic/nodular tumours have the best prognosis – a 10-year survival rate of 84% (Millard and Braganca, 2016).

The subgroup is defined by aberrant activity of the SHH signalling pathway. Most patients have germline or somatic mutations for critical genes of this pathway this includes *SMO* (smoothened), loss-of-function mutations or deletions of PTCH1 (protein patched homolog 1), and *SUFU* (Suppressor of Fuse Homology) (Northcott et al., 2012; Kool et al., 2014). Mutations in *TP53* (tumour supressing protein 53) are also a contributing factor to 5-year survival rates; mutant TP53 SHH tumours are associated with a decreased 5-year survival rate of 40% (Thomas and Noel, 2019; Orr et al., 2020).

SHH tumours are further divided into four subtypes: SHH-α (29%), characterised by frequent *TP53* mutations and a poor outcome, SHH-β (16%), occurring in infants and frequently metastatic, SHH-γ (21%), also occurring in infants, and SHH-δ (34%), the subtype with the best 5-year prognosis and occurring in adults (Cavalli et al., 2017).

1.1.2.2.3.   Group 3

Group 3 accounts for 25–30% of medulloblastoma cases, with a patient population that typically comprises children under 3 and occurs twice as likely to occur in males compared to females (Kool et al., 2012; Taylor et al., 2012) (Table 1.1.). Group 3 is the most aggressive subgroup; tumours often present with metastasis at diagnosis (45%) which may contribute to the poor prognosis, a 5-year survival rate of 50–60% (Northcott et al., 2019;

Taylor et al., 2012). These tumours have a midline location adjacent to the fourth ventricle and show either classic or large cell/anaplastic histology (Kool et al., 2012).

Unlike WNT and SHH subgroups, a specific driver pathway has not been identified and only a few somatic mutations and no germline mutations have been associated with group 3 (Gajjar and Robinson, 2014). However, the amplification of *MYC* (MYC proto-oncogene, BHLH transcription factor) is common in group 3 tumours (17%), as well as mutations in *OTX2* (orthodenticle homeobox 2) and *SMARCA4* (transcription activator BRG1) (Northcott et al., Jones et al., 2012; Adamson et al., 2010)*.* Cytogenetically, Group 3 medulloblastomas exhibit extensive aneuploidy, including frequent isochromosome 17q (duplication of q arm paired with a complete/partial loss of p arm), a feature also shared by some group 4 tumours (Koczkodaj et al., 2021).

There are three subtypes of Group 3 tumours : Group 3-α (47%), mostly comprises of infants and often metastasises, Group 3-β (25%) and Group 3-γ (28%) with the latter having the worst prognosis (a 5-year survival rate of 42%) and associated with *MYC* amplification (Cavalli et al., 2017).

1.1.2.2.4.   Group 4
Group 4 is the most common subgroup, comprising 35% of medulloblastoma cases (Kool et al., 2012). This group is more prevalent in males and primarily affects children aged 3–16 (Northcott et al., 2012). Group 4 tumours generally have an intermediate prognosis, with a 75% 5-year survival rate despite often presenting with metastasis at diagnosis (30-40%) (Ramswamy et al., 2016). Tumours are typically located in the midline region and the majority are of classic histology (Kerleroux et al., 2020).

The most prominent commonality between Group 3 and 4, as well as the most common cytogenic change in group 4, is isochromosome 17q (Kool et al., 2012; Sharma et al., 2019; Cavalli et al., 2017).). Other features of this subgroup include a loss of an X chromosome and mutations in *KCNA1* (potassium voltage-gated channel subfamily A member 1) and a deletion of *KDM6A* (lysine demethylase 6A) (Taylor et al., 2012; Menyhart et al., 2019).

Group 4 can be subdivided into three subtypes: Group 4-α (30%), Group 4-β (33%) and Group 4-γ (37%), molecular features of Group 4-α include *MYC* amplification and also it is associated with poor prognosis (Cavalli et al., 2017).

1.1.3. Treatment Strategy for Medulloblastoma

The standard treatment for medulloblastoma involves maximal surgical resection, followed by craniospinal irradiation and chemotherapy (Millard and de Braganca, 2016). Chemotherapeutic agents typically include platinum-based compounds (cisplatin, carboplatin) and alkylating agents (cyclophosphamide) (Millard and de Braganca, 2016). This approach achieves a 5-year survival rate of ~70% across all medulloblastoma patients (Ramaswamy et al. 2016).

However, several challenges remain such as the need to account for long-term toxicity. Craniospinal irradiation can cause neurological, endocrine and cognitive impairments, particularly in young children (Grill et al., 2005). Dose reduction and radiation avoidance strategies help minimise these effects but often lead to higher relapse rates (Michalski et al., 2021). Additionally, medulloblastoma subgroups respond differently to treatment, yet targeted therapies remain elusive and existing therapies limited due to significant intra-subgroup heterogeneity. For example, SHH inhibitors are only effective in tumours with mutations upstream of *SMO*, rendering them ineffective for many SHH patients (Kool et al., 2014).

Given the limitations of current treatments, adjuvant therapies that enhance efficacy could allow for lower therapeutic doses, reducing toxicity and long-term side effects. Mounting evidence indicates that high-dose intravenous vitamin C may act as a potent adjuvant therapy by generating reactive oxygen species (ROS), selectively targeting tumour cells (Böttger et al., 2021). While its potential is being explored in various cancers, its role in medulloblastoma remains unclear.

1.2. The Biochemistry of Ascorbic Acid

AA, commonly known as Vitamin C, is a water-soluble vitamin and key antioxidant (Doseděl et al., 2021). Humans are unable to synthesise AA and therefore rely on exogenous sources, primarily from citrus fruits, to meet their dietary needs. If these needs are not met the condition scurvy persists; characterised by fatigue, bleeding gums, bruised skin and potentially fatal complications including neuropathy, fever, convulsions and death (Du et al., 2012).

Central to all functions of AA is its ability to rapidly undergo oxidation and donate two electrons. Following two consecutive one-electron oxidations, AA forms first an ascorbyl radical then dehydroascorbic acid (DHA) (Figure 1.4). AA can readily oxidise but is dependent on pH and accelerated by the presence of catalytic metals (Du et al., 2012). Spontaneous autoxidation occurs at low rates in their absence (Du et al., 2012).
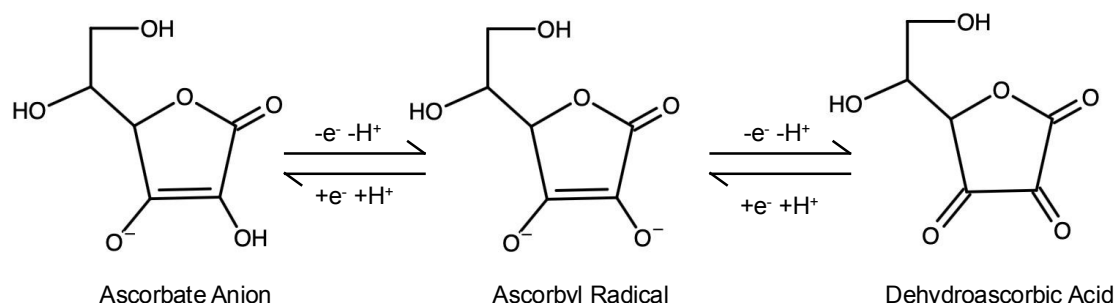
Figure 1.4 The oxidation of ascorbic acid to dehydroascorbic acid. The ascorbate anion donates one electron to form the ascorbyl radical and a second electron to form dehydroascorbic acid.

1.2.1. Ascorbic acid an antioxidant

ROS are inevitable byproducts of cellular metabolism, primarily generated in the mitochondria during oxidative phosphorylation, where electron leakage from the electron transport chain leads to the formation of superoxide radicals. Other significant sources include the endoplasmic reticulum, where protein folding generates ROS, and peroxisomes, which produce hydrogen peroxide as a byproduct of fatty acid oxidation. ROS levels escalate during periods of cellular stress, and if unchecked, these radicals can damage cellular components and trigger harmful signalling pathways, including p53, JNK, and ASK1, which promote apoptosis and cell death through mitochondrial dysfunction and activation of caspases. (Sies et al., 2022). To maintain redox balance, cells rely on a complex interplay of enzymatic and non-enzymatic antioxidants to neutralise radicals and prevent oxidative damage.

AA plays a crucial role in this defence by donating an electron to a wide range of oxidising radicals (Table 1.2A). Its one-electron oxidation product, the ascorbyl radical, also reduces radicals, often more rapidly than AA itself (Table 1.2B). This dual oxidation potential allows AA to significantly contribute to radical detoxification (Du et al., 2012).

Table 1.2 – The antioxidant reactions of (A) ascorbic acid and (B) ascorbyl radical. *Adapted from Njus et al., 2020. AA ascorbic acid; O_2^- superoxide; H^+ proton, AA^- ascorbyl radical; H_2O_2 hydrogen peroxide; TyrO tyrosine phenoxyl radical; Trp tryptophan indolyl radical; TO alpha tocopheroxyl radical; OH^- hydroxyl; H_2O water; $^1O_2$ singlet oxygen; AH^- dehydroascorbic acid*

A)

Radical	Reaction	Rate Constant ($M^{-1}s^{-1}$)
Superoxide	$AA + O_2^- + H^+ \rightarrow AA^- + H_2O_2$	1×10^5
Tyrosine Phenoxyl Radical	$AA + TyrO + H^+ \rightarrow AA^- + TyrOH$	9.3×10^7
Tryptophan Indolyl Radical	$AA + Trp + H^+ \rightarrow AA^- + TrpH$	1×10^8
Alpha-Tocopheroxyl Radical	$AA + TO + H^+ \rightarrow AA^- + TOH$	1.3×10^7
Hydroxyl	$AA + OH^- + H^+ \rightarrow AA^- + H_2O$	1.1×10^{10}
Singlet Oxygen	$AA + {}^1O_2 + H^+ \rightarrow AA^- + H_2O_2$	3×10^8

B)

Radical	Reaction	Rate Constant ($M^{-1}s^{-1}$)
Superoxide	$AA^- + O_2^- + H^+ \rightarrow AA + HO_2^- + OH^-$	2.6×10^8
Tocopheroxyl Radical	$AA^- + TO + H^+ \rightarrow AA + H_2O + TOH$	7×10^7
Ascorbyl Radical (Disproportionation)	$A^- + A^- + H^+ \rightarrow AH^- + AA + H_2O$	

AA supports the action of vitamin E (**α**-tocopherol) to protect lipids from oxidative damage. During the inhibition of lipid peroxidation by α-tocopherol the potentially harmful α-tocopheroxyl radical is formed (Niki et al., 1987). AA prevents the irreversible loss of α-tocopherol by reducing this radical back to its active form. Additionally, AA can also directly reduce lipid peroxyl radicals in plasma (Frei et al., 1989). Thus, AA action both directly and indirectly inhibits lipid peroxide-dependent cell death, ferroptosis (Lőrincz et al., 2019).

In organelles such as the nucleus, where enzymatic antioxidants are absent, small molecule antioxidants like AA are indispensable to prevent free radical damage to DNA (Zhitkovich, 2020). AA is crucial for scavenging specific radicals that lack these dedicated enzymatic defences, such as nitrogen dioxide, carbonyl radicals, and amino acid radicals like tryptophanyl and tyrosyl radicals. Furthermore, AA is the primary defence against singlet oxygen, a highly reactive and mutagenic form of oxygen produced in photoreactions (Devasagayam et al., 1991). This is especially important in tissues like the corneal epithelium and skin, where AA concentrations are high due to constant exposure to visible light and UV (Brubaker et al., 2000).

1.2.2. Ascorbic acid as a pro-oxidant

The excellent reducing capacity of AA paradoxically defines its pro-oxidant activity at high millimolar concentrations. AA donates electrons to free transition metal ions, like Fe^{3+} and Cu^{2+}, reducing them and consequentially generated high levels of hydrogen peroxide (H_2O_2) (Buettner et al., 1996). Additionally, reduced iron (Fe^{2+}) produced in this reaction can react further with H_2O_2 via the Fenton reaction and produce highly reactive hydroxyl radicals (OH^-) (Du et al., 2012; Figure 1.5). These hydroxyl radicals are potent oxidising agents that indiscriminately damage biological molecules, including macromolecules, lipids, and DNA.

$$1) \quad Fe^{3+} + AA \longrightarrow Fe^{2+} + AA^- + 2H^-$$

$$2) \quad Fe^{2+} + O_2 \longrightarrow Fe^{3+} + O_2^-$$

$$3) \quad 2O_2^- + 2H^+ \longrightarrow H_2O_2 + O_2$$

$$4) \quad H_2O_2 + Fe^{2+} \longrightarrow Fe^{3+} + OH^-$$
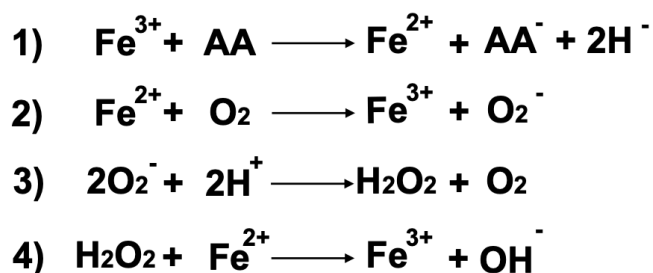
Figure 1.5 The Fenton reaction mediated by ascorbic acid; (1) ascorbic acid reduces ferric iron to ferrous iron, **(2)** ferrous iron reacts with oxygen to produce superoxide, **(3)** the dismutation of superoxide leads to formation of hydrogen peroxide, **(4)** hydrogen peroxide reacts with ferrous iron to form hydroxyl radicals. *AA, ascorbic acid; Fe^{3+}, ferric iron; Fe^{2+} ferrous iron*; AA^-, ascorbyl radical; O_2^-, superoxide; H_2O_2, hydrogen peroxide; OH^-, hydroxyl radical.

The pro-oxidant effect of AA is concentration-dependent (>1mM) and relies on the availability of free transition metal ions, particularly iron (Fe) and copper (Cu). At physiological concentrations of AA (75-100μM), this effect does not occur (Carr et al., 1999). Additionally, in healthy individuals, the cellular availability of free metal ions is tightly regulated. However, in pathological conditions such as cancer or chronic inflammation, cellular iron levels are increased to compensate for an elevated metabolic and proliferative capacity (Du et al., 2015). One mechanism by which this occurs is the upregulation of *TFR1* (transferrin receptor 1), which facilitates iron uptake via transferrin internalisation (Du et al., 2015; Zhang et al., 2020).

AA-induced oxidative stress is primarily dependent on the accumulation of H_2O_2, which is generated through the redox cycling of Fe^{3+} and Fe^{2+} via the Fenton reaction. Vitamin C enhances this process by reducing Fe^{3+} to Fe^{2+}, increasing its availability for ROS generation. Cancer cells, which often exhibit higher labile Fe^{2+} levels and reduced catalase activity, are particularly vulnerable to this oxidative stress. Catalase, a key enzyme responsible for neutralising H_2O_2, can mitigate the pro-oxidant effect of AA (Klingelhoeffer et al., 2012). This suggests that both metal ion availability and the presence of antioxidant defences like catalase contribute to the shift toward a pro-oxidant effect, selectively targeting cancer cells.

1.2.3. Ascorbic acid a co-factor for collagen production

AA maintains the active Fe^{2+} state of 2-oxoglutarate-dependent dioxygenases (2-ODDGs), a large enzyme superfamily responsible for a variety of hydroxylation and demethylation processes that include prolyl and lysyl hydroxylases. These enzymes are strictly localised to the endoplasmic reticulum (ER) and are crucial for collagen maturation. The hydroxylation of prolyl residues is needed for the formation of a stable procollagen, without which collagen cannot form triple helices (Salo and Myllyharju, 2021). These residues also contain functional motifs which increase the avidity of integrin binding. Hydroxylated lysine residues are sites for the covalent cross-links between adjacent collagen fibrils by lysyl oxidases (LOX). The mechanical properties of fibril-forming collagens (types I, II, III, V, and XI) rely on these cross-links for strength and elasticity (Ricard-Blum 2011). Additionally, hydroxylated lysine residues are attachment sites for post-translational modifications, such as glycosylation which for some collagens (type IV and VI) has been shown to be crucial for their assembly and secretion (Salo and Myllyharju, 2021; Sipilä et al., 2007).

Evidence also exists that as well as being necessary for collagen structural integrity, AA also may regulate expression of collagen. For example, fibroblasts cultured *in vitro* with AA produced a collagen matrix with alignment of collagen fibrils mimicking *in vivo* (Murad et al., 1981; Grinell et al., 1989; Geesin et al., 1988). Interestingly, AA also led to a 3-4-fold increase in expression and/or stability of mRNA for procollagens I and III (Pinnell et al., 1987; Tajima et al., 1996; Kim et al., 2013). The potential mechanism suggested was an accumulation of immature procollagen depressing further expression of collagen in the absence of AA and hydroxyproline residues. Hence, AA can influence collagen production in roles independent to being a co-factor for 2-ODDGs.

1.2.4. The recycling of DHA and AA

As humans cannot synthesise AA, efficient recycling of AA is crucial for the maintenance of its intracellular concentrations. Several enzymatic systems are responsible for recycling DHA (Figure 1.6). DHA is unstable at physiological pH with a half-life of 5-15 minutes thus must be rapidly reduced in order to avoid a loss of AA. Principally, DHA's reduction is facilitated by glutathione (GSH) which can either directly transfer electrons to DHA or with the further assistance of glutaredoxin (GRX) and protein disulphide isomerase (PDI) (Winkler et al.,1994; Wells et al., 1990). Thus glutathione-reductase (GSR), which regenerates GSH, is important in the recycling of DHA. Whilst this reduction is thought to be largely GSH-dependent, thioredoxin and thioredoxin reductase function as an NADPH (nicotinamide adenine dinucleotide phosphate) dependent DHA reductase (May et al., 1997). Thus, DHA

can be reduced via multiple pathways, underscoring the cellular importance of efficient recycling for sustaining AA levels and enabling repeated cycles of oxidation.
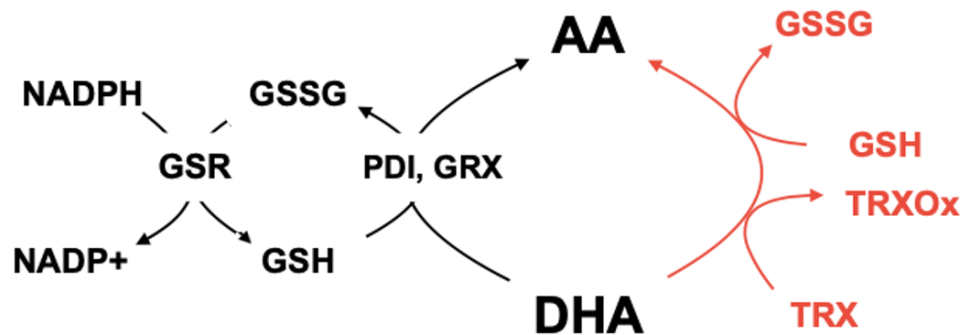
Figure 1.6, The enzymatic (black) and direct (red) recycling of DHA to AA. Thioredoxin and glutathione can donate electron/s directly to dehydroascorbic acid to recycle ascorbic acid. Protein disulfide isomerase and glutaredoxin can facilitate the transfer of electrons from glutathione to dehydroascorbic acid. Glutathione reductase and thioredoxin reductase can regenerate glutathione and thioredoxin. *AA, ascorbic acid; DHA, dehydroascorbic acid; GSH, glutathione; TRX, thioredoxin; PDI; protein disulfide isomerase; GRX, glutaredoxin; GSR, glutathione reductase; NADPH, nicotinamide adenine dinucleotide phosphate.*

1.3. Transmembrane transport of ascorbic acid

Due to its size and charge, AA cannot diffuse across membranes (Wilson, 2005). To facilitate its transport, specialised sodium-dependent vitamin C transporters (SVCT), encoded by the solute carrier family 23 (SLC23) genes, have evolved. However, AA is not the only form of Vitamin C transported across membranes. DHA (the oxidised form of Vitamin C) is transported by certain members of the glucose transporter (GLUT) family, encoded by the solute carrier family 2 genes (SLC2) (Rumsey et al., 1997). This process is a facilitative transport that competes with glucose (Table 1.3).

Table 1.3. – Ascorbic acid and dehydroascorbic acid transporters. Individual transporters', gene names, transporter classification database (TCDB) ID, known substrates, tissue distribution, and subcellular location. AA transporters are coloured blue, and DHA transporters are coloured red – for continuance of colour key. *References: Mueckler et al., 2013; Banheygi et al., 2014.*

Protein	Gene	TCDB ID	Substrate	Tissue Distribution	Subcellular Location
SVCT1	*SLC23A1*	2.A.40.6.5	***Ascorbic Acid***	Epithelial tissues including kidney, intestines, liver, lung	Plasma membrane
SVCT2	*SLC23A2*	2.A.40.6.2	***Ascorbic Acid***	***Brain*** (neurons), retina, placenta, spleen, prostate, testis, ovary	Plasma membrane, mitochondrial inner membrane, endoplasmic reticulum
GLUT1	*SLC2A1*	2.A.1.1.130	Glucose, galactose, mannose, glucosamine, ***dehydroascorbic acid***	Erythrocytes, ***brain***, blood–brain barrier	Plasma membrane, Golgi apparatus, mitochondrial inner membrane
GLUT2	*SLC2A2*	2.A.1.1.29	Glucose, galactose, fructose, mannose, glucosamine, ***dehydroascorbic acid***	Liver, islet of Langerhans, intestine, kidney, ***brain***	Plasma membrane
GLUT3	*SLC2A3*	2.A.1.1.91	Glucose, galactose, mannose, xylose, ***dehydroascorbic acid***	***Brain*** (neurons), testis, lymphocytes	Plasma membrane
GLUT4	*SLC2A4*	2.A.1.1.80	Glucose, glucosamine, ***dehydroascorbic acid***	Adipose, skeletal and cardiac muscle	Endosomal pathway, plasma membrane
GLUT8	*SLC2A8*	2.A.1.1.89	Glucose, galactose, fructose, ***dehydroascorbic acid***	Testis, ***brain***, adrenal gland, liver, spleen, adipose tissue, lung	Plasma membrane, lysosome, late endosome, rough endoplasmic reticulum
GLUT10	*SLC2A10*	2.A.1.1.59	Glucose, galactose, ***dehydroascorbic acid***	Heart, lung, ***brain***, liver, skeletal muscle, pancreas, placenta and kidney	Plasma membrane, mitochondrial inner membrane, nuclear envelope, endoplasmic reticulum

1.3.1. SVCTs – ascorbic acid transporters

SVCT1 and SVCT2, encoded by *SLC23A1* and *SLC23A2* are the only functional members of this family. SVCT3 is an orphan transporter and *SLC23A4P* is a pseudogene (Bürzle, 2013). SVCT1 and SVCT2 exhibit 66% sequence identity and are highly specific for L-AA, showing stereoselectivity over D-AA, D-AA has similar physiochemical properties but does not act as an enzymatic co-factor (Wilson, 2005). The resolved structure of SVCT1 shows it forms a homodimer, with each protomer consisting of 14 transmembrane helices organised into a core and gate domain and an intracellularly located N- and C- termini (Kobayashi et al., 2024; Figure 1.7). AA transport is an active process that co-transports two Na^+ ions across the membrane.

Despite their homology, SVCT1 and SVCT2 differ in both kinetics and tissue distribution. SVCT1, a high-capacity/low-affinity transporter (K_M of 65-237µM) is primarily found in epithelial tissues such as the intestines and kidneys, where it regulates systemic AA levels through absorption and reabsorption (Wilson, 2005). Conversely, SVCT2, a low-capacity/high-affinity transporter (K_M of 15-20µM), is widely expressed in tissues with high oxidative demands, such as the brain and cornea (Wilson, 2005). The essential role of SVCT2 is underscore by the fact that knockout mice do not survive beyond birth (Sotiriou, 2002).

SVCTs are regulated by environmental factors, including pH and ion concentrations. Notably, SVCT2 is sensitive to intracellular Ca^{2+} and Mg^{2+} concentrations, adopting a low-affinity conformation in their absence (Wilson, 2005). SVCT1 and SVCT2 can localise intracellularly, in organelles such as mitochondria and the ER.
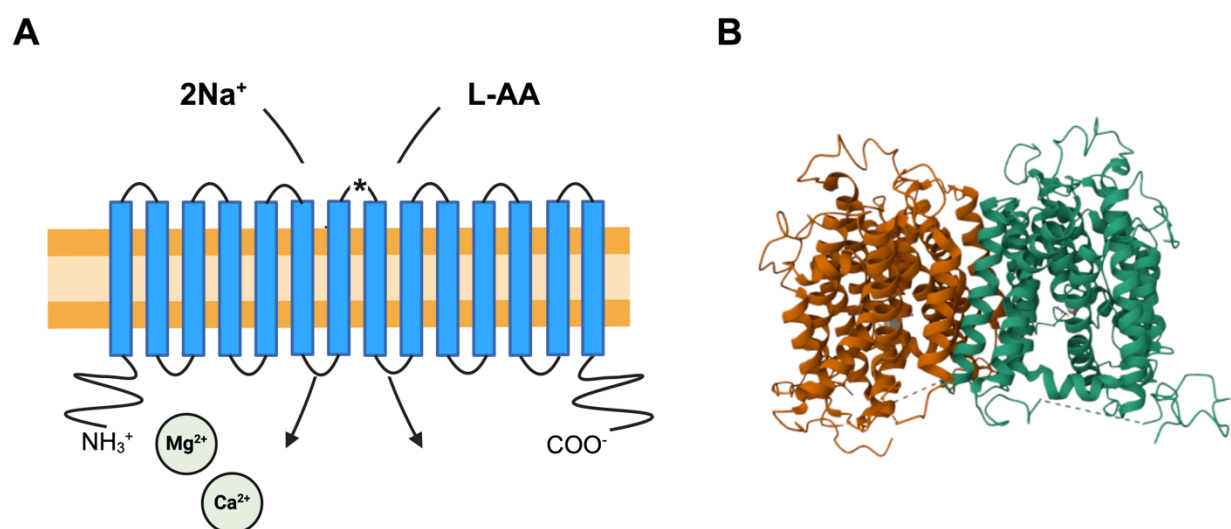
Figure 1.7 Structural features of SVCT transporters and SVCT1 electron microscopy structure
A) An SVCT transporter protomer contains 14 transmembrane helices with intracellularly localised N- and C- termini. Conserved proline residues (*) in the extracellular loop between 7 and 8 transmembrane domains are needed for transport. This transport is dependent on 2Na$^+$ to provide the energy for this active process. Specific to the SVCT2 transporter is the necessity of intracellular Ca^{2+} and Mg^{2+} to adopt a high-affinity conformation. **B)** The dimeric structure of SVCT1 resolved by electron microscopy (3.2Å resolution) with correct topography. *SVCT1 structure obtained from Wang et al., 2023*.

1.3.2. GLUTs – dehydroascorbic acid transporters

The GLUT family is composed of 14 isoforms encoded by the *SLC2* genes and belongs to the major facilitator superfamily (Mueckler et al., 2013). These transporters typically contain 12 transmembrane helices arranged into two pseudo-symmetrical domains (Mueckler et al., 2013; Figure 1.8A/B). The structure of GLUT1, as a reference, is depicted in Figure 1.8C (Deng et al., 2014). GLUTs catalyse the facilitative import of hexoses across membranes, this includes but is not limited to glucose. Based on sequence identity and functional characteristics, GLUTs are classified intro three subclasses: Class I, II and III. Whilst Class I and II share a high degree of sequence homology, Class III is less well understood and has only ~35% sequence similarity between its members (Mueckler et al., 2013; Long et al., 2015; Joost et al., 2002; Figure 1.8D).

D
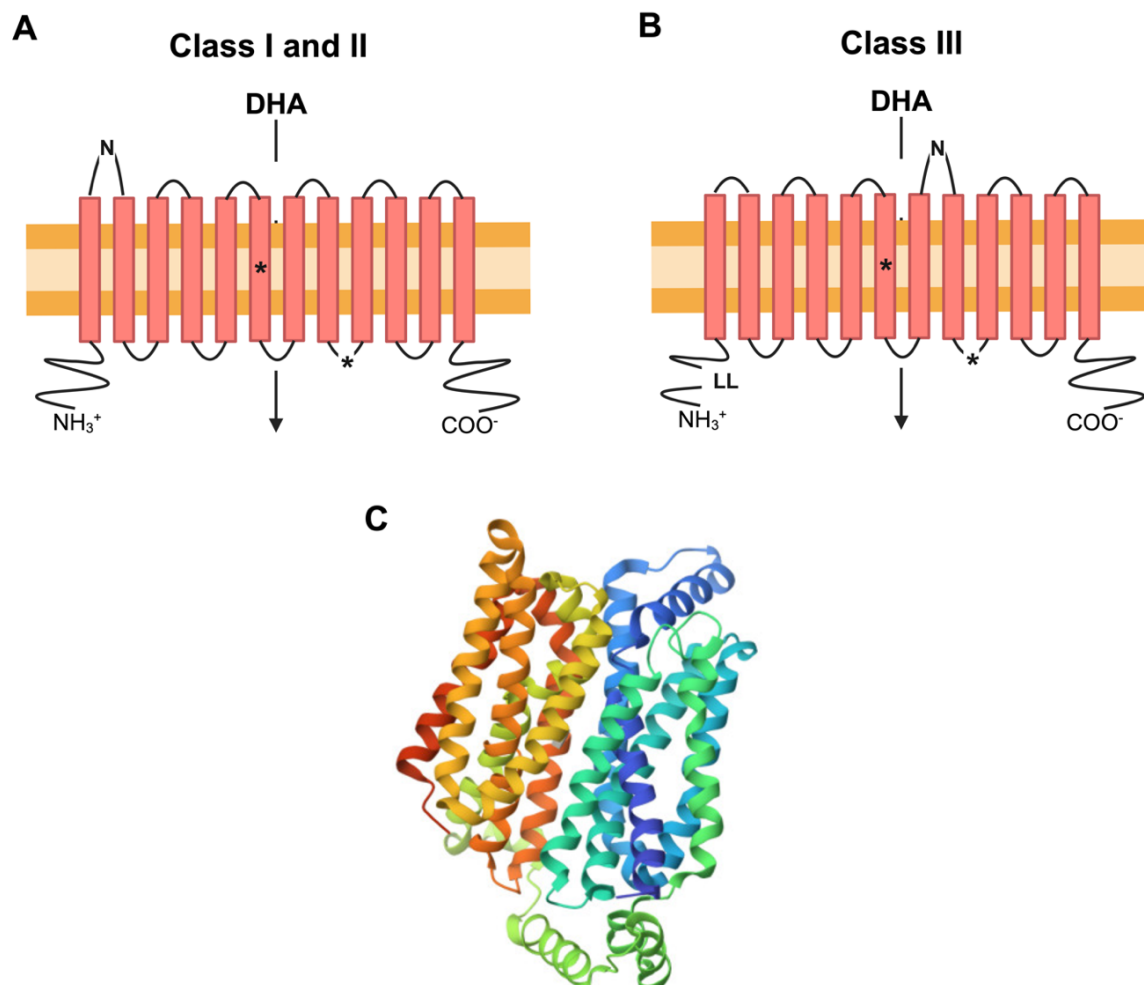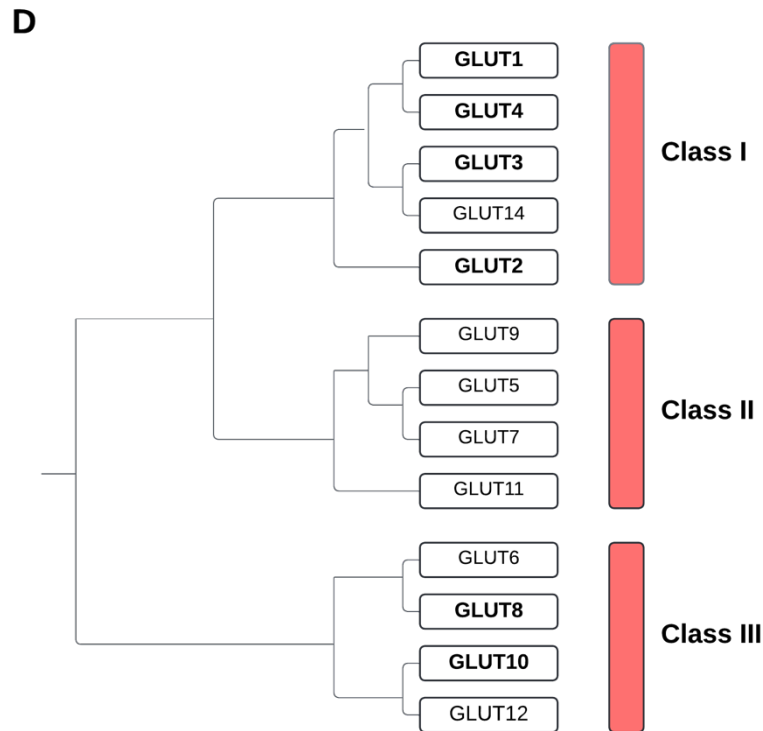
Figure 1.8 Structural features of Class I, II and III GLUT transporters, GLUT1 structure and a dendrogram of all members of the GLUT family. GLUT transporters contain 12 transmembrane domains with intracellularly localised N- and C- termini. Proposed substrate binding sites (*) are located in the 7th transmembrane domain (QLS sequence) and the intracellular loop between 10 and 11 in all classes. **(A)** Class I and II transporters have N-linked glycosylation sites on the intracellular loop between 1 and 2 **(B)** and for Class III transporters this is located between transmembrane domains 9 and 10. Class III transporters additionally have a dileucine motif (LL), an intracellular localisation signal, in the N- terminus. **(C)** GLUT1 structure resolved from X-ray diffraction (resolution 3.17Å). **(D)** The evolutionary relationships of all GLUT transporters (GLUTs that transport DHA are **in bold**). *GLUT1 structure obtained from Deng et al., 2014. Dendrogram adapted from Joost et al., 2002*

Due to the structural similarity of glucose and the bicyclic hemiketal form of DHA (formed when in solution), the transport of DHA by GLUTs had been hypothesised (Figure 1.9). Expression of cloned GLUTs in *X. laevis* oocytes demonstrated that GLUT1, GLUT3, and GLUT4 are efficient transporters of DHA (K_m values of 1.5mM, 2mM and 1mM respectively) (Rumsey et al., 1997; Rumsey et al., 2000). These transporters all belong to Class I, the most extensively studied class of GLUTs. This facilitative transport of DHA was competitively inhibited by glucose and known pan-GLUT inhibitors (e.g., cytochalasin B). GLUT2 and GLUT8, which are expressed in the intestine, are also involved in DHA transport (K_m values of 2mM and 3mM respectively) (Corpe et al., 2013). Additionally, GLUT10, a Class III member, can also transport DHA; this has been observed in mitochondria and endomembranes of smooth-muscle cells and fibroblasts (Lee et al., 2010; Németh et al., 2016). Genetic silencing of GLUT10 results in a significant reduction of DHA within immortalised human fibroblasts (Németh et al., 2016).

Dehydroascorbic acid
(bicyclic hemiketal)
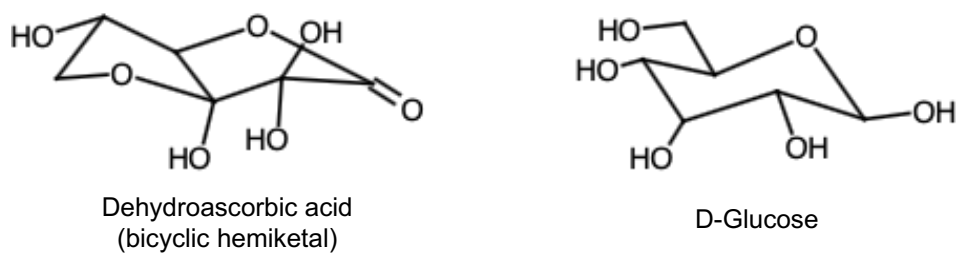
D-Glucose

Figure 1.9. The structure of dehydroascorbic acid and d-glucose.

The contribution of DHA transport to intracellular AA accumulation is context- and cell-type specific. For instance, in erythrocytes, which lack SVCT expression, GLUT1 predominately functions as a DHA transporter, and as a glucose transporter secondly, to ensure these cells which are continuously exposed to oxidative stress in the blood remain protected (Montel-Hagen et al., 2008). Moreover, DHA is transported by GLUTs across the blood-brain barrier, as SVCTs are exclusively localised to the choroid plexus, this has been an implicated mechanism in the accumulation of AA in the brain, where AA concentrations can be 10-fold higher than in plasma (up to 1mM in neurons) (Agus et al., 1997; Angelow et al., 2003).

1.4. Collagen and the extracellular matrix in cancer

The extracellular matrix (ECM) is dramatically reorganised by many solid tumours and can account for up to 60% of the tumour mass (Huang et al., 2021). ECM components can promote tumorigenesis by interacting with cell surface receptors such as integrins, that activate a plethora of intracellular pathways (Popova and Jucker, 2022; Kadry et al., 2020). Overexpression of certain ECM proteins, particularly collagen, is linked to worse clinical outcome. This has been best reported in breast cancer, where tumour-associated collagen boundaries (TACs) have been identified (Li et al., 2024; Brett et al., 2020). TACs have their own distinct organisation and composition of collagens that contribute to tumorigenesis. Collagen deposition, along with increased collagen cross-linking mediated by elevated LOX activity and the reorientation of collagen into parallel fibrils, can locally stiffen tissue (Fang et al., 2012). Enhanced ECM stiffness activates downstream integrin signalling and increases adhesion at the tumour-stroma interface. Imbalanced biomechanic forces, exacerbated by the growing tumour mass, are a key trigger for initiating the epithelial-mesenchymal transition (EMT) of tumour cells (Torzilli et al., 2012). Under mechanical stress, cells become deformed adopting a spindle-like fibroblastic morphology with reduced adhesion and enhanced motility (Fang et al., 2012).

1.4.1. The extracellular matrix of medulloblastoma

In medulloblastoma, the ECM remains less understood than in other solid tumours, but recent studies have identified unique ECM signatures. Comparative proteomics of decellularised patient tumours reveal distinct ECM compositions compared to normal brain tissue, with seven collagens (including collagens I, IV, V and VI) being upregulated in medulloblastoma (Trombetta-Lima et al., 2021). This ECM signature is particularly prominent in the SHH and WNT subgroups, suggesting a role of the ECM in tumour progression in these subgroups.

Indeed, 3D spheroid models have demonstrated that SHH tumours form a distinct ECM shell, absent in Group 3 or 4 tumours (Linke et al., 2023; Roper et al., 2021; Figure 1.10). These models closely replicate *in vivo* spatial organisation, cell-cell interactions and metabolic gradients, providing a physiologically relevant platform for drug screening (Roper et al., 2021). Notably, collagens I and VI are highly expressed in these ECM structures alongside small leucine-rich proteoglycans like lumican and fibromodulin, essential for collagen fibrillogenesis (Linke et al., 2023). The presence of this collagen-rich shell correlates with better survival outcomes in SHH patients, potentially by restricting tumour spread and therefore limiting progression.

Thus, ECM dynamics in medulloblastoma, particularly in SHH tumours, may influence both tumour progression and treatment response. Further investigation could uncover new therapeutic strategies that exploit ECM-related vulnerabilities in medulloblastoma.
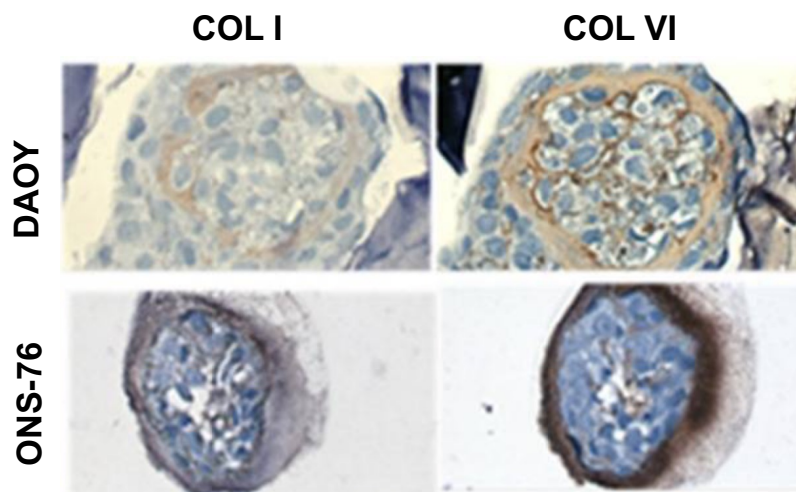
Figure 1.10. The collagen outer shell of SHH nodules. Immunohistochemical staining of DAOY and ONS-76 (two SHH-derived medulloblastoma cell lines) nodules for type 1- and type VI- collagens (stained brown) identifies a subgroup-unique rich collagen outer shell. *Image adapted from Linke et al., 2023.*

1.4.2. Ascorbic acid, collagen and cancer

As discussed in section 1.2.3, AA at physiological concentrations is a co-factor for collagen synthesis, increases collagen mRNA expression and promotes collagen production in human skin fibroblasts (Salo and Myllyharju, 2021). As discussed in section 1.4, collagen deposition is typically elevated in cancer with either prognostic benefits, as observed in SHH medulloblastoma, or detrimental effects, as seen in breast cancer (Linke et al., 2023; Li et al., 2024). However, despite a hypothesis by McCormick (1959) which proposed a potential connection between AA and collagen in cancer, there remains a notable lack of direct research investigating if this physiological link extends to cancer biology.

In vitro studies have offered some insight into a possible association. In a study by Polireddy et al (2017), high-dose AA administered to an orthotopic mouse model of human pancreatic cancer led to tumour reduction, decreased metastasis, enhanced tumour stroma deposition alongside an increase in collagen mRNA and secretion. In their phase I/IIa study, they also found increased collagen levels in a patient who became suitable for tumour resection. Similarly, a study by Cha et al (2013) utilising an orthotopic mouse model of breast cancer, observed that oral AA administration increased collagen type I production, forming a capsule around the tumour and creating more defined tumour boundaries compared to controls. Whether this is an effect of tumour cells or cancer-associated fibroblasts remains unclear and requires further investigation.

This is particularly relevant as high-dose AA has been shown to reduce metastasis in multiple *in vitro* studies, though the underlying mechanism remains unclear, with little attention given to its potential relationship with collagen (Bottger et al., 2021). Notably, a study by Chen et al (2011) found that AA significantly inhibited the activity of MMP-2 and MMP-9 (metalloproteinase-2/-9), enzymes responsible for collagen degradation, in xenografted mice with lung carcinoma. The proposed mechanism involved the AA-dependent increase in the protein expression of TIMP-1 and TIMP-2 (tissue inhibitor of metalloproteinase-1/-2), further supporting a wider association of AA with ECM remodelling in cancer.

1.5. Redox balance and oxidative stress

Cancer cells typically exhibit elevated basal ROS levels due to their increased metabolic activity. ROS can promote tumour proliferation, growth and metastasis (Nakamura et al., 2012; Figure 1.11). However, excessive ROS production can lead to oxidative damage and programmed cell death. To maintain ROS levels within the range that supports tumour growth without triggering cell death, cancer cells adapt by minimising ROS production, for example, by reducing their reliance on mitochondrial oxidative phosphorylation. They also upregulate antioxidant systems, such as GSH, to neutralise excess ROS (Nakamura et al., 2012).

Tumour sensitivity to ROS is being exploited in various cancer therapies. Therapeutic approaches either increase ROS production or suppress antioxidant defences. For instance, anlotinib, a multi-target tyrosine kinase inhibitor, enhances ROS production by upregulating ROS-producing oxidative enzymes such as NADPH oxidase (Huang et al., 2021). Conversely, β-phenylethyl isothiocyanate inhibits GSH recycling, resulting in ROS-dependent cell death in pancreatic ductal adenocarcinoma cells (Ju et al., 2015). This dual strategy of increasing oxidative stress or disabling the tumour's antioxidant defences represents a promising therapeutic avenue.
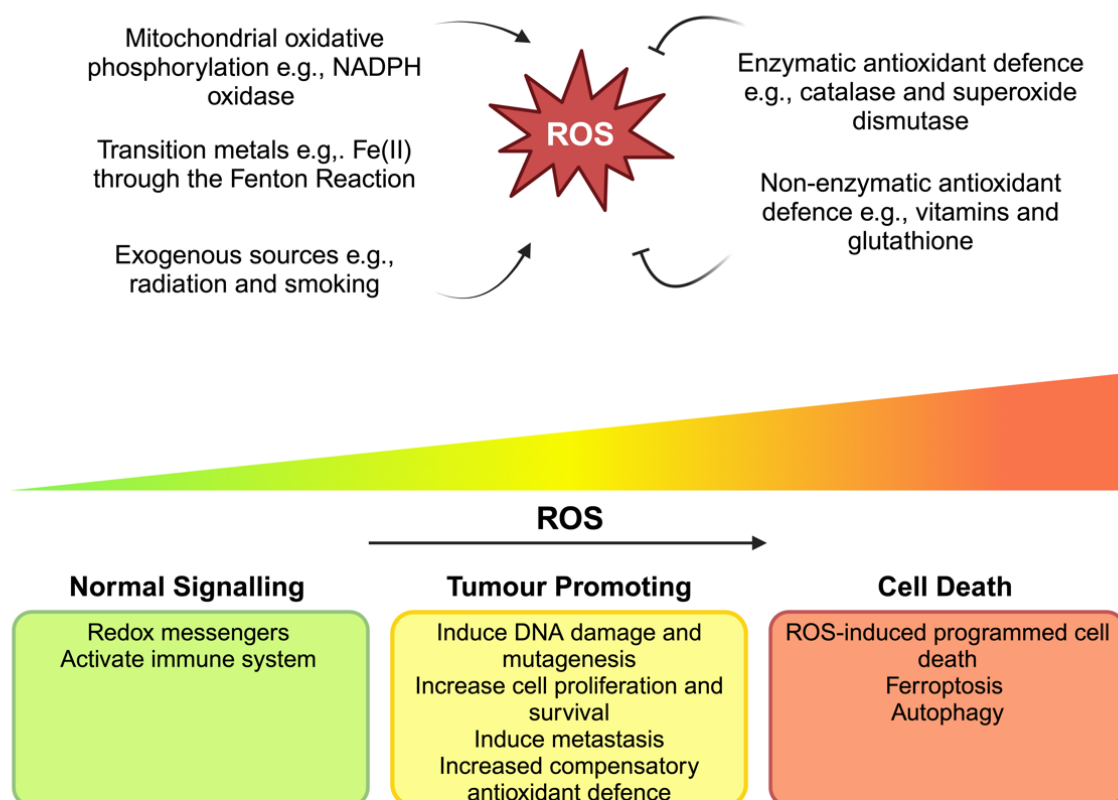
Figure 1.11 The formation and roles of reactive oxygen species. ROS are generated through endogenous processes like mitochondrial oxidative phosphorylation and the Fenton reaction, as well as through exogenous sources such as radiation. Cells defend against ROS through enzymatic (e.g., catalase, superoxide dismutase) and non-enzymatic (e.g., vitamins, glutathione) antioxidant mechanisms. At low levels, ROS function in normal redox cell signalling and activate the immune system. Elevated ROS levels promote tumorigenesis by inducing DNA damage, enhancing cell proliferation, and increasing metastasis. Excessive ROS leads to cell death through mechanisms like ferroptosis and autophagy.

1.5.1. Oxidative stress in medulloblastoma

The brain is particularly vulnerable to oxidative stress, but the specific role of oxidative stress in medulloblastoma tumorigenesis is not fully understood. A study using radioresistant medulloblastoma stem cell clones (ONS-76; a SHH derived cell line) showed reduced mitochondrial ROS levels and oxidative stress markers compared to their radiosensitive counterparts, suggesting that medulloblastoma cells develop adaptive redox mechanisms to resists oxidative damage during treatment (Sun et al., 2017). In support of this, increased expression of Nrf2 (nuclear factor erythroid 2-related factor 2), the principal regulator of antioxidant defence, has been observed in medulloblastoma tissue samples compared to adjacent non-tumour brain tissues (Tang et al., 2017; Barrera et al., 2017). This suggests an overall increased antioxidant capacity in medulloblastoma.

The potential redox sensitivity of medulloblastoma cells has been observed *in vitro* by a number of adjuvant therapies that increased cell death in an ROS-dependent manner (Yang et al., 2009; Oshima-Hosoyama et al., 2011; Li et al., 2022). An example is the topoisomerase I inhibitor Camptothecin which significantly increased cell death via increasing ROS production, an effect reversed by GSH treatment (Yang et al., 2009). This suggests a potential efficacy of treatments targeting redox in medulloblastoma.

1.5.2. Ascorbic acid as an antioxidant in cancer

Given its physiological role as an antioxidant, AA has been investigated for its potential anti-carcinogenic properties. AA has been shown to prevent the initiation of skin tumours in rodent models exposed to carcinogens (Slaga and Bracken, 1977) and reduce the mutagenicity of these agents (Shamberger et al., 1979). This large body of early research spurred interest in the possible link between AA intake and a reduced cancer risk. Some studies suggest an association (Chen et al., 2022) and even suggest prenatal AA supplementation lowers the risk of brain tumours in children (Preston-martin et al., 1998), while others challenge the significance of this relationship (Lee et al., 2015). The conflicting findings illustrate the complexity of studying diet and cancer risk, especially when confounding factors such as multivitamin use are involved.

Upon tumour formation, AA's protective antioxidant properties could extend to cancer cells, as it is known that cancer cell's increase their antioxidant defence. Several studies have reported elevated AA concentrations in various tumour types (Moriarly et al., 1977; Liebes et al., 1981; Fiaschi et al., 2005), alongside decreased plasma concentrations (Huijskens et al., 2016; Nigar et al., 2021; Khanzode et al., 2004). Tumour-sequestered AA can be accompanied with increased expression of antioxidant enzymes, suggesting that AA might contribute to an enhanced detoxification capacity of cancer cells (Fiaschi et al., 2005). However, the implications of elevated AA in tumours are complex, in glioblastoma multiforme, higher AA levels have been associated with decreased HIF-pathway activity and improved patient survival (Burgess et al., 2022), indicating that AA's antioxidant role may vary by tumour type and context. Thus, with this in consideration, AA supplementation during cancer therapy remains controversial as antioxidants may reduce the effectiveness of treatment (Krejbich et al., 2022). In accordance with these concerns, preincubating myeloid leukaemia cells with DHA reduced the level of apoptosis following ionising radiation (Witenberg et al., 1999). However, this protective capacity of AA can also extend to non-tumour cells. AA supplementation during radioiodine therapy has been shown to reduce the adverse effects of treatment-induced oxidative stress in thyroid cancer patients (Jafari et al., 2018). This highlights a potential of AA to mitigate treatment-induced side effects.

1.5.3. Ascorbic acid as a pro-oxidant in cancer

High-dose AA (>1mM) induces ROS production and cytotoxicity to cancer cells through its action as a pro-oxidant. As discussed in section 1.2.2, at these concentrations, AA oxidation culminates in the production of excessive ROS which causes cell death in numerous cancer cell lines (Tronci et al., 2021; Chen et al., 2019; Takemura et al., 2010; Du et al., 2012; Figure 1.11). This cytotoxic effect is dependent on H_2O_2 production, as demonstrated by the sensitisation of an AA-resistant cancer cell line to high-dose AA following the silencing of catalase, the key enzyme responsible for scavenging H_2O_2 (Klingelhoeffer et al., 2012). While extracellularly generated H_2O_2 contributes to AA's pro-oxidant activity, intracellular AA plays key roles. This is evidenced by the decreasing effect of high-dose AA on differentially expressing SVCT2 cell lines (Cho et al., 2018). In addition, iron chelators that sequester the pool of labile iron can diminish AA-induced cytotoxicity (Du et al., 2015).

Interestingly, this pro-oxidant effect appears to be selective to cancer cells (Figure 1.12). High-dose AA does not induce apoptosis in normal cell lines, nor does it elevate H_2O_2 levels in blood plasma (Chen et al., 2005). The selectivity can be attributed to several differences between cancerous and normal cells. Whilst cancer cells typically increase antioxidant defences, compromised catalase activity has been observed impairing their ability to metabolise H_2O_2 efficiently (Doskey et al., 2016). Additionally, cancer cells frequently exhibit a heightened glycolytic phenotype, leading to increased expression of GLUTs that facilitate the uptake of DHA. This, in turn, depletes intracellular antioxidants as DHA is rapidly reduced back to AA (Yun et al., 2015). Furthermore, cancer cells typically contain elevated levels of labile iron because they require it for rapid proliferation, DNA synthesis and metabolic adaptation to oxidative stress (Torti et al., 2013). This dependency drives increased iron uptake and retention, creating a larger labile iron pool that enhances their susceptibility to oxidative damage induced by high-dose AA.
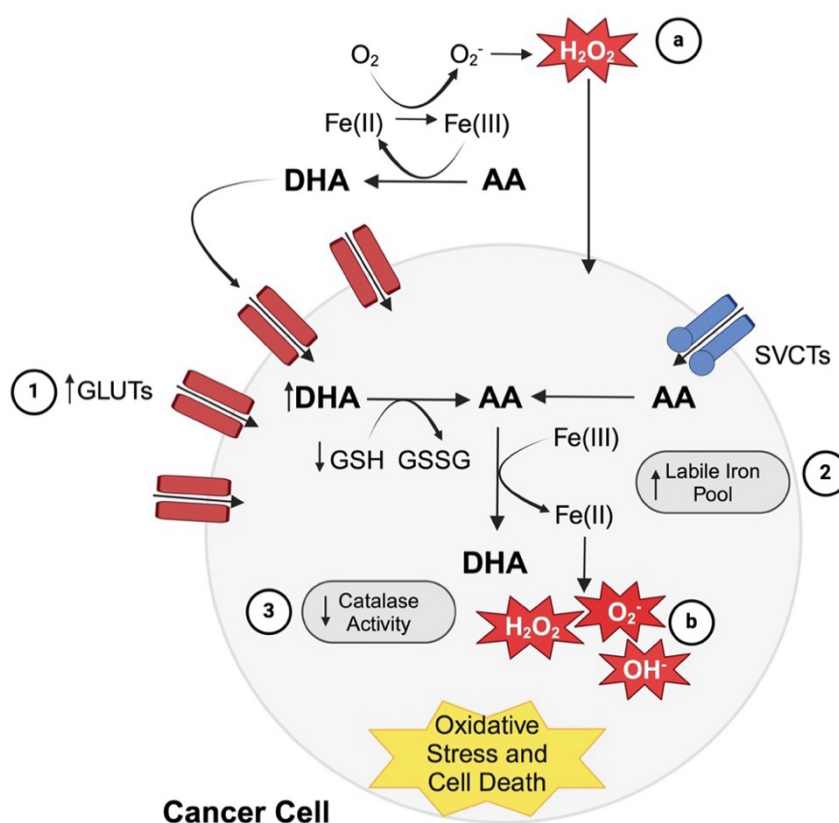
Figure 1.12. The mechanisms of H_2O_2 and radical production by high-dose ascorbic acid and its selective toxicity to cancer cells. High-dose AA, in the presence of catalytic metals like Fe(III), is oxidised DHA, generating extracellular H_2O_2 through the reduction of Fe(III) to Fe(II). **(a)** Extracellular H_2O_2 is produced as Fe(II) interacts with AA. **(b)** Intracellularly, AA and DHA are transported into cells via SVCTs and GLUTs, further generating ROS such as H_2O_2, O_2-, and $OH-$, which cause oxidative damage. The selective toxicity of high-dose AA toward cancer cells is thought to arise from: **(1)** increased expression of GLUT transporters, which are upregulated in cancer cells due to their glycolytic phenotype, facilitating greater DHA uptake; **(2)** an elevated labile iron pool, enhancing AA's pro-oxidant effects; and **(3)** reduced catalase activity, the key metaboliser of H_2O_2 and depletion of glutathione GSH via DHA recycling in cancer cells, reduce the antioxidant defence and thereby promote oxidative stress-induced cell death.

1.5.3.1. Clinical trials of high-dose ascorbic acid

AA's potential as an anti-cancer agent was first proposed by Linus Pauling and Ewan Cameron in the 1970s, who reported that high-dose AA prolonged survival in terminal cancer patients (Cameron and Campbell, 1974; Cameron and Pauling 1976). However, subsequent trials by the Mayo Clinic failed to replicate these results, casting doubt on AA's efficacy. Whilst these trials administrated the same dose of AA they differed in the route of AA administration. Pauling's trials used intravenous AA, achieving high plasma concentrations that could induce a pro-oxidant effect, whereas the Mayo Clinic trials used orally supplemented AA, which produces only modest and transient increases in plasma levels (Creagan et al., 1979; Moertel et al., 1985). This distinction is critical because high-dose intravenous AA can achieve plasma concentrations >1.5 mM, levels at which AA shifts from an antioxidant to a pro-oxidant and exerts cytotoxic effects on cancer cells (Sebastian et al., 2004).

Preclinical studies show high-dose AA can inhibit tumour growth and reduce metastasis, but clinical trials using AA monotherapy have been less successful, with no significant anti-tumor responses observed (Stephenson et al., 2013; Riordan et al., 2005; Nielsen et al., 2017). However, AA has been shown to be safe and tolerated, even at high doses such as 20mM, and individual case reports of prolonged survival and tumor regression in patients suggest that some patients may benefit from AA monotherapy (González et al., 2016; Seo et al., 2015). It should be noted these trials consisted of patients that received heavy chemotherapy and radiation prior to AA treatment. More promising results have emerged from trials combining high-dose AA with chemotherapy or radiotherapy. Preclinical studies have demonstrated that AA can enhance the efficacy of chemotherapeutic agents such as cisplatin and carboplatin and act as a radiosensitiser (O'Leary et al., 2018; Schoenfeld et al., 2017). This synergy likely arises from exacerbating oxidative stress (Böttger et al., 2021). Early-phase clinical trials in pancreatic cancer, ovarian cancer and glioblastoma multiforme have reported reduced toxicity and trends towards improved progression-free survival with combination therapies, though further research is needed to confirm these effects (Bruckner et al., 2017; Ma et al., 2014; Allen et al., 2019)

1.6. Hypothesis and aims

High-dose AA as a potential adjuvant cancer therapy has garnered renewed interest in recent years leading to numerous clinical trials. AA is reported as safe and can increase the efficacy of standard treatments including cisplatin. This thesis aims to explore the effect of AA in SHH medulloblastoma tumours in two critical contexts:

1. Due to AA's role in collagen production, can AA contribute to the prognostically beneficial deposition of collagen encapsulating SHH tumours?
2. Can high-dose AA alone and in combination with the chemotherapeutic cisplatin exert anti-tumour effects in medulloblastoma?

As AA is transported into and within the cell by transporter proteins an underpinning aim of this thesis is to identify AA/DHA transporter/s that could potentially regulate AA availability in medulloblastoma.

The objectives outlined in this thesis are therefore:

- To investigate the expression of the 8 known candidate AA/DHA transporters and association with outcome in medulloblastoma.
- To investigation correlation of candidate transporter gene expression with antioxidant and collagen genes in medulloblastoma.
- To characterise the impact of AA treatment on SHH spheroid growth alone and alongside co-treatment with cisplatin.
- To assess if the potentially cytotoxic effects of high-dose AA and cisplatin in SHH spheroids are ROS-dependent.

2. Materials and Methods

2.1. Analysis of publicly available patient datasets

In this study three publicly available gene expression array datasets (Cavalli and Pfister (medulloblastoma) and Roth (normal cerebellum)) were accessed and analysed using the R2: Genomics Analysis and Visualisation Platform (http://r2.amc.nl) (Roth et al., 2006; Cavalli et al., 2017; Northcott et al., 2017; Table 2.1).

Table 2.1 Datasets used in analysis

Author	Tumour/Tissue	N	Survival Data	Material	Normalisation	Platform
Cavalli	Medulloblastoma	763	Yes	Bulk RNA	rma_sketch	hugene11t
Pfister	Medulloblastoma	223	No	Bulk RNA	MAS5.0	u133p2
Roth	Normal Cerebellum	9	No	Bulk RNA	MAS5.0	u133p2

2.1.1. Analysing gene expression in medulloblastoma vs normal Cerebellum

In order to analyse the expression of a gene across two datasets the 'R2:MegaSampler' tool was used in R2. For this comparison the Pfister medulloblastoma dataset and Roth normal cerebellum dataset were used as they were generated by the same expression array technology. The Pfister medulloblastoma dataset can be separated into medulloblastoma subgroups. All data was then exported to GraphPad Prism® (version 9.4.1), where significant differences in gene expression between groups were calculated using a Kruskal-Wallis test with Dunn's multiple comparisons. This non-parametric test was chosen as gene expression data often do not follow a normal distribution, making it a suitable alternative to one-way ANOVA. The Kruskal-Wallis test allowed for comparison across multiple independent groups, while Dunn's post-hoc test identified specific group differences while controlling for multiple comparisons.

2.1.2. Gene expression-based survival analysis

The Cavalli dataset was used to conduct gene expression-based survival analysis as it provided patient survival data. Using the R2:KaplanScan tool, Kaplan-Meier curves based on the expression of a gene of interest were generated. The R2:KaplanScan tool determines the most statistically significant cut-off for survival analysis based on gene expression data. This is achieved by splitting the dataset into two groups (minimum of 8 samples per group) based on the expression of a gene of interest ('high' and 'low' expression groups). Starting with the 8 samples with the lowest level of gene expression versus the rest of the samples in the dataset, the R2:KaplanScan then uses every increasing expression value as a new cut-off to create two groups and determine the statistical significance of the difference in survival between them in a logrank (Mantel–Cox) test. The two groups which yield the most significant p-value are then returned with a Kaplan Meier curve.

2.1.3. Correlated gene expression analysis

The R2 function 'Find Correlated Genes with a Single Gene' was used to find significant gene expression correlations with candidate genes in patients. To filter genes specific to the hypothesis two GO terms were chosen; 'Antioxidant Activity' (GO-id:16209) and 'Collagen Metabolic Process' (GO-id:32963). The results of this analysis provided an overview of the combinations that met the significance criteria of $p < 0.05$, it provides the individual gene's R-value (correlation coefficient of expression) and p-value (significance of that correlation). The individual gene, their R-values and p-values were exported to GraphPad Prism® (version 9.4.1) and plotted on scatterplots.

2.2. Cell culture

Four cell lines were cultured during this study, ONS-76 and DAOY are SHH-patient derived cell lines (Table 2.3), HEK293Ts were transfected with GLUT10 plasmid and SH-SY5Y is a neuroblastoma cell line that served as a positive control for SVCT2 expression. All cell lines were cultured in an incubator at 37°C with 5% CO_2 in cell culture medium. Cells were cultured in treated T-25 or T-75 flasks. The cell culture medium used for each cell line can be found in Table 2.2.

Table 2.2 Composition of cell culture media and purpose for each cell line cultured in this study.

Cell Line	Media	Purpose
ONS-76	Roswell Park Memorial Institute-1640 (RPMI-1640) + 10% (v/v) foetal bovine serum (FBS)	For pellet harvesting for western blotting, for spheroid generation
DAOY	Dulbecco's modified Eagle's medium (DMEM) + 10% (v/v) FBS	For pellet harvesting for western blotting, for spheroid generation
HEK293T	DMEM + 10% (v/v) FBS + 1% (v/v) penicillin/streptomycin	For transfection with GLUT10 plasmid for the generation of a GLUT10 positive cell line
SH-SY5Y	DMEM/F12 (Gibco^{TM},11320033) + 10% (v/v) FBS + non-essential amino acids (0.1 mM of: glycine, L-alanine, L-asparagine, L-aspartic acid, L-glutamic acid, L-proline and L-serine; Gibco^{TM}, 11140035) + 1% (v/v) penicillin/streptomycin	As an SVCT2 positive cell line

2.2.1. Recovering cell lines from frozen stocks

Cryogenic vials of cells were thawed at 37°C. The contents of vials were gently pipetted into a T-25 flask with fresh cell culture medium and left overnight. Depending on the observed recovery, the cells were left for an additional 24-48 hours, with a medium change to ensure optimal recovery.

2.2.2. Cell maintenance

All cell lines cultured were adherent and thus sub-cultured by complete removal of the previous culture medium. The cells were then washed with 1X PBS and incubated with 1X trypsin-EDTA (ethylenediaminetetraacetic acid; Sigma, T4174) to detach the cells. Once cells were visibly detached, pre-warmed cell culture medium (as detailed in Table 2.1) was added to the flask to neutralise the trypsin, The contents of the whole flask were centrifuged at 800 x g for 5 minutes. After centrifugation, the cell pellet was resuspended in fresh culture medium, and cells were seeded into new cell culture flasks at a split ration of 1:7.5 - 1:15, depending on cell density and future need. All flasks were incubated at 37°C in a humidified atmosphere with 5% CO_2.

2.2.3. Cell counting

Following cell culture as described, cells were harvested and resuspended in 1ml of cell culture medium. A 10µl aliquot of this suspension was pipetted into the glass chamber of a haemocytometer, and cells were manually counted per square of the chamber using a brightfield microscope. The cell concentration (cells per ml) was calculated using the following formula:

Cells per ml = Average number of cells per square x 10 000

2.2.4. Preparation of cell pellets for molecular analysis

Following cell culture as described, the remaining cell suspension following the passage was centrifuged at 800 x g to generate a cell pellet. This pellet was resuspended in 1mL of cell culture medium and transferred to an Eppendorf tube. This cell suspension was centrifuged again at 800xg for 5 minutes and resuspended in 1mL of 1X PBS to wash the cells. Following another identical centrifugation, the supernatant was discarded, and pellets placed in the -80°C freezer.

2.2.5. Preparation of cells for cryo-storage

Following cell culture as described, the remaining cell suspension following the passage was centrifuge at 800 x g to generate a cell pellet. The resultant pellet was resuspended in 1ml of freezing medium (90% FBS and 10% DMSO) and then transferred to a cryogenic vial. The vials were placed in a Mr Frosty™ container and stored at -80°C overnight before being transferred to liquid nitrogen for long-term storage.

2.3. Spheroid culture and assays

Spheroid culture and analysis methodologies were previously optimised by Dr Sophie Roper, a former PhD student in Dr Beth Coyle's lab (Roper and Coyle, 2022).

2.3.1. Neurosphere media

All spheroids were cultured in neurosphere medium, which was composed of DMEM/F-12, 2% (v/v) B-27 supplement (Gibco™, 17504044), 1% (v/v) N-2 supplement (Gibco™, 17502048), 2µg/mL Heparin (Stem Cell Technologies, 07980), 20ng/mL epidermal growth factor (EGF; Gibco™, PHG0315), and 10ng/mL basic fibroblast factor (bFGF; Gibco, PHG0266). Fresh neurosphere medium was prepared and stored at 4°C for up to 3 days before use.

2.3.2. Spheroid generation and maintenance

DAOY and ONS-76 cell lines were cultured under standard tissue culture conditions (section 2.2.2) until they reached ~70% confluency. Cells were trypsinised, resuspended in standard cell culture medium and prepared for either stock propagation or spheroid generation. For spheroid generation, cells were centrifuged at 800 x g for 5 minutes and then resuspended in 2-3ml of neurosphere medium. After cell counting, DAOY cells were seeded at a density of 250 cells/well and ONS-76 cells at 200 cells/well into the inner-wells of 96 well Ultra Low Attachment (ULA) plates (Corning, 7007) in a total volume of 200µl of neurosphere medium. To minimise medium loss, 200µl of HBSS was added to the outermost wells. The plate was placed in an incubator at 37°C with 5% CO_2. At Day 4, half of the media was replaced with 100µl of fresh neurosphere medium to maintain the spheroids (Figure 2.1).
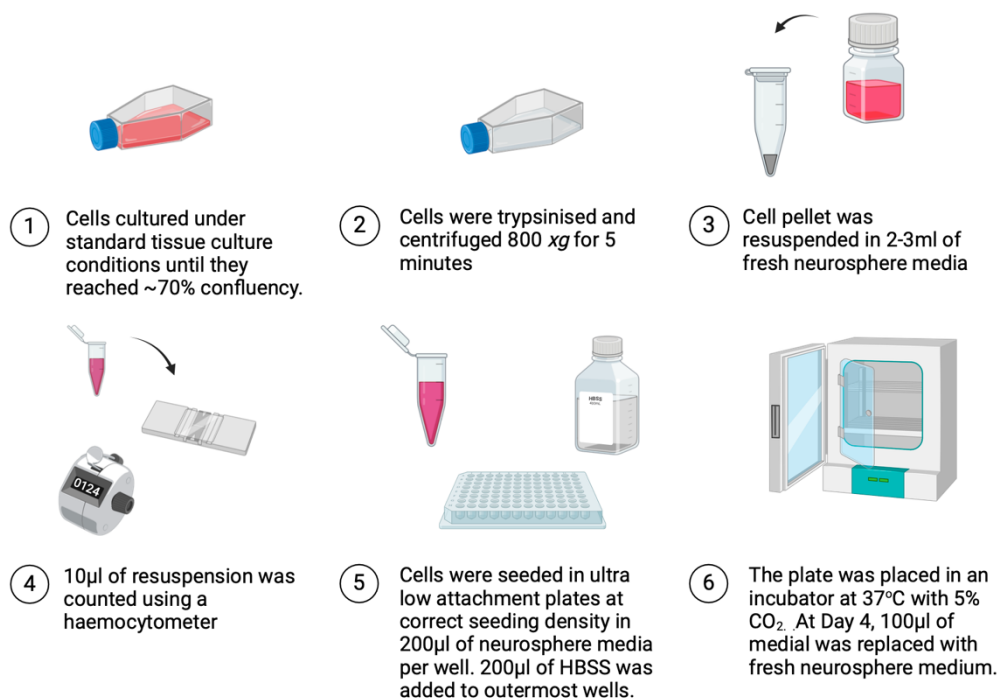
Figure 2.1. Cell culture workflow of SHH spheroid generation. (1-2) Cells were cultured, trypsinised and centrifuged as normal. **(3)** The cell pellet was resuspended in fresh neuropshere media and **(4)** counted. **(5)** After appropriate dilution to correct seeding density, 200µl of cell suspension was seeded in ULA plates and 200µ; of HBSS was added to outermost wells. **(6)** The plate was incubated at 37°C with 5% CO_2 till Day 4 where a half-media change is performed.

2.3.3. Imaging spheroids and assessing dimensions

Spheroid growth was assessed through capturing images using the ZOE Fluorescent Cell Imager (BioRad) which featured an inbuilt 100µm calibration scale. ImageJ software was used for measuring spheroid area. A global scale was set to the length of the calibration bar. Using the 'Freehand Selection' tool the spheroid was outlined manually to calculate the area (A). Data was exported to Microsoft Excel and from these measurements, spheroid radius (r) and volume (V) were derived using the following formulas:

$$R = \sqrt{A/\pi} \qquad V = 4/3\pi r^3$$

2.3.4. Ascorbic acid and cisplatin treatment of spheroids

The effects of AA alone and in combination on the growth of SHH spheroids was assessed using DAOY and ONS-76 spheroids. Spheroids were grown to Day 4 and then treated with varying concentrations of AA and/or cisplatin. Pre-treatment images were taken on Day 4 and then every 24 hours for 72 hours following treatment (Day 5 – 7).

AA concentrations were selected based on physiological and pharmacological relevance: 100µM (physiological blood plasma level; Carr et al., 1999), 1mM (physiological neuronal level; Angelow et al., 2003), and 2.5mM (high dose). Cisplatin concentrations were: 0.5µM (low dose, IC_{10}), 1µM (IC_{50},), and 5µM (high dose, IC_{90}), according to Roper (et al., 2022). AA and cisplatin were prepared and stored as indicated in Table 2.3. Treatments were prepared at 2X concentrations in Eppendorf tubes with 100µl of fresh neurosphere media and diluted upon addition to the wells (after 100µl of existing media was removed). Untreated spheroids and cisplatin-only treated spheroids served as controls. The plates were incubated at 37°C with 5% CO_2 for 72 hours. Triplicate wells were used for each condition and the entire experiment was repeated three times (n=3) for both DAOY and ONS-76 spheroids.

Table 2.3 Details of compounds used in this study

Compound	Stock Solution	Vehicle	Storage	Product Details
Ascorbic Acid	1M	PBS	Room temperature protected from light as a powder. In -80°C freezer as a stock solution.	SigmaAldrich, A92902
Cisplatin	1mM	DMF or DMSO	In 2-8°C fridge protected from light as a powder. In -80°C freezer as stock solution.	SigmaAldrich, 232120
DCFH-DA	10mM	DMSO or Ethanol	In -20°C freezer protected from light as a powder. Should not be stored long-term as a solution.	Invitrogen, D399

2.3.5. DCFH-DA assay for reactive oxygen species detection in spheroids

To investigate the effects of AA alone and in combination with cisplatin on ROS production in SHH spheroids, the fluorescent probe DCFH-DA (2' 7'-dichlorodihydrofluorescein diacetate; Table 2.3) was used (Figure 2.2). DCFH-DA permeates cell membranes and in the presence of ROS is oxidised to the fluorescent compound DCF (2',7'-dichlorofluorescein). The fluorescent signal is proportional to the ROS present and can be detected using a FlexStation® 3 Multi-Mode Microplate Reader at 495/535nm with a bottom-well read. Initially trialled as an endpoint assay after 72 hours of incubation, the protocol was later optimised to a shorter assay focusing on Day 4 spheroids to monitor the acute effects of AA and cisplatin on ROS production.

The experimental set up of this assay was based on previous assays detecting ROS production in AA-treated cells (Bardyn et al., 2021; Oh et al., 2020; Figure 2.2). All media and washes were phenol-red free as the optimisation stage indicated that phenol-red in media oxidised DCFH. This assay was completed in subdued light conditions as DCFH-DA is light sensitive. DCFH-DA was dissolved in DMSO to make a 10mM stock solution, this solution was diluted with DMEM/F12 to a 2X working solution of 20μM. Day 4 spheroids, that were grown in phenol-red free neurosphere media, had 100μl of media removed and replaced with 100μl of DCFH-DA supplemented DMEM/F12 (The 2X working solution allows for the dilution at this stage). Plates were wrapped in foil and incubated for 1 hour at 37°C with 5% CO_2. After 1 hour, two half-media washes with phenol-red free HBSS were performed to remove excess DCFH-DA and basal fluorescence of the spheroids was measured on the FlexStation®.

AA and cisplatin were used in the same concentrations as described previously (Section 2.3.4). AA and cisplatin solutions were prepared in PBS and DMF, respectively, at a 20X stock solution so that 10μl added to the existing 200μl in the wells allowed a 1X working dilution. AA was added first, and fluorescence was measured every 15 minutes for 1 hour. Cisplatin was then added relevant wells, and fluorescence was again measured every 15 minutes for 1 hour. Control wells included DCFH-DA treated alone in media and untreated spheroids with DCFH-DA. This experiment was repeated three times (n=3), each with technical triplicates, for both DAOY and ONS-76 spheroids. Additionally, an exploratory experiment (n=1) was performed where the order of treatment, i.e. cisplatin first then AA, was reversed.

Raw fluorescence values were exported to Microsoft Excel. Mean fluorescence from media-only wells treated with DCFH-DA was subtracted at each time-point to correct for media background. The values were normalised to pre-treatment fluorescence values and plotted on GraphPad Prism® to show changes in ROS production over time.
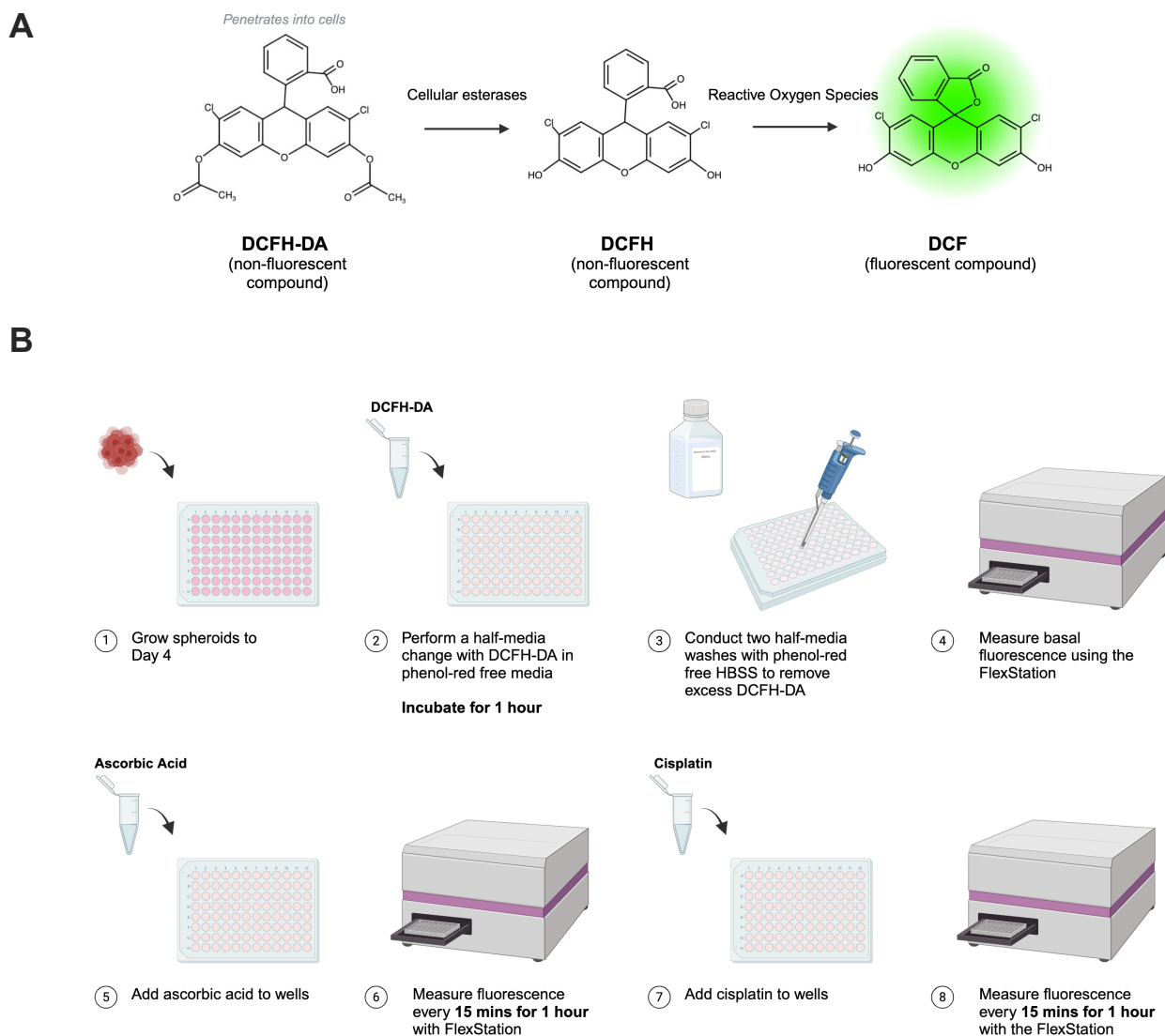
Figure 2.2 Experimental basis and set-up for the detection of ROS by DCFH-DA in SHH spheroids
A) The conversion of the non-fluorescent 2',7'-dichlorodihydrofluorescein diacetate (DCFH-DA) to the fluorescent dichlorofluorescein (DCF) via acetylation by cellular esterases to the intermediate dichlorodihydrofluorescein (DCFH) and subsequent oxidation by cellular reactive oxygen species to DCF. **B)** The experimental setup for ROS detection following ascorbic acid and cisplatin treatment in SHH spheroids. Day 4 spheroids were cultured (1) and incubated for 1 hour with 10μM DCFH-DA in phenol-red free media after a half-media change (2). Excess DCFH-DA was removed via two half-media washes (3) to prevent spheroid loss, and basal fluorescence was measured using the FlexStation® 3 Multi-Mode Microplate Reader (4). Ascorbic acid was then added, and fluorescence was recorded every 15 minutes for 1 hour (5,6). Cisplatin was subsequently added, with fluorescence measured at the same intervals for another hour (7,8). Plates were incubated at 37°C and 5% CO_2 when not being measured.

2.4. Protein analysis

To assess the presence and relative quantity of GLUT10 and SVCT2, western blotting of patient-derived cell lines was performed. Pellets were obtained from six medulloblastoma cell lines that were derived from SHH, Group 3 and Group 4 patients (Table 2.4). The HD-MB03, D425, CHLA-01 and CHLA-01R pellets were kindly obtained from Dr Susannah Entwistle and Connor Levers.

2.4.1. Cell lysis

To create cell lysates, washed cell pellets were thawed on ice and then resuspended in 500µl of ice-cold PBS with 10% glycerol, 5µl of thawed protease inhibitor (Merck Complete Protease Inhibitor Cocktail III, 539134) was then added. Using a clean sonicator probe, the samples were sonicated thrice for 10s (at no higher that 50% power) with incubation on ice for at least 20-30s between pulses.

2.4.2. Protein quantification from Lowry protein assay

To determine protein concentration of the lysates, a standard curve of known protein concentrations was generated using dilutions of BSA (bovine serum albumin; 2µg/µl stock). Triplicate dilutions of BSA were prepared, ranging from 0 to 10µg. Cell lysates were added in volumes of 5µl, 2.5µl, and 1µl, each in triplicate, with all wells made up to 5µl using distilled water. Following this, 20µl of Reagent A (BioRad DC Protein Assay) was added to each well, followed by 200µl of Reagent B. The plate was gently agitated at room temperature for 15 minutes. After incubation, the absorbance of the wells was measured at 700nm on SpectraMax iD3 plate reader. The data was then exported to Microsoft Excel, and the absorbance values from the distilled water blank were subtracted from triplicate averages. The protein concentration of each lysate was then calculated using the standard curve. Lysates were either used immediately or stored at -20 °C.

Table 2.4 Medulloblastoma cell lines used in western blotting with clinical information.

Cell Line	Sub-group	Sub-type	Metastatic Stage	Clinical Information	Reference
DAOY	SHH	Putative SHH-a, *TP53* mutant	Non-metastatic (M0)	4-year-old male. *TP53* mutated cerebellar medulloblastoma of posterior fossa.	(Jacobsen et al., 1985)
ONS-76		Putative SHH-b, *TP53* wild-type	Metastatic tumours present at the right prepontine cistern (M2)	2-year-old female. Large midline cerebellar medulloblastoma.	(Yamada et al., 1989)
HD-MB03	Group 3	n/a	Metastatic (M3)	3-year-old male. Large cell anaplastic mass in midline, spinal metastasis in CSF.	(Milde et al., 2012)
D425		n/a	Non-metastatic (M0)	6-year-old male. Tumour harbours *MYC* amplification and found in posterior fossa.	(Bigner et al., 1990)
CHLA-01	Group 4	n/a	Non-metastatic (M0)	8-year-old male. Cerebellar tumour with leptomeningeal dissemination.	(Xu et al., 2015)
CHLA-01-R		n/a	Metastatic recurrence 8 months after diagnosis (M3)	Matched pair to CHLA-01. Recurrent metastatic cells from pleural fluid.	

1.4.3 SDS-Page

Samples were thawed and 20μg of protein from each lysate was transferred to an Eppendorf. The samples were prepared by supplementing to a fixed volume (40µl) with PBS/10% glycerol and adding 6x sample buffer (See Table 2.5 for all buffer compositions). Samples were then vortexed and denatured in a 90°C heat block for 10 minutes. 10% (w/v) acrylamide sodium dodecyl sulphate (SDS) resolving gels were used for all analysis. These were prepared (See Table 2.6 for electrophoresis gels composition) and pipetted between the pre-prepared 1.5mm spacer plate and the short plate. The gel was overlaid with water saturated butanol to ensure level setting, and to remove air bubbles. After polymerisation, the butanol was gently removed, and the stacking gel (Table 2.6) was pipetted on top. A 10-well 1.5mm comb was immediately placed into the gel, which was allowed to polymerise for 30 mins to an hour. Once set, the gel was either used immediately or wrapped in damp tissue and clingfilm and stored at -4°C for a week.

Table 2.5 Composition of buffers used in western blotting. All buffers made up in distilled water (dH$_2$O).

Buffer	Materials
6X Loading Buffer	125mM Tris-HCl pH 6.8, 10% (w/v) SDS, 10%(v/v) glycerol, 0.5M EDTA, 0.2% (w/v) Bromophenol blue in ethanol, 0.5% (v/v) 2-Mercaptoethanol
10X Running Buffer	1.9M Glycine, 250mM Tris-Base, 1% (w/v) SDS
1X Running Buffer	100ml 10X Running Buffer, 900ml dH$_2$O
10X Transfer Buffer	1.9M Glycine, 250mM Tris-base
1X Transfer Buffer	100ml 10X Transfer Buffer, 200ml Methanol, 700ml dH$_2$O
1X PBS-Tween 20	100ml 10X PBS, 1ml Tween-20, 899ml dH$_2$O

Table 2.6. Composition of 2 X 10% SDS gels.

Material	10% Resolving Gel	4% Stacking Gel
1M Tris pH 8.8	4.5ml	n/a
1M Tris pH 6.8	n/a	3ml
40% (w/v) Acrylamide	4.5ml	1.2ml
dH$_2$O	8.5ml	7.5ml
10% (w/v) SDS	135µl	90µl
10% (w/v) Ammonium Persulphate (APS)	270µl	180µl
N,N,N′,N′-Tetramethyl ethylenediamine (TEMED)	10µl	7.5µl

Denatured cell lysates were carefully loaded into the wells of the gel alongside a molecular weight marker (SeeBlue Plus2). Gels were then electrophoresed at 40mA, until the samples had reached the resolving gel, at which point the current was increased to 80mA. Once the samples had reached the bottom of the resolving gel, the gels were removed from the gel electrophoresis tank and running module.

2.4.3. Western blotting

Proteins were then transferred from the polyacrylamide gel to a nitrocellulose membrane on which they could be detected and quantified. Gels were carefully removed from their casting plates and the stacking gel was discarded. Protein was transferred by a wet blotting method (Towbin et al.,1979) in transfer buffer (Table 2.5) by electrophoresis at 200mA for two hours or overnight at 20mA.

To blot for target proteins, post transfer-membranes were initially blocked with 5% w/v non-fat milk powder (in 1X PBS-Tween 20) for one hour with gentle agitation at room temperature (Table 2.5). The blocking buffer was discarded and using the protein ladder for guidance the membrane was cut so individual sections could be stained using a different antibody. The primary antibody (Table 2.7) was then added to the membrane at an

appropriate dilution in minimal volume of blocking buffer at 4°C for at least 2 hours or overnight, continuously rotating. The antibody was removed and could be reserved for future use if kept at 4°C. The membrane was washed three times with 1X PBS-Tween 20 for at least 10 minutes each. The secondary antibody was then added to the membrane at a dilution of 1:10,000 in blocking buffer and incubated at room temperature with gentle agitation for one hour (Table 2.8). The secondary antibody was removed, and the membrane was again washed three times with 1X PBS-Tween 20 for 10 minutes.

Table 2.7. Details of primary antibodies used for western blotting in this study.

Target Protein	Host Species	Dilution	Clonality	Source
GLUT10	Mouse	1:250-1:2000	Monoclonal	Santa Cruz, sc-398496
	Mouse	1:250-1:2000	Polyclonal	Invitrogen, PA1-46137
SVCT2	Rabbit	1:1000	Polyclonal	AbCam, Ab229802
Calnexin	Goat	1:2000	Polyclonal	SciGen, AB0041-200

Table 2.8. Details of secondary antibodies used for western blotting in this study.

Used in the detection of:	Species Reactivity	Dilution	Detection System	Source
GLUT10	Anti-Mouse	1:2000	Horse Radish Peroxide (HRP) conjugated – ultra-sensitive ECL	Dako,P0447
SVCT2	Anti-Rabbit	1:2000		Dako, P0217
Calnexin	Anti-Goat	1:10 000	LI-COR, IRDye 800CW	LI-COR, 926-32214

For SVCT2 and GLUT10 antibody detection we utilised enhanced chemiluminescence (ECL) using the SuperSignal™ West Femto Maximum Sensitivity Substrate (ThermoFisher Scientific, 10391544) for increased sensitivity in the detection of our target bands. Reagent a and B from the kit were mixed in a 1:1 dilution on clingfilm, this was left to react for 1 minute, and then the membrane was placed face down onto the clingfilm and left for a further minute. Using a BioRad ChemiDoc imaging system, the function 'single-chemiluminescence' was used to image the bands from 30 seconds to 5 minutes, depending on level of expression in order to capture a fluorescent image. The 'multi-colorimetric' function was used to visualise the protein ladder. For imaging of the calnexin bands the 'colorimetric IR-800' was used. These images were exported to ImageJ where the lanes and protein ladder are superimposed to one image using the 'Merge Channels' tool.

2.1.1. Quantifying protein expression by densitometry analysis

Visualised protein bands were quantified by densitometry analysis using ImageJ software. Firstly, under the 'Set Measurements' tool only the 'Grey Mean Value' was checked. Rectangles were then drawn around each protein band and their density were determined using the 'Measure' tool. The relative density of each protein was calculated by subtracting background and normalising to the housekeeping protein calnexin. These values were exported to GraphPad Prism® (version 9.4.1) and significant differences in relative protein density were calculated using a two-way ANOVA.

2.1.2. Transfection of HEK293Ts with GLUT10 plasmid

For optimisation of GLUT10 antibodies a positive control in HEK23T cells was produced. Firstly, competent NEB-5α cells were used for GLUT10 plasmid amplification (Sino Biological; HG13982-NF). The GLUT10 plasmid was dissolved in 50µl of autoclaved distilled water and 0.5µl of plasmid DNA was added to thawed competent cells, followed by incubation on ice for 30 minutes. The cells were heat-shocked at 42°C for 30 seconds, then placed on ice for 2 minutes. Lysogeny broth was added, and cells were shaken at 37°C for 1 hour at 250 rpm. Transformed cells were plated on LB agar plates containing hygromycin (the vector contained a hygromycin resistance gene) and incubated at 37°C overnight.

Colonies were picked for plasmid purification using a miniprep kit (Qiagen). Bacterial cells were harvested, lysed, and plasmid DNA was isolated using a silica membrane spin column. DNA was eluted in 50µl of buffer and quantified by the NanoDrop. The concentration of samples was then calculated from the absorbance of the sample at 260nm. The 260/280nm ratio of absorbance was used as an indication of DNA 'purity' (~1.8).

HEK293T cells were seeded at a density of 300,000 per well in 6-well plates 24 hours before transfection. Three hours before the transfection, the media was replaced with DMEM with 5% (v/v) FBS. GLUT10 Plasmid DNA and polyethyleneimine (PEI) were mixed at a 1:7.5, 1:10 or 1:15 ratio (molar ratio of DNA phosphorus to PEI nitrogen) incubated, and added to the cells. After 24 hours media was replaced with DMEM with 10% (v/v) FBS. Control cells were transfected with a GFP-encoding plasmid (SinoBiological). After 48 hours, when control well showed GFP fluorescence, cells were harvested by the removal of media, the addition of 100µl of trypsin followed by 1ml of PBS to wash and collect cells to transfer to an Eppendorf. The Eppendorf was centrifuged at 800 $x\ g$ for 5 minutes, the supernatant discarded, and then placed in the -80°C freezer.

3. Investigating AA and DHA transporters in Medulloblastoma

The association and/or differential expression of AA and DHA transporters has not yet been investigated in medulloblastoma; thus, we first assessed their gene expression using publicly available genomic patient datasets. To achieve this, we used the R2: Genomics Analysis and Visualisation Platform (http://r2.amc.nl) to analyse medulloblastoma datasets (Pfister, n=223, Northcott et al., 2017; Cavalli, n=763, Cavalli et al., 2017), along with a normal cerebellum dataset (Roth, n=9; Roth et al., 2006).

The objective was to identify a candidate among the eight known DHA/AA transporter genes (Table 1.3) that may potentially play a role in medulloblastoma tumour biology. Our investigation included the overall medulloblastoma cohort but given the potential link between AA and collagen production in the SHH subgroup, we paid particular attention to the expression of these transporters within this subgroup.

3.1. Analysis of DHA/AA transporter expression across the medulloblastoma subgroups and normal cerebellum

Candidate gene expression was compared across medulloblastoma subgroups and normal cerebellum using the Pfister and Roth datasets. Significant differences were determined using a Kruskal-Wallis test with Dunn's multiple comparisons. The objective of this analysis was to identify candidate transporters with differential gene expression in medulloblastoma patients, specifically patients in the SHH subgroup.

The expression of GLUT1, GLUT3 and SVCT2 were elevated in normal cerebellum compared to other candidate transporter gene expression, this is consistent with their proteins established brain functions (Wohlrab et al., 2017; Figure 3.1). GLUT1, GLUT3, GLUT4 (excluding the WNT subgroup), GLUT10 and SVCT2 expression was significantly differential in medulloblastoma subgroups compared to normal cerebellum (p<0.01 for all comparisons). Notably, GLUT10 was the sole candidate among these transporters with a significantly elevated expression in medulloblastoma subgroups compared to normal cerebellum (p<0.01 vs Group 3 and Group 4, p<0.0001 vs SHH and WNT).
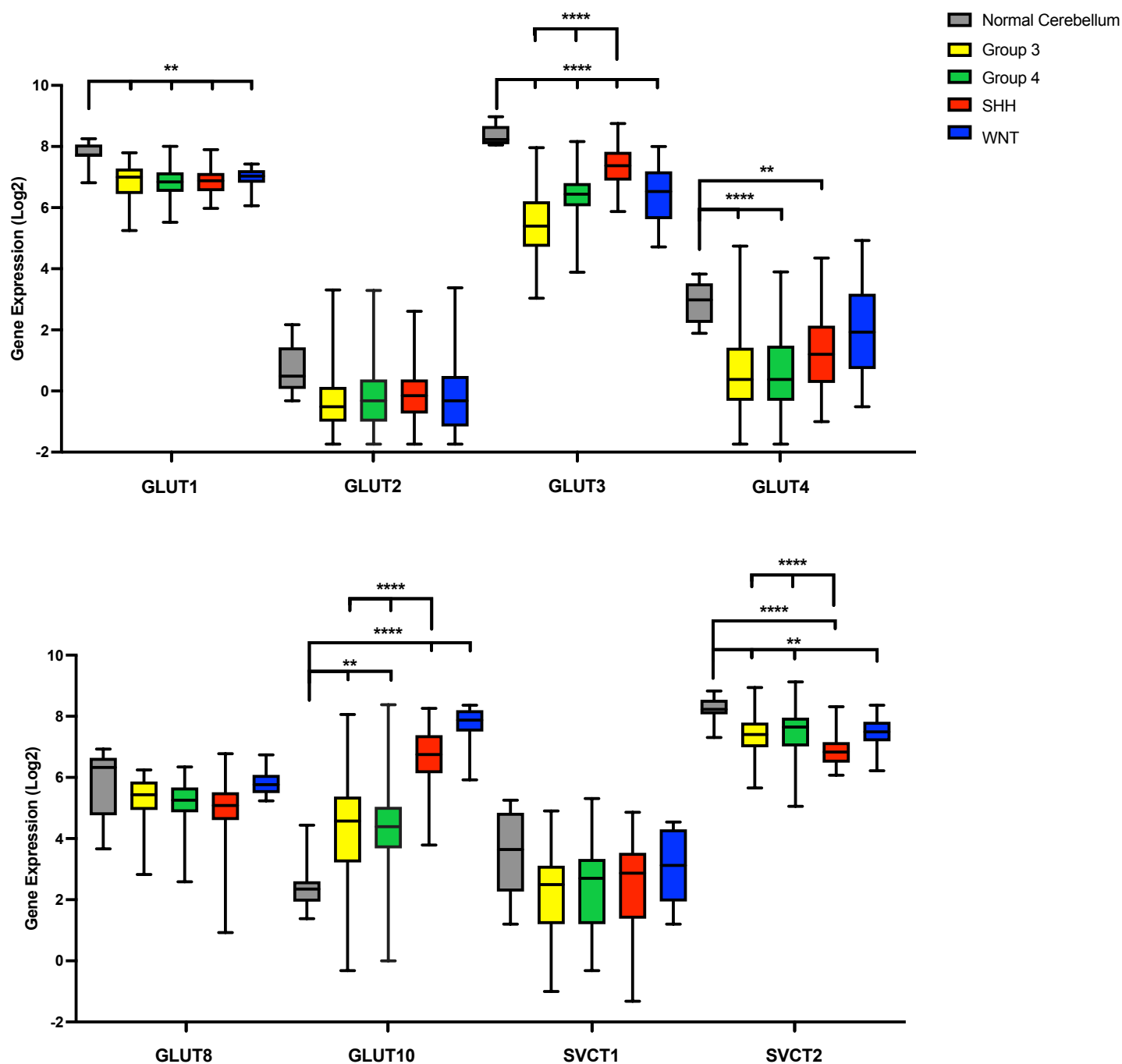
Figure 3.1. Gene expression of AA/DHA transporter candidates in the normal cerebellum and medulloblastoma subgroups. Log2 gene expression was determined using the normal cerebellum Roth dataset (n=9; Roth et al., 2006) and the medulloblastoma Pfister dataset (n=223; Northcott et al., 2017). Group 3 **(yellow)** n=56; Group 4 **(green)** n=91; SHH **(red)** n=59; WNT **(blue)** n=17. Statistical significance of gene expression of each transporter within each subgroup compared to both other subgroups and normal cerebellum was assessed using Brown-Forsythe and Welch analyses with Dunnett's T3 multiple comparison test. ** p ≤ 0.01, *** p ≤ 0.001, **** p ≤ 0.001. The larger end of the significance bar points to the reference expression group. This figure provides a simplified representation of the significance bars for clarity.

There were significant differences in the gene expression of candidates between the subgroups. Figure 3.1 displays simplified significance bars to highlight the significant differential expression of GLUT3, GLUT10, and SVCT2 (p<0.0001 for all comparisons) in the SHH subgroup compared to their expression in Group 3 and 4. Group 3 and 4 are transcriptionally similar to each other but exhibit minimal genetic overlap with the SHH subgroup, which could suggest a potential significance of these genes in SHH biology (Cavalli et al, 2017). This analysis provides initial insights into potential target candidates, specifically GLUT3, GLUT10 and SVCT2 which exhibit differential expression in SHH tumours compared to other subgroups.

3.2. Analysis of medulloblastoma patient survival outcomes associated with DHA/AA Transporter expression

We explored the association between candidate gene expression and patient prognosis using Kaplan-Meier survival curves from the Cavalli dataset (Cavalli et al., 2017). The R2:KaplanScan tool divided the patient population into 'high' and 'low' expression groups for each gene. The split between expression was based upon the most significant p-value between the two patient groups, calculated using a log-rank test (Mantel-Cox).

To facilitate analysis of multiple Kaplan-Meier analyses, key parameters from each Kaplan-Meier curve was plotted on a single "bubble" graph (e.g. Figure 3.2). The x-axis represents FDR-corrected log p-values, with positive values indicating that high gene expression correlates with better patient outcome, and negative values indicating high expression correlates with worse outcomes. The shaded area highlights where these p-values are not statistically relevant (p=0.05). The y-axis shows the percentage of patients in the 'high' expression group, with shaded areas marking extremes (5% or 95%), where uneven group sizes could compromise statistical power. Each gene is represented as a circle, with the radius indicating average log2 gene expression and the colour reflecting differences in 5-year survival rates between expression groups.

The initial analysis included all medulloblastoma patients (n=613) and is summarised in Figure 3.2A, with selected individual Kaplan-Meier plots in Figure 3.2B-E. High expression of GLUT4 (log p=-2.156) and GLUT8 (log p=-1.620) was associated with poorer outcomes (Figure 3.2B-C). Notably, patients in the 'low' GLUT4 expression group had a 48% increase in 5-year survival rate compared to those in the 'high' group. However, the 'high' GLUT4 group comprised only 8 patients, suggesting that while the result is statistically significant, its
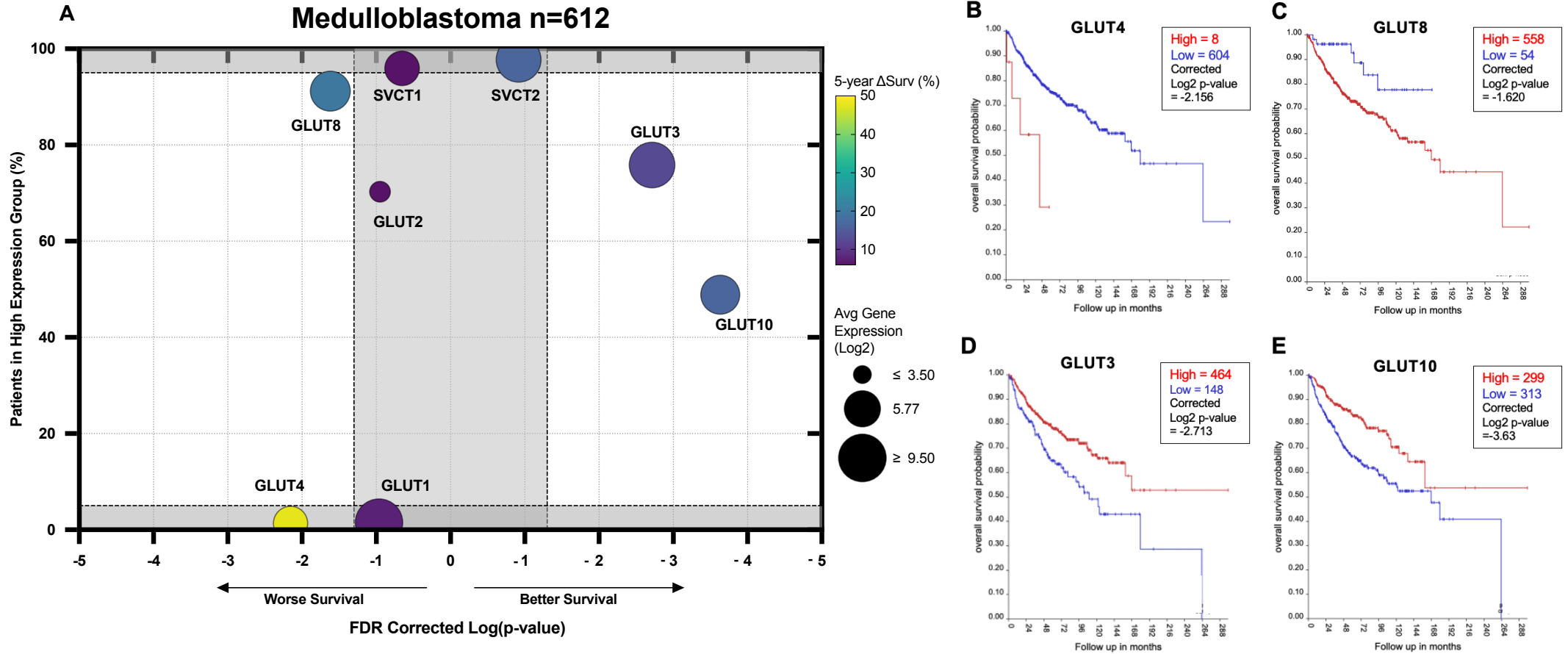
Figure 3.2. (A) Association of transporters with patient survival across a large clinical cohort of medulloblastoma (B-E) individual Kaplan-Meier survival analysis. (A) Kaplan-Meier survival curves produced using survival data (n=612) from the Cavalli dataset on R2: Genomics analysis and visualisation platform. The x-axis represents the FDR corrected log-transformed p-value, values plotted on the right indicates that high gene expression correlates with better outcomes, and values on the left indicate worse outcomes. The percentage of patients within the 'high' expression group is plotted on the y-axis. Shaded areas denote either p-values that are not statistically significant (>0.05) or heavily skewed sample populations. The candidate genes are plotted as circles whose radius correlates with the log2 of average gene expression and whose colour represents the differences between the 5-year survival rates of the 'high' and 'low' expression groups. Kaplan-Meier survival analysis of **B**), GLUT4; **C**), GLUT8; **D**) GLUT3; **E**) and GLUT10 expression on medulloblastoma patients in the Cavalli dataset (n=612). Survival curves were compared using the Log-rank (Mantel-Cox) test. Log2 P-values were adjusted for FDR corrections amongst other candidates. Significant differences in survival were considered those where p<0.05.

clinical relevance may be limited to a small subpopulation. Conversely, high expression of GLUT3 (log p=-2.713) and GLUT10 (log p=-3.630) was linked to better outcome (Figure 3.2D-E). These results are more robust, especially for GLUT10, where patient groups were evenly split.

The Cavalli dataset has large numbers of samples from each molecular subgroup of medulloblastoma, this enables survival analysis to be refined to the subgroups. For Group 3 and WNT, no candidate transporter genes were significantly associated with survival. For Group 4, high expression of GLUT1, GLUT4, and SVCT2 correlated with better prognosis, while GLUT2 and GLUT3 were linked to worse outcomes. However, the findings of the SHH subgroup (n=172) are of particular interest as the collagen shell is specific to this subgroup.

In the SHH subgroup, all candidates significantly impacted prognosis yet GLUT1 (log p=-2.155) and GLUT2 (log p=-2.011) observed largely skewed patient populations (Figure 3.3A). High expression of GLUT4 (log p=-5.133), GLUT8 (log p=-2.022), SVCT1 (log p=-2.187), and SVCT2 (log p=-2.356) were associated with worse outcomes (Figure 3.3B-E), while high expression of GLUT2 (log p=-2.011), GLUT3 (log p =-2.414), and GLUT10 (log p=-3.641) were associated with better outcomes (Figure 3.3F-G). The differences in 5-year survival probabilities between expression groups were more pronounced in the SHH subgroup, ranging from 17% to 50%. The results from the collated survival analyses highlight GLUT3, GLUT4, GLUT8 and GLUT10 as promising candidates for further investigation.

3.3. Correlation of candidate gene expression with genes within relevant GO terms

To guide the selection process further, we used gene expression correlation analysis. This is based upon the assumption that genes with significantly correlated expression may share functional relationships, such as an involvement in similar pathways or cellular processes. However, it is crucial to acknowledge the limitations of this approach. A correlation in gene expression does not necessarily equate to a direct functional relationship, as gene expression patterns may not reflect protein levels or activity. Despite these limitations, this analysis remains a valuable tool to uncover biologically relevant relationships, particularly when combined with other approaches. By integrating these results with the previously collected data, we can provide stronger context and validation in identifying promising candidate transporters.

A

SHH n=172

Worse Survival ← → *Better Survival*

FDR Corrected Log(p-value)

B GLUT4
High = 12
Low = 160
Corrected log
p-value = -5.133

C GLUT8
High = 23
Low = 149
Corrected log
p-value = -2.022

D SVCT1
High = 15
Low = 157
Corrected log
p-value =-2.187

E SVCT2
High = 36
Low = 136
Corrected log
p-value =-2.356

F GLUT3
High = 112
Low = 80
Corrected log
p-value =-2.414

G GLUT10
High = 157
Low = 15
Corrected log
p-value =-3.641
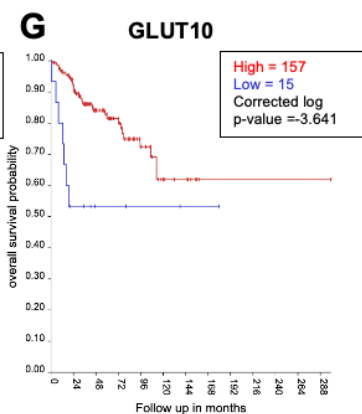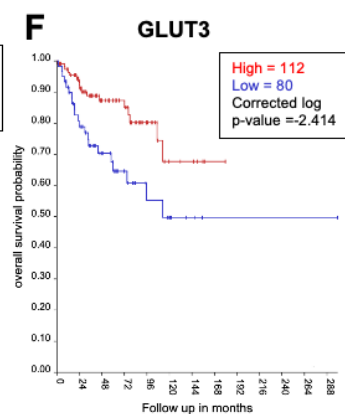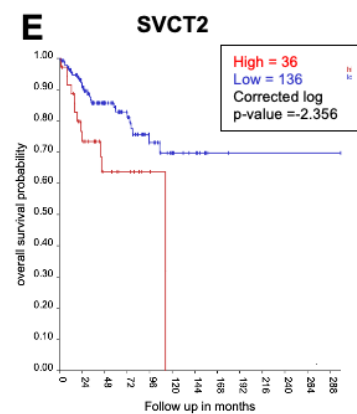
Figure 3.3. (A) Association of transporters with patient survival across SHH patients (B-G) individual transporter Kaplan-Meier survival analysis. (A) Kaplan-Meier survival curves produced using survival data (n=172) from the Cavalli dataset on R2: Genomics analysis and visualisation platform. See figure 3.2 for detailed description. Kaplan-Meier survival analysis of **B),** GLUT4; **C)**, GLUT8; **D)** SVCT1; **E)** SVCT2; **F)** GLUT3; **G)** GLUT10 expression on medulloblastoma patients in the Cavalli dataset (n=612). Survival curves were compared using the Log-rank (Mantel-Cox) test. Log p-values were adjusted for FDR corrections amongst other candidates. Significant differences in survival were considered those where log(p)<-1.3.

In order to refine our findings, we selected two GO terms for correlation analysis. The first, 'Antioxidant Activity' (GO:0016209, n=72), was chosen as AA is a well-established antioxidant. Hence, we hypothesised that AA/DHA transporters would be co-expressed with genes involved in antioxidant defence mechanisms. The second GO term 'Collagen Metabolic Process' (GO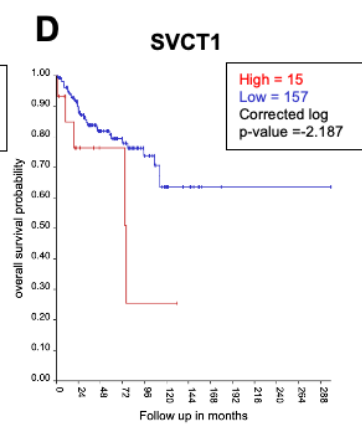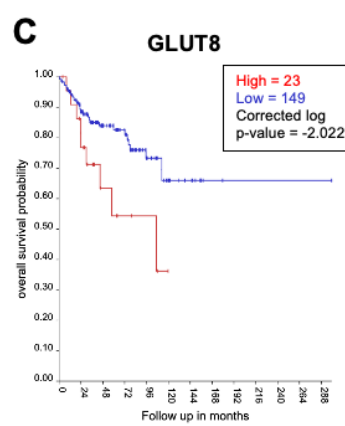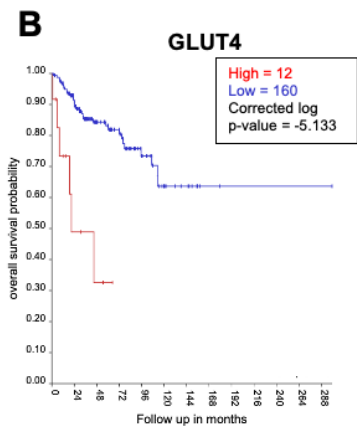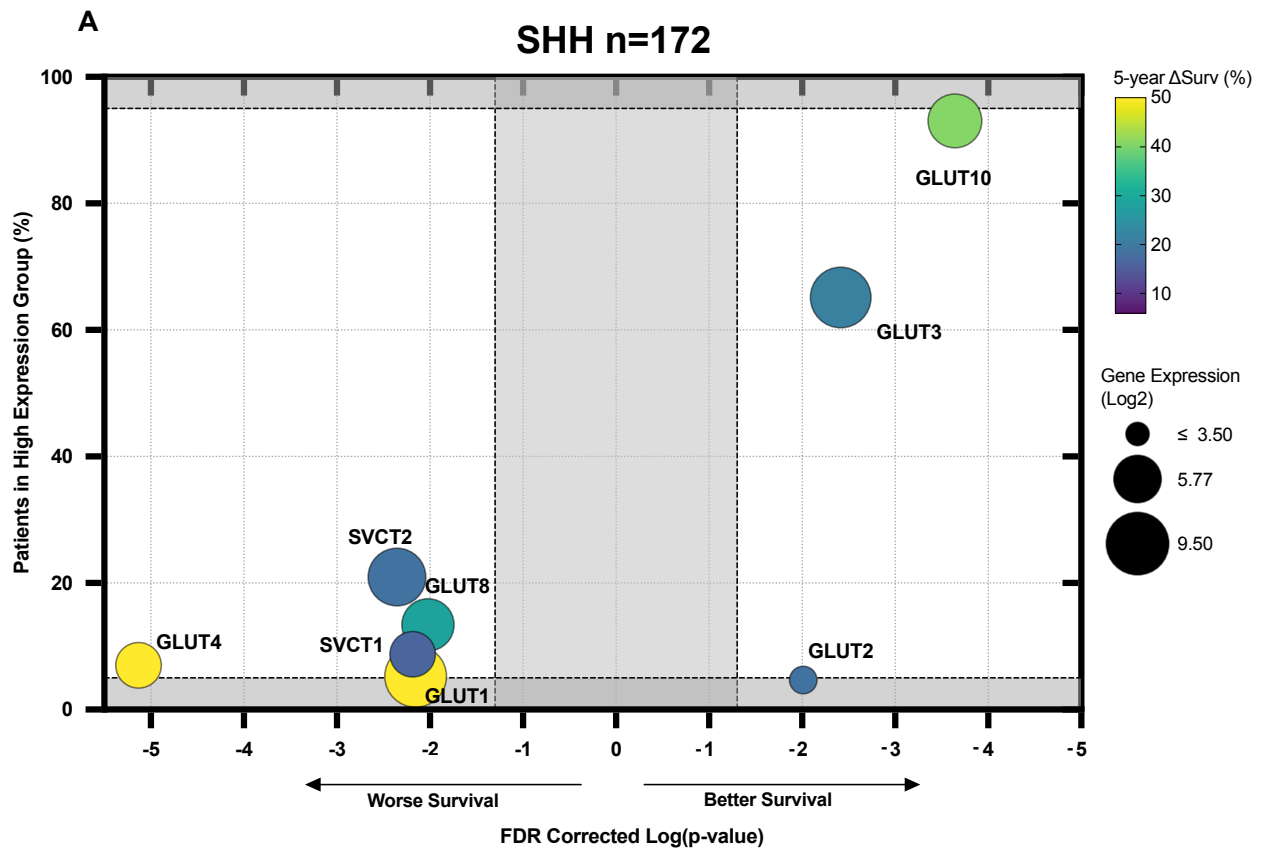:0032963, n=106), was chosen to investigate the hypothesis. We hypothesised that a transporter associated with collagen production would be co-expressed with genes involved in collagen metabolism, especially in the SHH subgroup.

We used R2 to calculate Pearson correlation coefficients (R values) to evaluate the linear relationship between the expression of candidate genes and the genes within the specific GO terms in medulloblastoma patients. The R value quantifies the strength and direction of the expression relationship between two genes and ranges from -1 (perfect negative correlation) to 1 (perfect positive correlation), with 0 indicating no correlation. Genes that were significantly correlated with candidate gene expression ($p<0.05$) had their R-values plotted on scatterplots, and an R value cut-off of ±0.3 was applied to highlight meaningful correlations (Schober et al., 2018). Genes that met this threshold were plotted in black and those that did not were plotted in grey.

3.3.1. Antioxidant Activity

Figure 3.4 presents the scatterplot of the significant correlations between the candidate transporter genes and the genes within the 'Antioxidant Activity' GO term, using gene expression data from all medulloblastoma patients. Significant correlations were observed for all candidate transporters ($p<0.05$), but most, including GLUT1-4, GLUT8, and SVCT1, had few genes that also met the R-value cutoff (n<7 for all candidates). GLUT10 was the only GLUT transporter with a large number of significant correlations that satisfied this cutoff (n=20; ~30% of the GO term), an overwhelming majority of which were positively correlated to GLUT10 expression. SVCT2 showed a moderate set (n=12), though with a 50:50 split between positive and negative correlations.
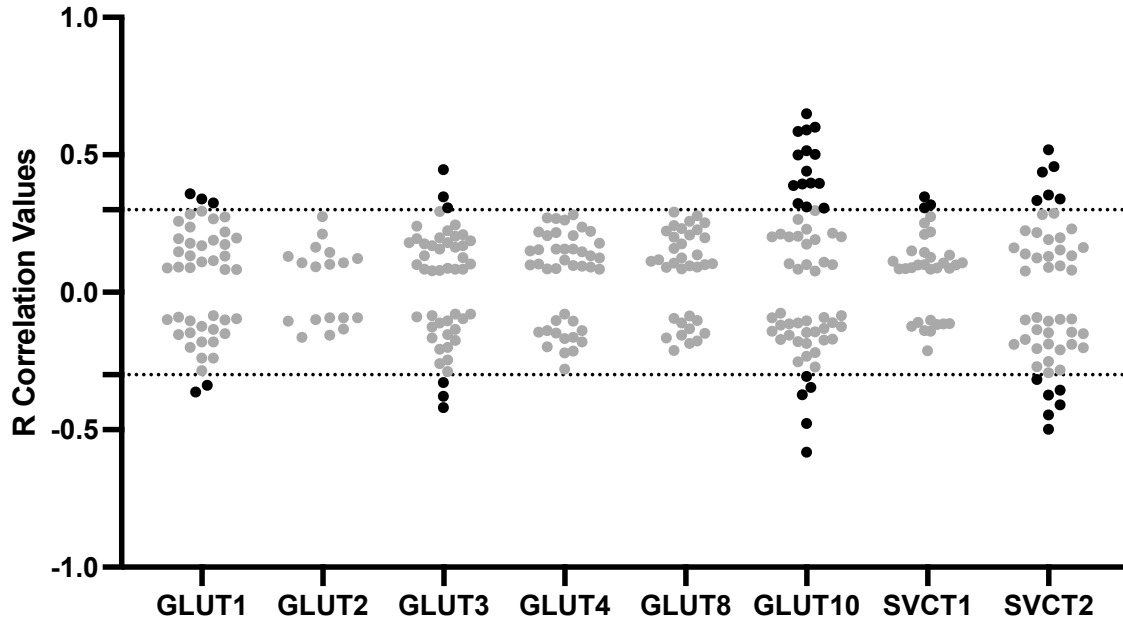
Figure 3.4. Significant gene correlations between the expression of candidate transporters and genes related to antioxidant activity. Each data point represents a gene within the GO term 'Antioxidant Activity' (n=72) whose expression is significantly correlated (p<0.05) with the candidate transporter gene shown on the x-axis. The corresponding R value is plotted on the y-axis, indicating the strength and direction of this relationship. Genes with R values above or below the cut-off threshold of ±0.3 (dotted line) are highlighted in **black.**
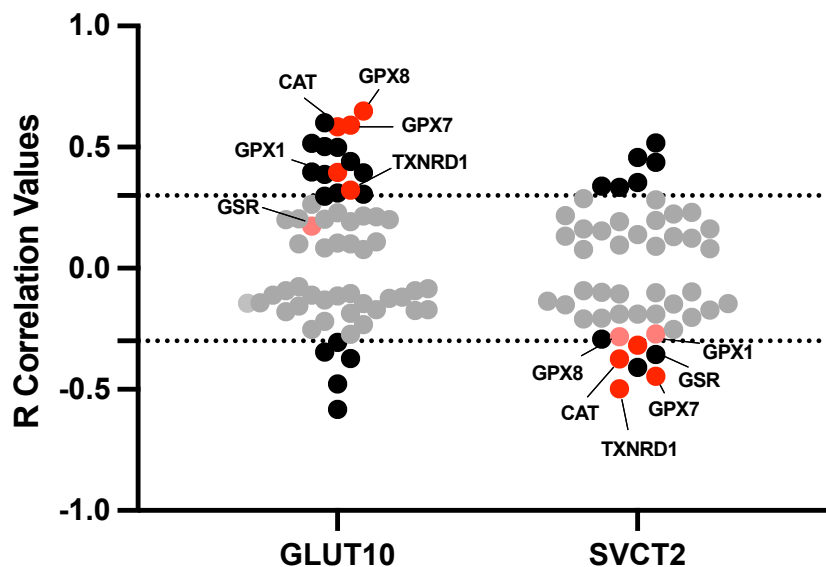

Figure 3.5. Significant gene correlations of interest between the expression of GLUT10 and SVCT2 and genes related to antioxidant activity. For full description of scatterplot see Figure 3.4. Genes of interest *(GSR, TXNRD1, CAT, GPX, GPX7, GPX8)* are labelled and highlighted in **red** if R±0.3 and **paler red** if 0.3>R<-0.3.

Upon further investigation of the positive significantly correlated genes with GLUT10 expression, 6 genes of interest were identified (highlighted in red in Figure 3.5). *TNXR1* (thioredoxin reductase) and *GSR* (glutathione reductase) are important enzymes for DHA recycling to AA (Du et al., 2012; Figure 1.6), whilst *CAT* (catalase)*, GPX1, GPX*7, and *GPX8* (glutathione peroxidase 1, 7, and 8) are genes encoding key cellular antioxidant enzymes. Catalase, as the key metaboliser of H_2O_2, has been observed to mitigate cytotoxic effects of high-dose AA (Klingelhoeffer et al., 2012). GPx7 and GPx8 are found in the ER, similarly the AA-dependent prolyl- and lysyl- hydroxylases are localised to the ER, suggesting AA availability in the ER could be linked to our hypothesis *(Pei et al., 2023; Table 3.1).* These genes were also investigated amongst SVCT2's significantly correlated genes, and contrastingly all 6 genes had a negative correlation with SVCT2 expression in medulloblastoma patients (Figure 3.5).

Table 3.1 – The genes of interest in the significant correlations of GLUT10 and SVCT2 within the GO Term 'Antioxidant Activity'. *References: (May et al., 1997; Pei et al., 2023; Klingelhoeffer et al., 2012; Chen et al., 1984)*

Gene	Protein	Function	Relevance to AA Biology
TXNRD1	Thioredoxin reductase 1	Belongs to the pyridine nucleotide disulfide oxidoreductases. Important for maintaining thioredoxin in a reduced state.	Contribute to the reduction of ascorbic acid to dehydroascorbic acid (see Figure 1.6).
GSR	Glutathione reductase	Belongs to the FAD-dependent proteins. Important for maintaining glutathione in a reduced state.	
CAT	Catalase	Common enzyme that catalyses the decomposition of hydrogen peroxide into oxygen.	Catalase activity mitigates the pro-oxidant and cytotoxic activity of ascorbic acid.
GPX1, GPX7, GPX8	Glutathione peroxidases 1, 7, and 8	Glutathione peroxidases are an enzyme family that catalyse the decomposition of ROS into water, typically using glutathione as a reducing agent. GPx1 ubiquitous in cytoplasm and mitochondria. GPx7 and GPx8 are found in the ER and play important roles in ER stress.	Ascorbic acid can increase the activity of this group of enzymes.

3.3.2. Collagen Metabolic Process

The analysis was replicated with genes in the GO term 'Collagen Metabolic Process', Figure 3.6 presents the scatterplot of the significant correlations between candidate genes and genes within this GO term using patient data from the overall cohort.

Similar to their lack of correlation with genes in the 'Antioxidant Activity' GO term, GLUT1, GLUT2, GLUT4, GLUT8, and SVCT1 exhibited minimal significant correlations that met the R-value cutoff with genes in this GO term (n<7 for all candidates). GLUT10 (n=45, 42% of the GO term) and SVCT2 (n=25), again, had a substantial number of significant correlations. GLUT10 showed predominantly positive correlations, while SVCT2 exhibited predominantly negative correlations. Interestingly, GLUT3 (n=32) also showed a moderate set of significant correlations.
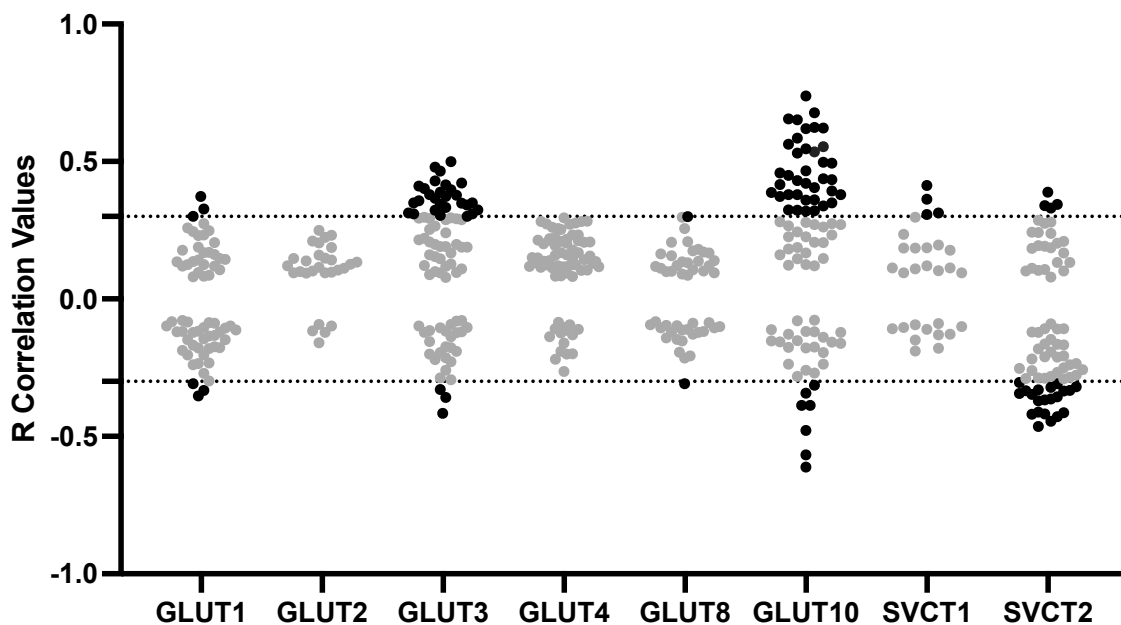
Figure 3.6. Significant gene correlations between the expression of candidate transporters and genes related to collagen metabolic process. Each data point represents a gene within the GO term 'Collagen Metabolic Process' (n=106) whose expression is significantly correlated (p<0.05) with the candidate transporter gene shown on the x-axis. The corresponding R value is plotted on the y-axis, indicating the strength and direction of this relationship. Genes with R values above or below the cut-off threshold of ±0.3 (dotted line) are highlighted in black.

In accordance with the previous GO term analysis, the significant gene correlations of GLUT3, GLUT10 and SVCT2 were further investigated (Figure 3.7). This identified six genes that were previously identified in the collagen outer shell of SHH patients (Linke et al., 2022) (Table 3.2). Consistent with the previous analysis, the genes were positively correlated to GLUT10 expression, as well as GLUT3 expression, and negatively correlated to SVCT2 expression (Figure 3.7). The genes encode collagen types I, III, and VI which have been associated with improved survival outcomes in SHH patients (Linke et al., 2022).

Figure 3.7. Significant gene correlations of interest between the expression of GLUT3, GLUT10 and SVCT2 and genes related collagen metabolism. For full description of scatterplot see Figure 3.6. Genes of interest *(COL1A1, COL1A2, COL3A2, COL6A1, COL6A2, COL6A3)* are labelled and highlighted in **red** if R±0.3 and **paler red** if 0.3>R<-0.3.

Table 3.2 – The genes of interest in the significant correlations of GLUT3, GLUT10, and SVCT2 within the GO Term 'Collagen Metabolic Process. *References: (Ricard-Blum et al., 2011; Linke et al., 2023)*

Gene	Protein	Function	Relevance to SHH Medulloblastoma Biology
COL1A1, COL1A2	Collagen I (α1 and α2 chain)	The most common type of fibril-forming collagen. Found in skin, tendons, ligaments, blood vessels, bone, lungs, and heart. The α1 homotrimer plays an essential role in wound healing.	Gene expression associated with a better prognosis of SHH patients. Present in the outer collagen shell surrounding SHH tumours.
COL3A1	Collagen III (α1 chain)	An essential fibril forming collagen in the structural integrity of hollow organs. Also functions in cell adhesion, migration and proliferation through integrin interactions.	
COL6A1, COL6A2, COL6A3	Collagen VI (α1, α2, and α3 chain)	A microfibrillar collagen found in connective tissues. Also has cytoprotective functions through inhibition of apoptosis and oxidative damage.	

We refined our investigation of GLUT3, GLUT10 and SVCT2 significantly correlated genes within this GO term to the gene expression of SHH patients to observe if this overall correlative relationship remains (Figure 3.8). The number of significant correlations decreased for GLUT10 (n=14) and SVCT2 (n=10), in comparison GLUT3 retained a modest set (n=4). We hypothesised this decrease in significant correlations could reflect the heterogeneity of SHH tumours, thus this analysis was further refined to individual SHH subtypes. Notably, the number of collagen-related genes correlated with GLUT10 expression increased substantially in the SHH-α(n=31), SHH- β (n=17), and SHH-δ (n=22) subtypes (Figure 3.8). In the SHH-α subtype, a subtype characterised with *TP53* mutations and poor prognosis, all six collagen genes found in the SHH-specific ECM shell were positively correlated with GLUT10 expression (Northcott et al., 2019). Conversely, only in the SHH-γ subtype was SVCT2 expression significantly correlated with a large set of genes (n=34). The significant gene correlations with GLUT3 within SHH subtypes was minimal, except in the SHH-γ subtype (n=16).
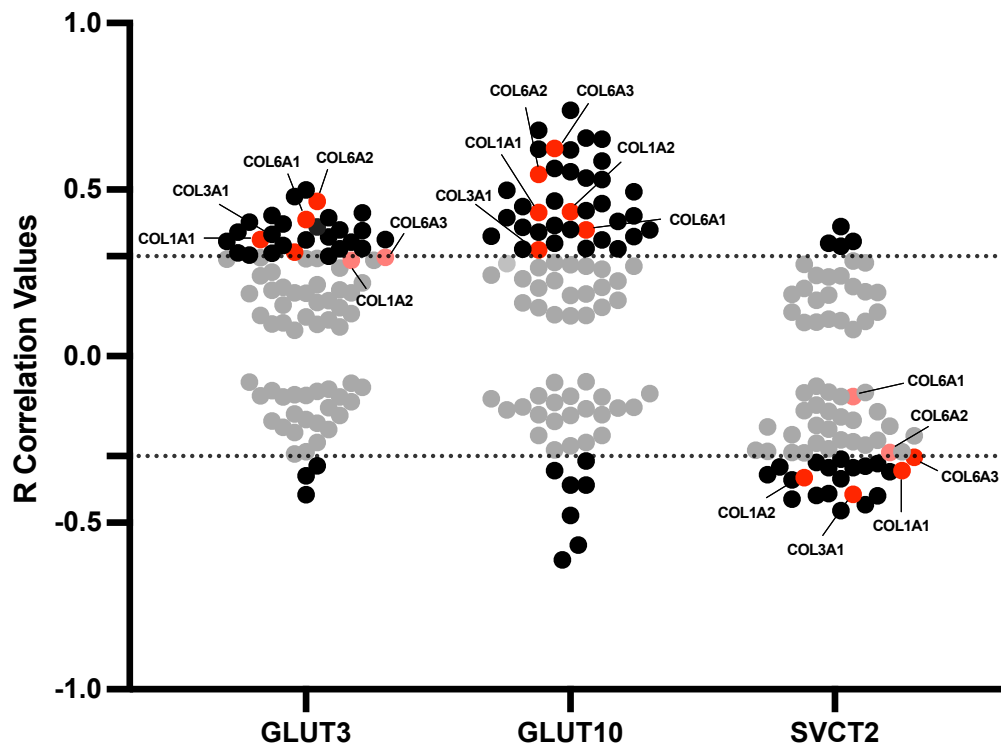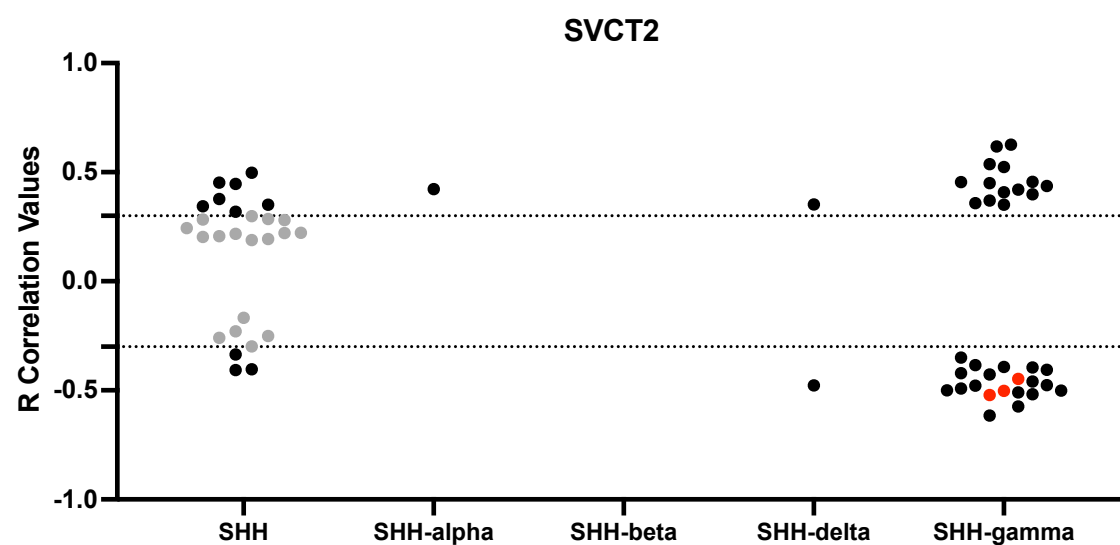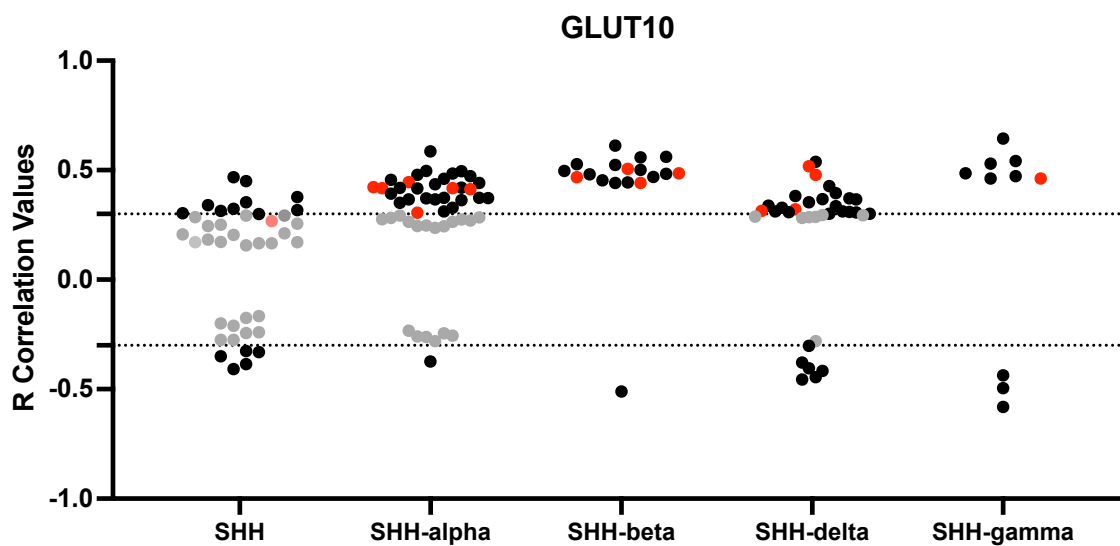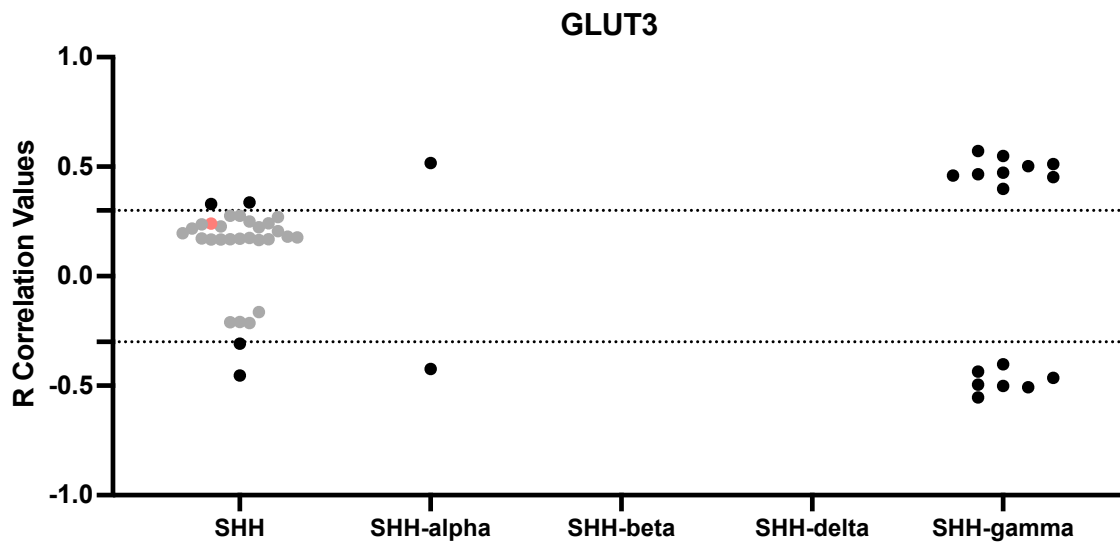
GLUT3

GLUT10

SVCT2

Figure 3.8. Significant gene correlations between the expression of GLUT3, GLUT10, and SVCT2 with genes related to collagen metabolic process in SHH and subtypes. Each data point represents a gene within the GO term 'Collagen Metabolic Process' (n=106) whose expression is significantly correlated (p<0.05) with the specific candidate transporter gene in SHH and the SHH subtypes (α, β, δ, and γ) that are plotted on the x-axis. The corresponding R value is plotted on the y-axis, indicating the strength and direction of this relationship. Genes with R values above or below the cut-off threshold of ±0.3 (dotted line) are highlighted in **black**. Genes of interest *(COL1A1; COL1A2; COL3A2; COL6A1; COL6A2; COL6A3)* are highlighted in **red** if R±0.3 and **paler red** if 0.3>R<-0.3.

3.3.3. SVCT2 vs GLUT10 Expression

The identified genes of interest all positively correlated with GLUT10 and negative correlated with SVCT2 (Figure 3.5 and Figure 3.7); we were interested to see if this inverse relationship continued with the wider significantly correlated genes with SVCT2 and GLUT10 expression in these GO terms, regardless of their meeting the R cutoff criterion. We utilised Venn diagrams, figure 3.9, to visualise any overlap. Specifically, 23 genes overlapped from the 'Antioxidant Activity' GO term (representing 39% of genes in the GO term) and 49 genes from the 'Collagen Metabolic Process' GO term (representing 46% of genes in the GO term) and). These findings strongly suggest an inverse relationship between GLUT10 and SVCT2.
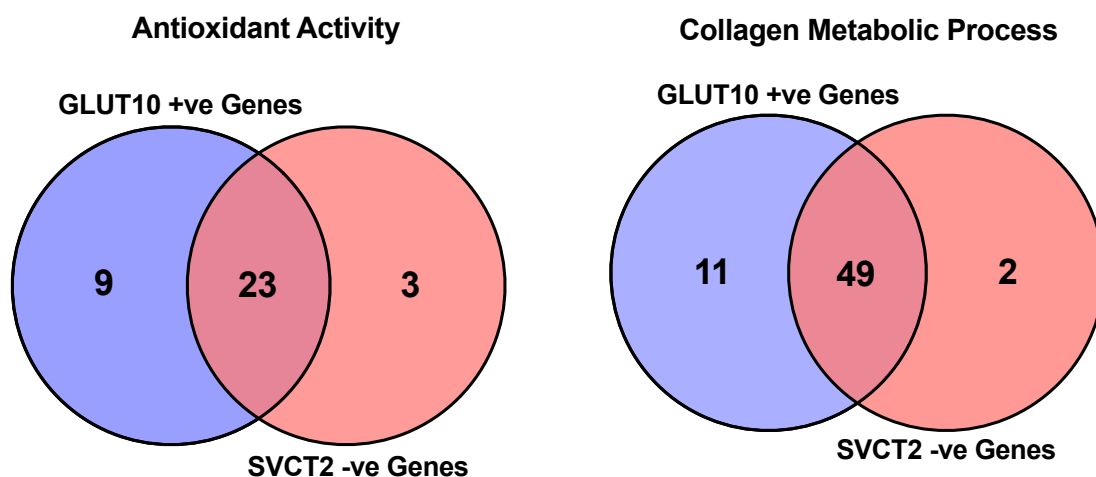
Figure 3.9. The reciprocal relationship of genes within the GO terms to GLUT10 and SVCT2 expression. GLUT10 significantly positively correlated genes (p<0.05; no R cutoff) **(red circle)** and SVCT2 significantly negatively correlated genes (p<0.05; no R cutoff) **(blue circle)** in the GO terms 'Antioxidant Activity' and 'Collagen Metabolic Process'

Thus, we directly investigated whether GLUT10 and SVCT2 expression *per se* exhibited an inverse relationship in patient samples (Figure 3.10). This was confirmed in the overall patient cohort, where a significant inverse correlation was observed (R =-0.325, p=3.40E-20). However, a weaker correlation was noted among SHH patients (R=-0.183, p=0.0062). The impact of the candidate's expression patterns on SHH patient survival was also inverse: patients with 'high' GLUT10 expression were associated with better survival outcomes, while those with 'high' SVCT2 expression were linked to a poorer survival in the SHH subgroup.
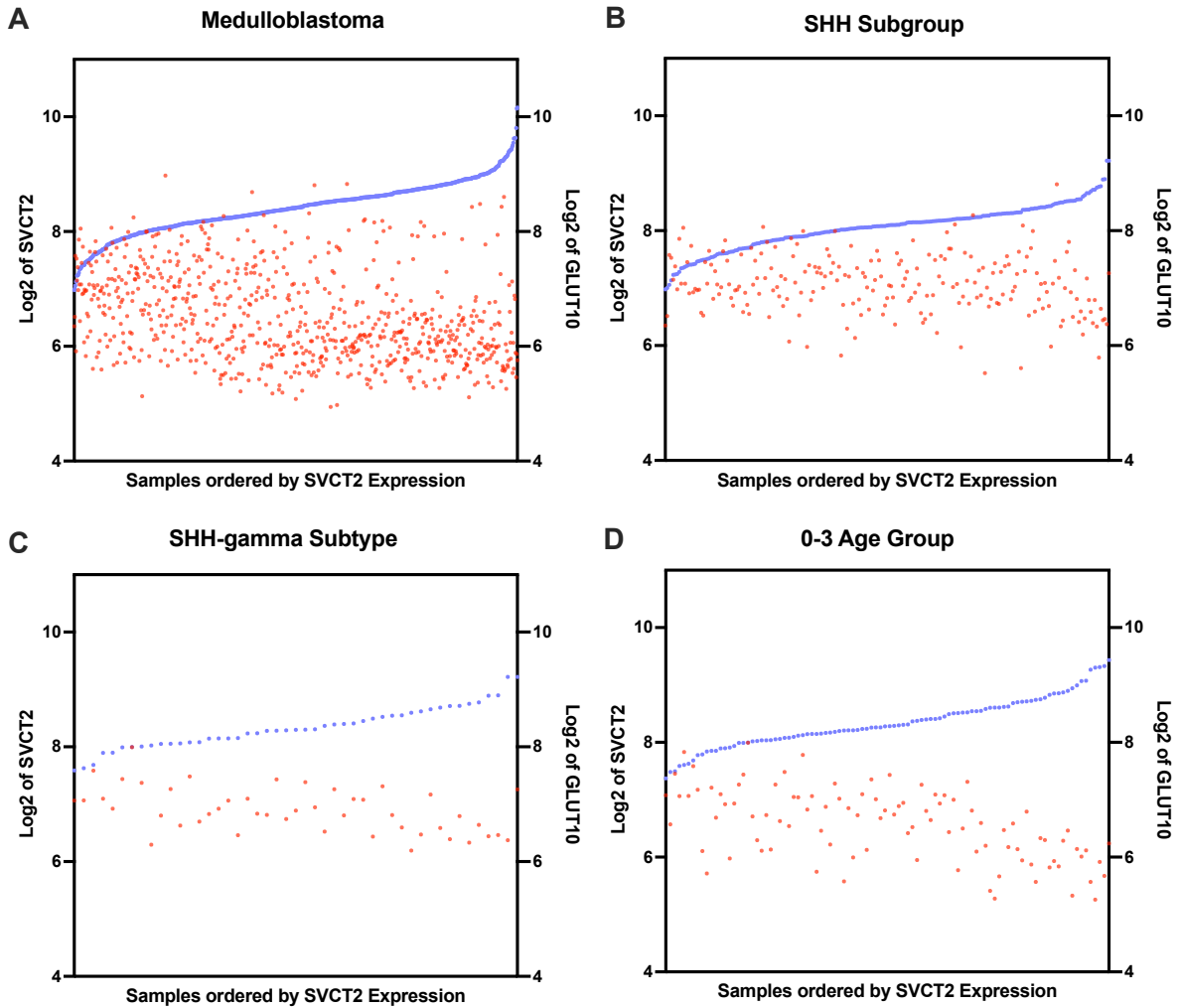
Figure 3.10. SVCT2 vs GLUT10 gene expression in A) medulloblastoma; **B)** SHH subgroup; **C)** SHH-gamma subtype; **D)** 0-3 age group. The Log2 of SVCT2 expression is plotted on the left y axis **(blue)** and the Log2 of GLUT10 expression is plotted on right **(red).** The samples are ordered on the x-axis according to their SVCT2 expression.

Notably, there was no significant correlation found in SHH-α, -β, -δ, subtypes.

However, the SHH-γ subtype exhibited a strong inverse correlation (R=-0.447, p=0.0017) (Figure 3.10C). This finding is intriguing given the consistent negative correlations of SVCT2 in the SHH-γ subtype. Since the SHH-γ subtype predominantly consists of infants aged 0-3 years, we extended the analysis to this age group across all subtypes. The results confirmed a significant and strong inverse correlation (R=-0.579, p=4.4E-10), which is clearly visualised in Figure 3.10D. This is of note due to medulloblastoma originating in the developmental stage, which may suggest developmental processes influencing the expression of these transporters.

3.4. GLUT10 and SVCT2 transporter genes are strong candidates for involvement in SHH biology

The primary objective of this screen was to identify candidate transporter genes potentially implicated in medulloblastoma biology. Selection criteria focused on; genes that exhibited differential expression in medulloblastoma, a significant impact on patient survival and strong significant correlations (R>±0.3) with genes associated with antioxidant activity and collagen metabolism, Table 3.3 summarises the genes that met these criteria. GLUT10 and SVCT2 met all criteria and subsequently were chosen to further study the impact of their activity in medulloblastoma.

Table 3.3 – The transporters and the criteria for selection for further study. If the transporter met the criteria, the box was coloured **green** and if it did not the box was coloured **grey**.

	Expression significantly associated with SHH patient survival	Differential expression in SHH Tumours compared to normal cerebellum, Group 3 and Group 4)	A moderate set of significant correlations that met an R cutoff of ±0.3 with genes within the GO term 'Antioxidant Activity'	A moderate set of significant correlations that met an R cutoff of ±0.3 with genes within the GO term 'Collagen Metabolic Process' in SHH patients
GLUT1	grey	grey	grey	grey
GLUT2	grey	grey	grey	grey
GLUT3	green	green	grey	grey
GLUT4	green	grey	grey	grey
GLUT8	green	grey	grey	grey
GLUT10	green	green	green	green
SVCT1	green	grey	grey	grey
SVCT2	green	green	green	green

3.5. Validation of SVCT2 and GLUT10 expression in medulloblastoma cell lines

Following the identification of SVCT2 and GLUT10 genes, we sought to investigate their protein expression in patient-derived cell lines. We achieved this through western blot detection of candidate protein expression in the medulloblastoma cell lines; DAOY, ONS-76, HD-MB03, D425, CHLA-01 and CHLA-01R (Table 2.4; Jacobsen et al., 1985; Yamada et al., 1989; Milde et al., 2012; Bigner et al., 1990; Xu et al., 2015). Three independently cultured cell pellets were analysed per cell line. This analysis aimed to determine basal protein expression in cell lines and explore potential differences in candidate expression within medulloblastoma subgroups to guide future research directions.

3.5.1. SVCT2 expression in medulloblastoma cell lines

To assess SVCT2 expression, a monoclonal SVCT2 primary antibody was utilised. Calnexin served as a loading control and a housekeeping gene, and SH-SY5Y cells were used as a positive control cell line (Uhlén et al., 2015, Human Protein Atlas proteinatlas.org). SVCT2 protein expression was observed in more than one pellet for each cell line. Notably, in two out of three DAOY pellets, SVCT2 was either undetectable or displayed a faint band (Figure 3.11A).

Relative SVCT2 protein levels were quantified by normalising to calnexin expression using ImageJ software. These values were plotted with error bars representing the standard error of the mean (SEM) (Figure 3.11B). Statistical analysis using a two-way ANOVA, followed by a multiple comparisons test, showed no statistically significant differences in SVCT2 expression between any of the cell lines. This suggests that SVCT2 expression is not significantly subgroup specific.
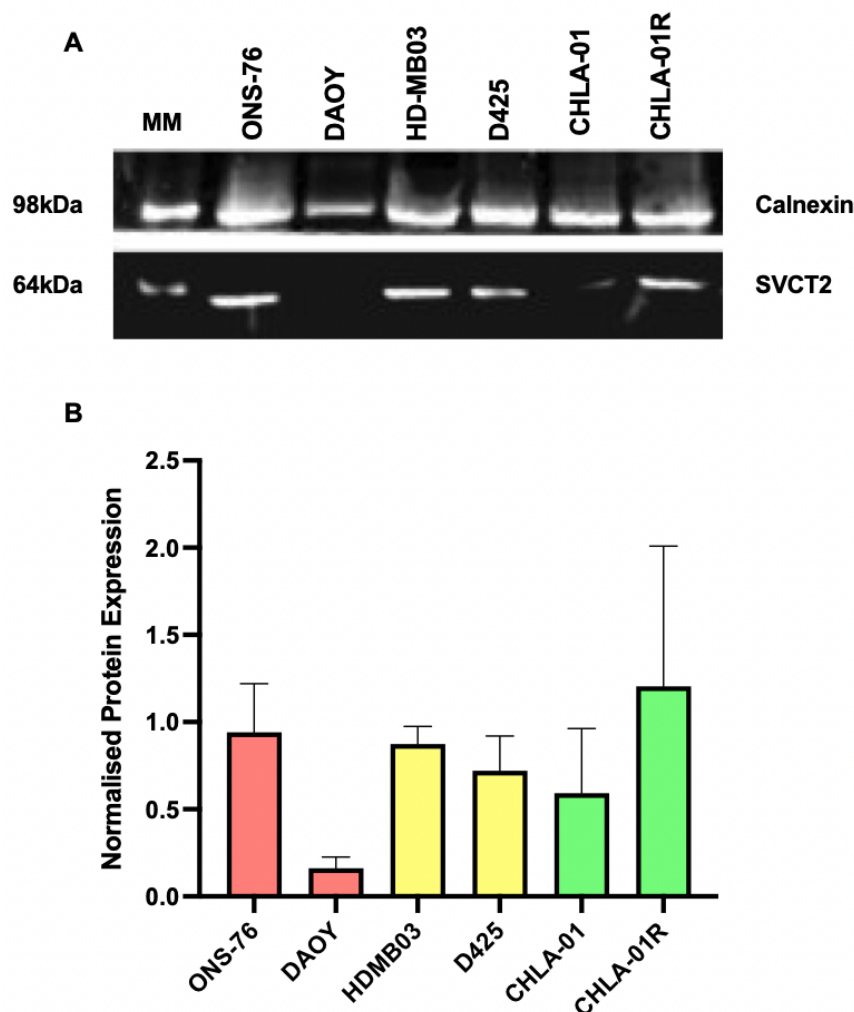

Figure 3.11. SVCT2 protein expression across medulloblastoma patient-derived cell lines. Expression of SVCT2 in; ONS-76 and DAOY (SHH), HD-MB03 and D425 (Group 3), and CHLA-01 and CHLA-01R (Group 4). **A)** Western blot of protein expression of one pellet repeat. Image obtained using

a LI-COR machine. Anti-calnexin (SciGen) used as housekeeping gene. SVCT2 (50kDa; 1:2000,) Calnexin (90kDa; 1:2000). **B)** Normalisation of SVCT2 protein expression with calnexin expression in western blots using arbitrary units (AU). Error bars represent standard error of the mean. SHH cell lines **(red)**, group 3 **(yellow),** and group 4 **(green)**. N=3. MM; molecular markers.

3.5.2. GLUT10 expression in medulloblastoma cell lines remained elusive

Assessing GLUT10 expression proved more challenging. Initially, we obtained a GLUT10 antibody and utilised HepG2 cells (human hepatocellular carcinoma-derived cell line) as a potential positive control due to high GLUT10 expression in liver (Uhlén et al., 2015, Human Protein Atlas proteinatlas.org). However, despite multiple optimisation efforts, non-specific bands were continuously observed with the strongest band at ~36kDa (GLUT10 - 57kDa) (Figure 3.12)
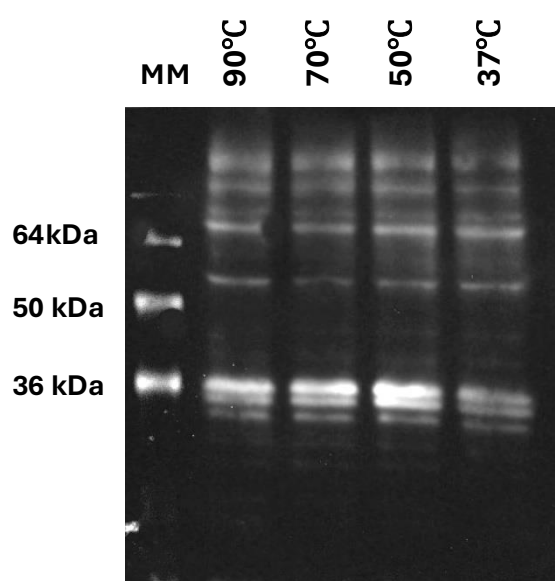
Figure 3.12. An example of the optimisation of GLUT10 antibody (1) in HepG2 cells. An example western blot of GLUT10 in HepG2 cells investigating the effect of varied denaturing temperatures during sample preparation. GLUT10 (57kDa; 1:1000). MM; molecular markers.

To overcome these issues, we sourced a new GLUT10 antibody and generated a positive control by transfecting HEK-293T cells with GLUT10 plasmid. Initial antibody optimisation in GLUT10-HEK293T cells revealed bands at the expected molecular marker (Figure 3.13A). Despite this, non-specific bands persisted when attempting to detect GLUT10 in medulloblastoma cell lines, even after further optimisation (Section 2.4**;** Figure 3.13B). Although a band corresponding to the correct molecular weight was observed (highlighted by a red box in Figure 3.13B), its validity is substantially compromised by the presence of non-specific bands, limiting the reliability of this finding. Unfortunately, we could not source a GLUT10 antibody that had been cited in literature independent to suppliers, thus were limited to these two. In addition, there is no known evidence for alternative proteoforms in cells (Dawson et al., 2001).
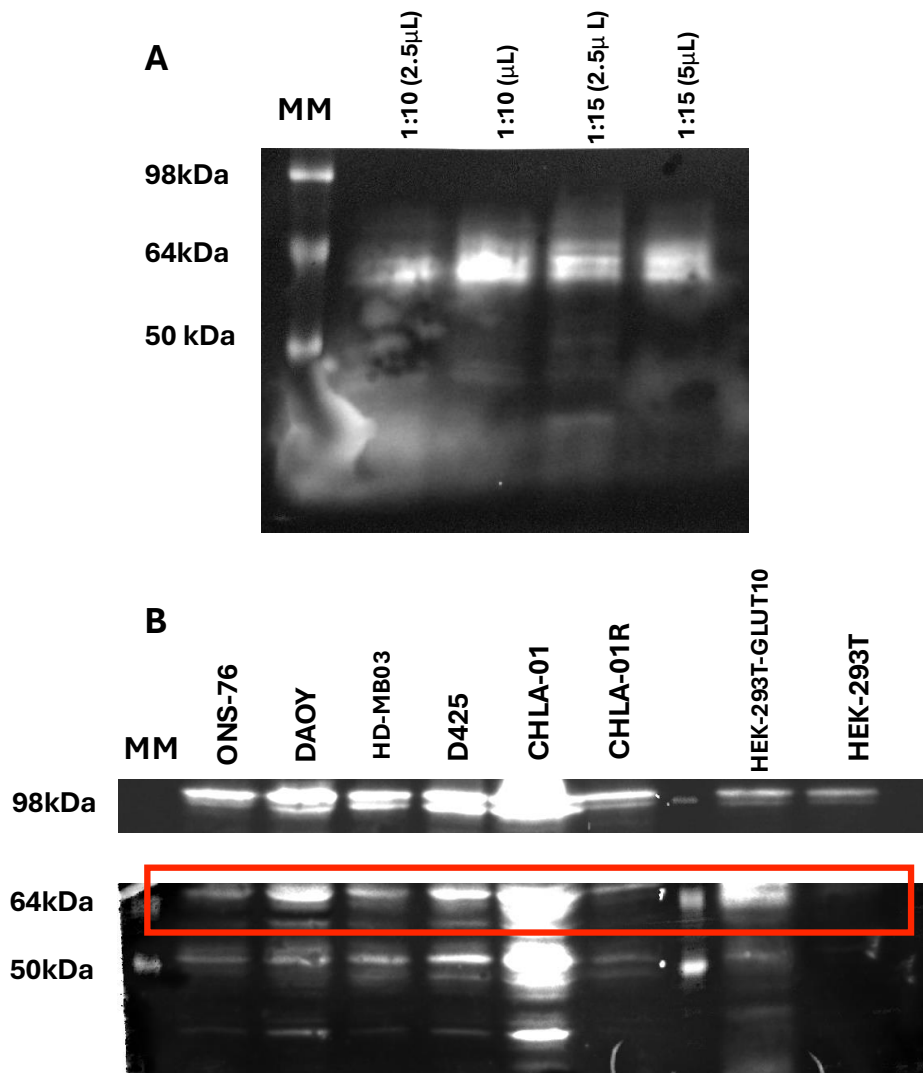
Figure 3.13. GLUT10 Antibody (2) unable to detect GLUT10 in medulloblastoma cell lines. A) Western blot of GLUT10 expression in HEK293T cells transfected with GLUT10 at 1:15 and 1:10 dilutions GLUT10 (57kDa; 1:1000). **B)** Western blot of GLUT10 expression in ONS-76 and DAOY (SHH), HD-MB03 and D425 (Group 3), and CHLA-01 and CHLA-01R (Group 4). A red box outlines the hypothesised band relating to GLUT10 however there are extensive non-specific bands. GLUT10 (57kDa; 1:1000). Calnexin (90kDa; 1:2000). MM; molecular markers.

3.6 Concluding statements

In this chapter, the eight known DHA/AA transporter genes were screened in medulloblastoma patient gene datasets (Pfister et al., 2011; Cavalli et a., 2017). This analysis identified GLUT10 and SVCT2 genes as significantly differentially expressed in SHH tumours, associated with survival outcomes of SHH patients and correlated with the expression of key antioxidant and collagen genes (Figures 3.1-3.8). This suggested that GLUT10 and SVCT2 transporter proteins could contribute to medulloblastoma biology through regulating AA/DHA uptake into cells and their compartments. Their protein expression was subsequently assessed using western blots, SVCT2 expression was detected but GLUT10 expression remained elusive in medulloblastoma cell line (Figures

3.11-3.14). Given these challenges, alternative approaches could have been employed to detect and quantify GLUT10 protein expression, such as mass spectrometry-based proteomics or immunoprecipitation-based enrichment prior to western blotting. Additionally, if the goal was to confirm gene expression rather than protein levels, RT-qPCR could have been used to measure GLUT10 transcript levels. Due to the lack of confidence in these results for CRISPR knock-out investigation, we shifted focus to assess the impact of varying AA concentrations on cultured SHH spheroids. Consequently, this chapter concludes our investigation of DHA/AA transporters but strengthens our confidence in exploring AA's effects in the next chapter, as GLUT10 and SVCT2 remain promising candidates in medulloblastoma biology.

4. Investigating Ascorbic Acid Action in SHH 3D Spheroids

SHH spheroids were used as a model for assessing the effects of AA alone and in combination with cisplatin on the growth of SHH tumours, as our hypothesis is rooted in SHH biology. Spheroids were cultured according to the protocol outlined by Dr Roper (Roper et al., 2022; Section 2.3; Figure 2.1). Sub-confluent DAOY and ONS-76 cells were seeded in ULA plates on Day 0, and imaged on Day 4, 5, 6 and 7 (Figure 4.1A). Both DAOY and ONS-76 spheroids increased in size during this period, although DAOY spheroids grew at a quicker rate than ONS-76 spheroids (Figure 4.1B). Additionally, ONS-76 spheroids appeared an irregular size in comparison to the more spherical DAOY spheroids, this is most likely a consequence of inaccurate seeding density and/or as the plates weren't shaken, however this morphology continues for all ONS-76 repeats. Spheroid volumes were measured at each time point using ImageJ software to determine area. At Day 4, spheroids were treated with the compounds of interest during a media change, and we performed a two-way ANOVA followed by a multiple comparison's test to assess statistical significance between the volume of differently treated SHH spheroids at Day 5, 6 and 7.

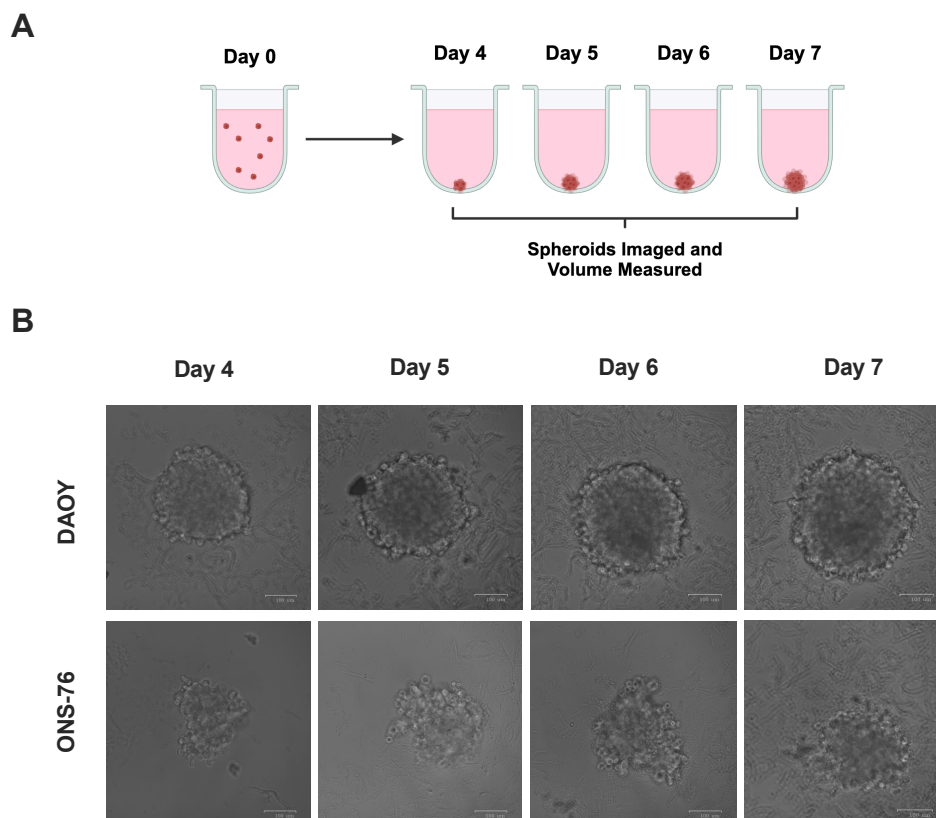**Figure 4.1. Day 4 to 7 Growth of DAOY and ONS-76 Spheroids. A)** Experimental set up for culturing 3D medulloblastoma spheroids. Sub-confluent cells are seeded in ultra-low attachment plates in neurosphere media at Day 0 and at Day 4 can be treated then imaged every 24 hours using a ZOE™ Fluorescent Cell Imager. **B)** Brightfield images of DAOY and ONS-76 spheroids at Day 4, 5, 6 and 7. Scale bar: 100μm.

4.1. Ascorbic Acid increases growth in SHH spheroids

Day 4 SHH spheroids were treated with one of three concentrations of AA: 100µM (physiological plasma concentration; Carr et al., 1999), 1mM (physiological neuronal concentration; Angelow et al., 2003), and 2.5mM, the high dose. Spheroid volumes at each time point were normalised to their pre-treatment volume (Day 4) (Figure 4.2). We hypothesised that physiological concentrations of AA (100µM and 1mM) would promote spheroid growth by increasing collagen deposition but the high AA concentration (2.5mM) would promote AA's pro-oxidant activities and inhibit spheroid growth.

Contrary to this hypothesis, AA stimulated growth in DAOY spheroids at all concentrations (Figure 4.2A). The significance of this growth compared to controls showed a concentration-dependent effect at different time points. Physiological concentrations of AA (100µM and 1mM) induced an earlier growth response, with the most significant differences in growth observed at Day 5 (48 hours post-treatment; p≤0.0001 for both concentrations). Whereas spheroids treated with 2.5mM AA showed a delayed significant growth response, and their growth was most significantly different to controls at Day 7 (p≤0.0001). Notably 2.5mM AA-treated spheroids also displayed the largest overall increase in size (2.5-fold increase relative to Day 4). The treatment of DAOY spheroids with 2.5mM AA also led to morphological changes, including cell dissociation (indicated by a red arrow in Figure 4.2C) and the appearance of dark speckles (indicated by white arrows in Figure 4.2C). These dark speckles were consistently observed across all wells treated with 2.5mM AA, in both cell lines. We hypothesised that these speckles may represent AA crystallising out of solution at high concentrations.

In contrast, ONS-76 spheroids displayed a generally more modest growth in response to AA (Figure 4.2B). The largest overall increase in size observed was 1.9-fold compared to a 2.5-fold increase in size for the DAOY spheroids and untreated spheroids only increased in size by 1.2-fold. Only 1mM and 2.5mM AA treatment induced a significant increase in size compared to controls and this was only observed at Day 7 (p≤0.05 and p≤0.001 respectively). Whilst 100µM AA (physiological plasma concentration) had no significant effect on ONS-76 spheroid size, which suggests ONS-76 spheroids require larger concentrations of AA to grow. Interestingly, 1mM and 2.5mM AA-treated ONS-76 spheroids had visible protrusions (indicated by red arrows in Figure 4.2C).

A DAOY

B ONS-76

Legend:
- Untreated Control
- 100μM Ascorbic Acid
- 1mM Ascorbic Acid
- 2.5mM Ascorbic Acid

C

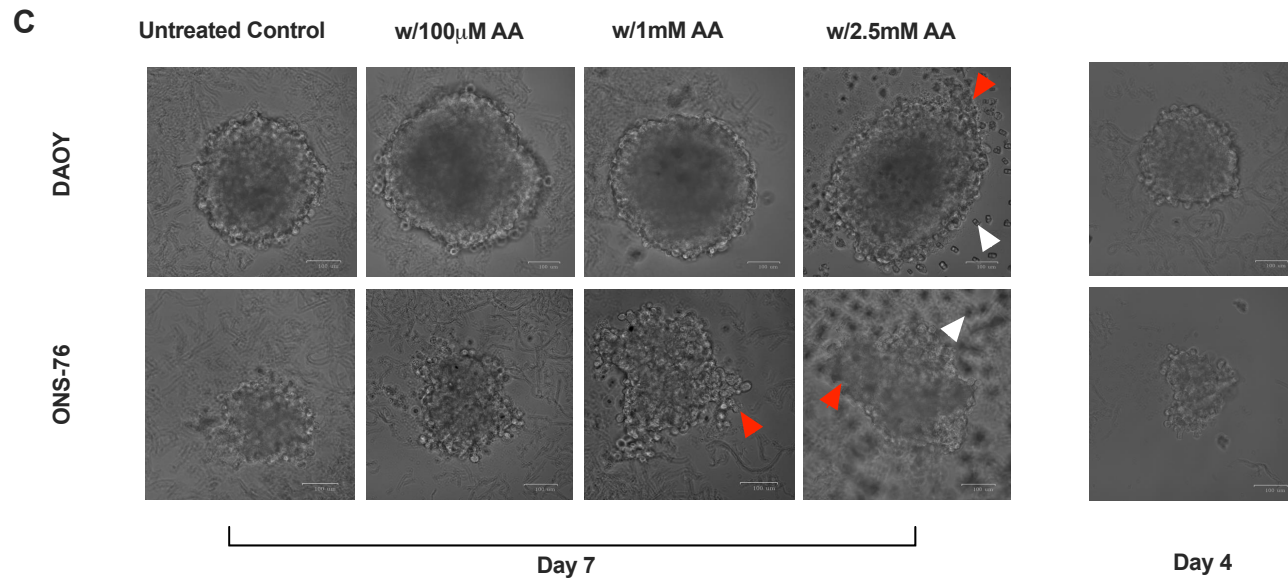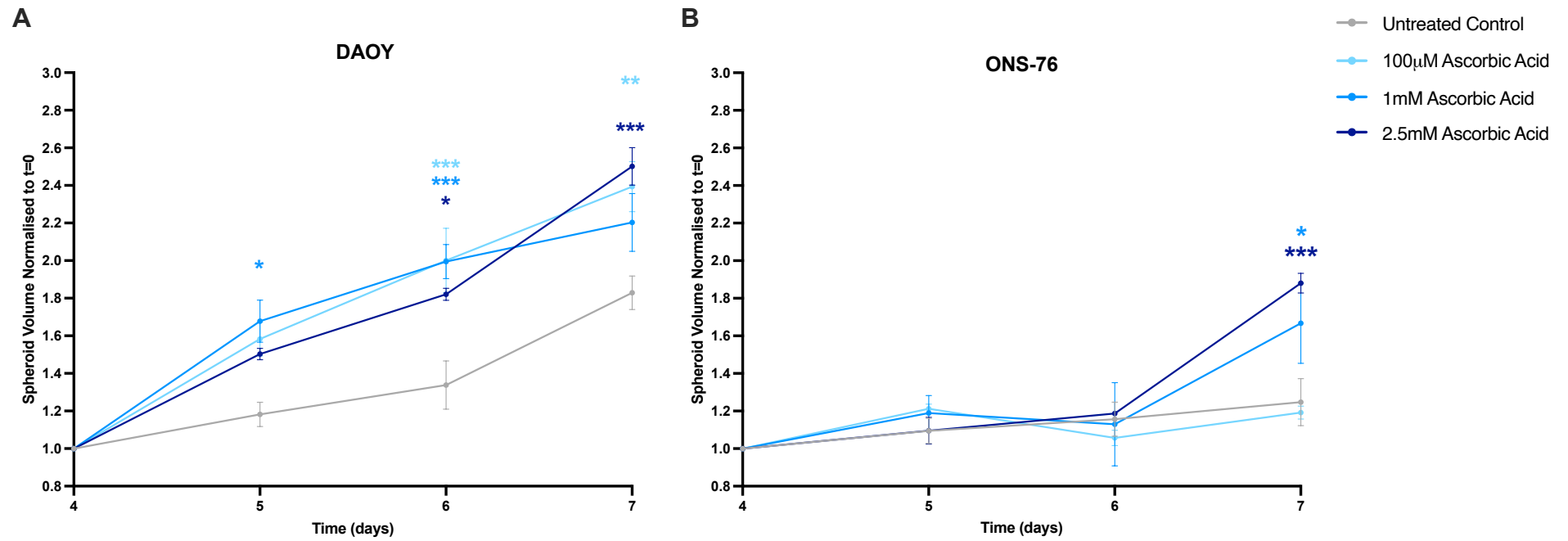|	Untreated Control	w/100μM AA	w/1mM AA	w/2.5mM AA	
DAOY					
ONS-76					

Day 7

Day 4

Figure 4.2. Ascorbic acid increases the size of DAOY and ONS-76 spheroids. The changes in volume of the spheroid over the time course for **A)** DAOY spheroids and **B)** ONS-76 spheroids. Spheroid volume was normalised to pre-treatment volume (Day 4). Error bars represent the mean ±SEM; n=3 with 3 internal replicates. Untreated control - grey; 100µM AA- pale blue; 1mM AA- blue; 2.5mM AA- midnight blue. **C)** Representative brightfield images of DAOY and ONS-76 spheroids at Day 7 for all conditions. Reference brightfield image of DAOY and ONS-76 spheroid at Day 4. Red arrows indicate structural changes in the spheroids. White arrows indicate dark hypothesised crystallised AA. Scale bar = 100µm. The results of the two-way ANOVA and multiple comparisons test between the size of AA-treated and untreated spheroids at Day 5, 6 and 7 are symbolised by ***** in the corresponding colour key. * $p<0.05$ ** $p<0.01$ *** $p<0.001$.

4.2. Investigating the Effect of Cisplatin and Ascorbic Acid Co-treatment in SHH Spheroids

As high-dose AA has been reported to potentiate chemotherapy response *in vitro* and *in vivo,* we next investigated the effect of AA in combination with cisplatin in SHH spheroids (Tronci et al., 2021; Chen et al., 2019; Takemura et al., 2010; Ghavami et al., 2020). Cisplatin is a platinum-based chemotherapeutic drug routinely used in the treatment of medulloblastoma with previously established IC values for SHH spheroids (REF; Roper et al., 2022). We used the same experimental set up as before but introduced cisplatin at 0.5µM, 1µM and 5µM concentrations alongside our previously tested concentrations of AA to Day 4 SHH spheroids (Figure 4.1).

We hypothesised that physiological concentrations of AA (100µM and 1mM) would protect spheroids from cisplatin-induced cytotoxicity through the inhibition of ROS production (Huang et al., 2023). While high-dose AA (2.5mM) would enhance cisplatin-induced cytotoxicity by increasing ROS production and decrease the size of spheroids compared to cisplatin-only controls (Huang et al., 2023).

4.2.1. High-dose ascorbic acid potentiates the cytotoxicity of chemotherapeutic agent cisplatin in DAOY spheroids

DAOY spheroids treated with 0.5µM cisplatin (IC$_{10}$) had a reduced overall growth (1.1-fold increase; Figure 4.3A). Co-treatment with 100µM or 1mM AA partially rescued spheroid growth by Day 7 (1.3-fold increase), suggesting at these concentrations AA partially protect spheroids from cisplatin-induced cytotoxicity. Co-treatment with 2.5mM AA led to a decrease in spheroid size (0.8-fold change) with boundary disintegration and cell shedding that was not observed in 0.5µM cisplatin alone-treated spheroids (indicated with red arrows in Figure 4.3C). However, none of the induced changes in spheroid size were statistically significant compared to 0.5µM cisplatin alone-treated spheroids.

A 0.5μM Cisplatin

B 1μM Cisplatin

Untreated Control
Cisplatin
w/ 100μM Ascorbic Acid
w/1mM Ascorbic Acid
w/ 2.5mM Ascorbic Acid

C

| | Untreated Control | Cisplatin | w/100μM AA | w/1mM AA | w/2.5mM AA |

0.5μM Cisplatin

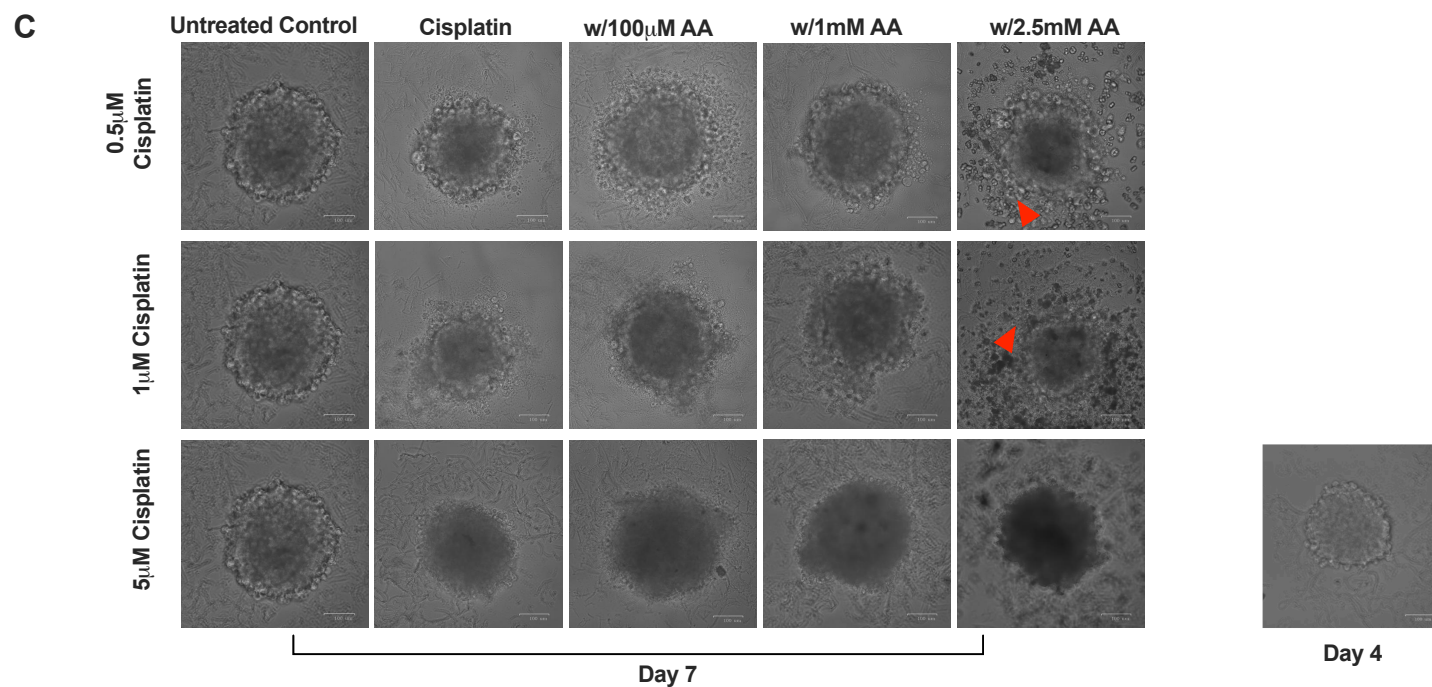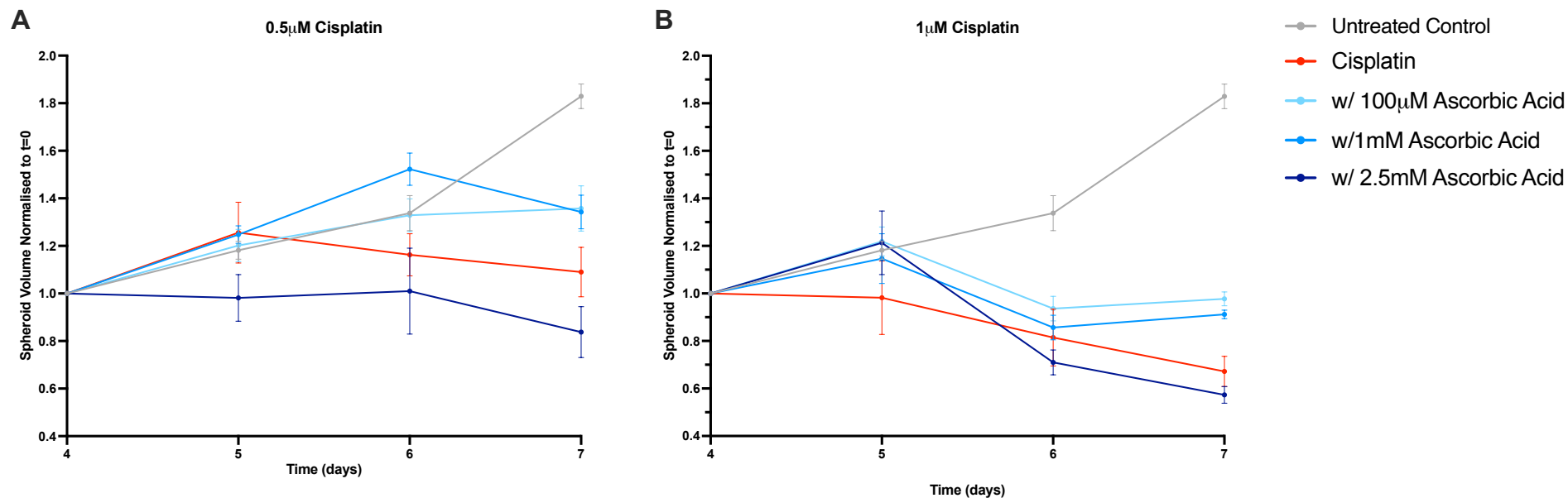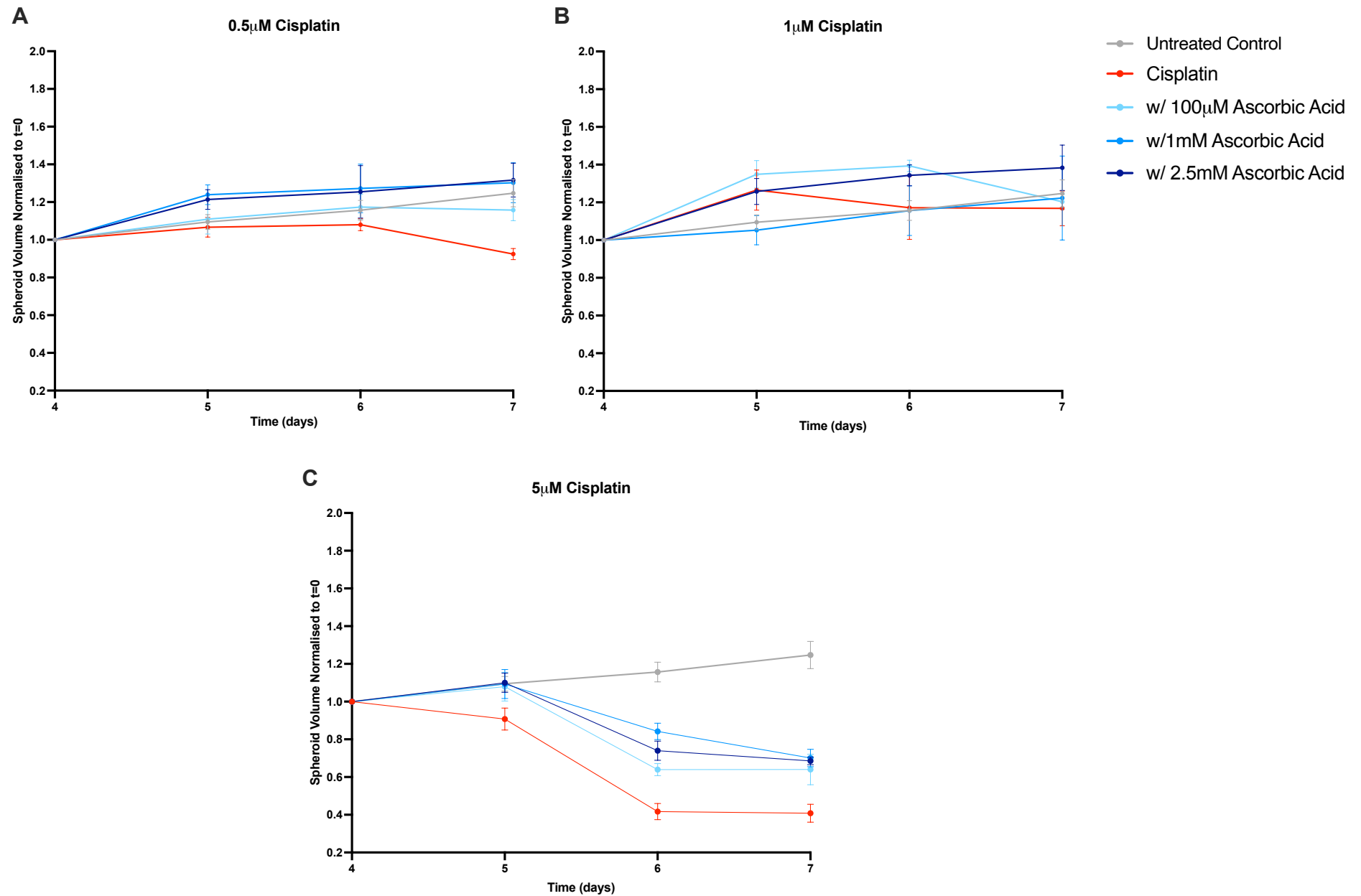1μM Cisplatin

5μM Cisplatin

Day 7

Day 4

Figure 4.3. High dose ascorbic acid can potentiate cisplatin response in DAOY spheroids. The changes in volume of the spheroid over the time course for DAOY spheroids treated with **A)** 0.5μM cisplatin and **B)** 1μM cisplatin alongside ascorbic acid conditions (100μM, 1mM and 2.5mM). Spheroid volume was normalised to pre-treatment volume (Day 4). Error bars represent the mean ±SEM; n=3 with 3 internal replicates. Untreated control - grey; Cisplatin only – red; with 100μM ascorbic acid - pale blue; with 1mM ascorbic acid - blue; with 2.5mM ascorbic acid - midnight blue. **C)** Representative brightfield images of DAOY spheroids at Day 7 for all conditions. Red arrows indicate structural changes in the spheroids. Reference brightfield image of DAOY spheroid at Day 4. Scale bar: 100μm.

$1\mu M$ (IC_{50}) cisplatin-treated DAOY spheroids reduced in overall size (0.7-fold change; Figure 4.3B) Again, co-treatment with $100\mu M$ or 1mM AA partially rescued spheroid growth (0.9-fold and 0.8-fold, respectively), but spheroids still exhibited a net decrease in size. Spheroids co-treated with 2.5mM AA and $1\mu M$ cisplatin showed the most pronounced shrinkage (0.6-fold), accompanied by extensive cell shedding (identified with red arrows in figure 4.3C). However, none of the induced changes in spheroid size were statistically significant compared to $1\mu M$ cisplatin alone-treated spheroids. It is noteworthy that at Day 5 (24 hours post-treatment), all AA concentrations with 1μM cisplatin led to an initial increase in spheroid size.

At the highest cisplatin concentration (5μM, IC_{75}), DAOY spheroids could not accurately be analysed as the spheroid boundary and the cells dissociating from it could no longer be confidently discerned (Figure 4.3C). However, co-treatment with 2.5mM AA and $5\mu M$ cisplatin produced visibly darkened spheroids, suggesting increased density and possible cell death. This would be consistent with our previous observations in 2.5mM AA and $0.5\mu M$ and $1\mu M$ cisplatin co-treated DAOY spheroids (Figure 4.3).

4.2.2. Enhancing cytotoxicity of high-dose ascorbic acid with cisplatin is not observed in ONS-76 spheroids

ONS-76 spheroids treated with $0.5\mu M$ cisplatin decreased in overall size (0.9-fold change; Figure 4.4A). When co-treated with AA at all concentrations, ONS-76 spheroids maintained their growth (1.15-1.3-fold increase), in fact increasing AA concentration led to an increased rescue of growth in the presence of $0.5\mu M$ cisplatin that was larger than the growth of untreated controls (1mM and 2.5mM AA with $0.5\mu M$ cisplatin: 1.3-fold increase; untreated controls: 1.2-fold increase). However, these differences were not statistically significant, suggesting that while AA may counteract the growth-reducing effects of cisplatin in ONS-76 spheroids, further investigation is needed to determine the extent of this effect.

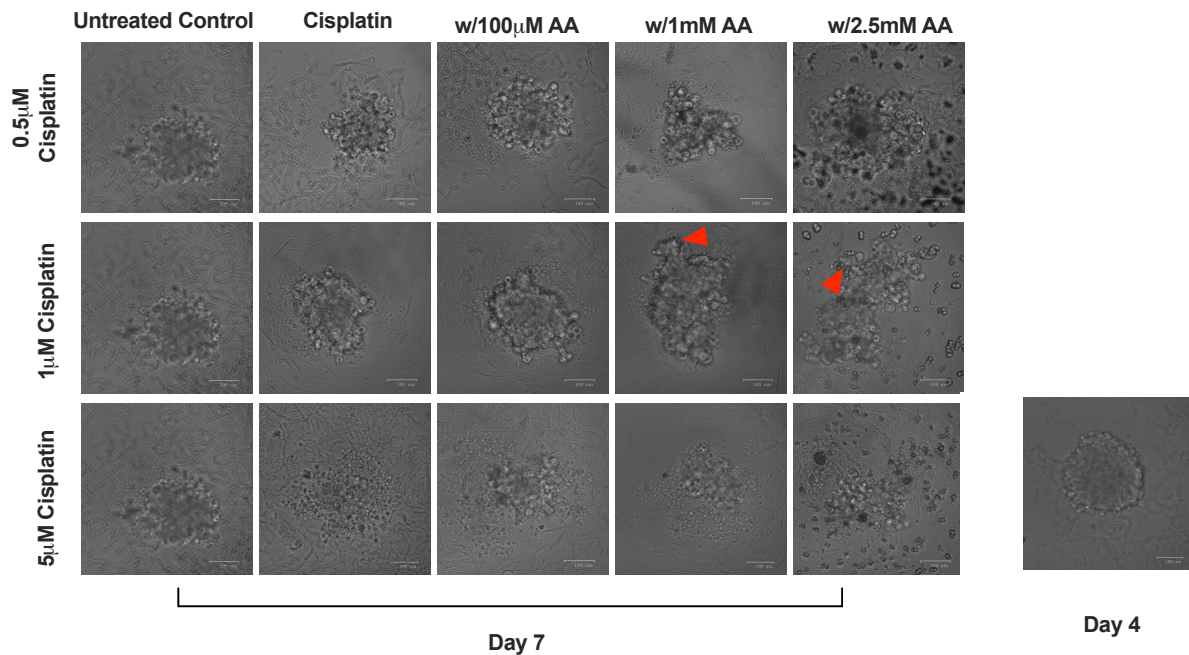**A** 0.5μM Cisplatin

B 1μM Cisplatin

C 5μM Cisplatin

Legend:
- Untreated Control
- Cisplatin
- w/ 100μM Ascorbic Acid
- w/1mM Ascorbic Acid
- w/ 2.5mM Ascorbic Acid

Y-axis: Spheroid Volume Normalised to t=0
X-axis: Time (days)

D

Figure 4.4. 2.5mM ascorbic acid does not potentiate cisplatin response in ONS...
The changes in volume of the spheroid over the time course for ONS-76 spheroids...
0.5μM cisplatin; B) 1μM cisplatin and C) 5μM cisplatin alongside ascorbic acid conditions...
and 2.5mM). Spheroid volume was normalised to pre-treatment volume (Day 4). Error bars represent
the mean ±SEM; n=3 with 3 internal replicates. Untreated control - grey; Cisplatin only – red; with 100μM
ascorbic acid - pale blue; with 1mM ascorbic acid - blue; with 2.5mM ascorbic acid - midnight blue. D)
Representative brightfield images of ONS-76 spheroids at Day 7 for all conditions and at Day 4. Red
arrows indicate structural changes in the spheroids. Scale bar: 100μm.

1μM cisplatin treatment, curiously, maintained ONS-76 spheroid growth (1.15-fold increase;

Figure 4.4B). Co-treatment with 100μM and 1mM AA similarly maintained growth (1.15-1.2-

fold increase) but spheroids co-treated with 2.5mM AA increased in size (1.4-fold increase).

However, this increase in growth was not statistically significant compared to cisplatin only

treatment. Observationally, 1mM and 2.5mM AA co-treated spheroids displayed peripheral

protrusions similar to the ones observed in ONS-76 spheroids treated with AA alone

(indicated with red arrows in Figure 4.4D).

ONS-76 spheroids treated with 5μM cisplatin showed a marked decrease in volume,

shrinking by a mean of 0.3-fold of their original size (Figure 4.4C). This severe reduction in

volume was accompanied by extensive cell dissociation, highlighting the strong cytotoxic

effect of 5μM cisplatin on ONS-76 spheroids (Figure 4.4D). Co-treatment with physiological

concentrations of AA partially mitigated this reduction in volume (~0.5-fold change for AA

concentrations) while cotreatment with 2.5mM AA spheroids resembled cisplatin controls.

However, despite this partial recovery in volume, spheroids exhibited signs of cell

dissociation at the periphery, suggesting that AA at any tested concentration was unable to

fully rescue the integrity of the spheroid.

## 4.3. Investigating the effect of ascorbic acid on reactive oxygen species production in SHH spheroids

To determine whether the mechanism underlying the potentially enhanced cytotoxicity of cisplatin in the presence of 2.5mM AA in DAOY spheroids was due to the pro-oxidant activities of AA we assessed the levels of ROS produced in SHH spheroids co-treated with AA and cisplatin. We utilised the fluorescent probe DCFH-DA to monitor ROS production (Figure 2.2A). DCFH-DA permeates cell membranes and is acetylated intracellularly to non-fluorescent DCFH. In the presence of ROS, DCFH can be oxidised to the highly fluorescent compound DCF. The fluorescence intensity of this signal is proportional to ROS levels. Although DCFH-DA is not specific for any particular oxidative species, it provides a reliable measure of overall oxidative stress, making it appropriate for the broad investigation of ROS in this context. The experimental set up is described in Section 2.3.4 and summarised in Figure 2.2B.

The methodology of this assay was in accordance with previous literature (Bardyn et al., 2021; Oh et al., 2020). SHH spheroids were loaded with DCFH-DA prior to treatment as this allowed for us to monitor real-time changes in ROS production. We treated with AA first and then cisplatin in order to distinguish the effects of each treatment on ROS levels, as well as their possible interaction. We reduced the assay duration to two hours due to our interest in capturing the acute ROS changes, which we hypothesised could be the trigger for longer-term spheroid structural changes that were observed in size analyses (Figure 4.3 and 4.4). We performed a two-way ANOVA followed by a multiple comparisons test to assess statistical significance between the ROS levels of AA co-treated and cisplatin-only spheroids at the last fluorescence read (t=135 mins). Given the assumption that cisplatin treatment would induce a significant ROS increase, we hypothesised that AA co-treatment at 2.5mM would exacerbate ROS production, specifically in DAOY spheroids, and at physiological concentrations (100µM and 1mM) would reduce ROS.

4.3.1. Pre-treatment of SHH spheroids with ascorbic acid depresses ROS levels upon addition of cisplatin

Contrary to this hypothesis, no significant increase in ROS was observed in DAOY spheroids treated with 2.5mM AA at any dose of cisplatin (Figure 4.5). Cisplatin did not show a dose or cell-line dependent increase in ROS - all concentrations of cisplatin led to a relatively comparable increase of ~2-fold compared to pre-treatment levels. Pre-treatment with AA, led to the maintenance of ROS levels following cisplatin treatment in both DAOY and ONS-76 spheroids. In fact, there was a slight trend in increasing AA concentration dampening ROS levels more significantly. Co-treatment with 2.5mM AA in all conditions, except with 5μM in DAOY spheroids, led to a significant difference of p≤0.001 in ROS levels compared with cisplatin-only controls (Figure 4.5). The degree of significance was better maintained in ONS-76 spheroids with a p≤0.01 for all conditions tested. These findings suggests that AA at all tested concentrations acted as an antioxidant, protecting the spheroid from cisplatin-induced oxidative stress.
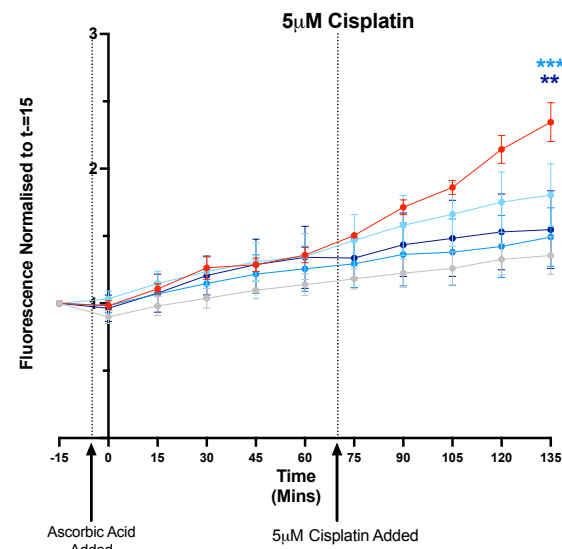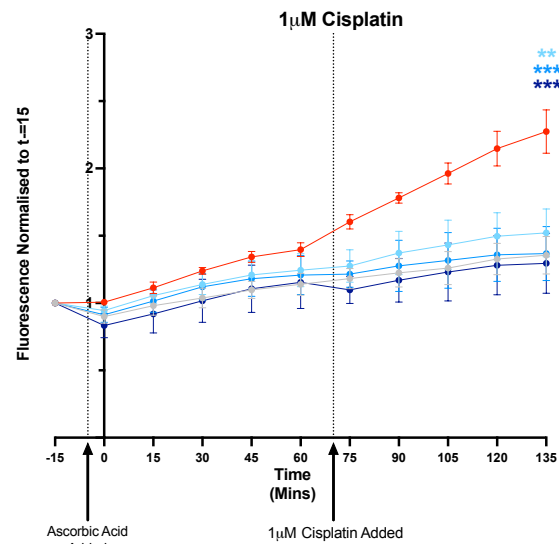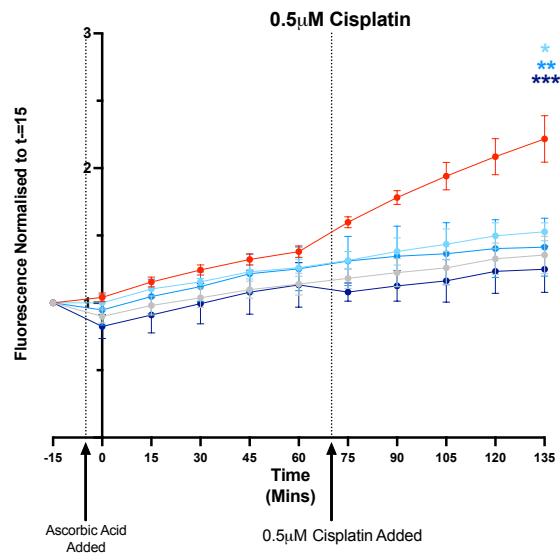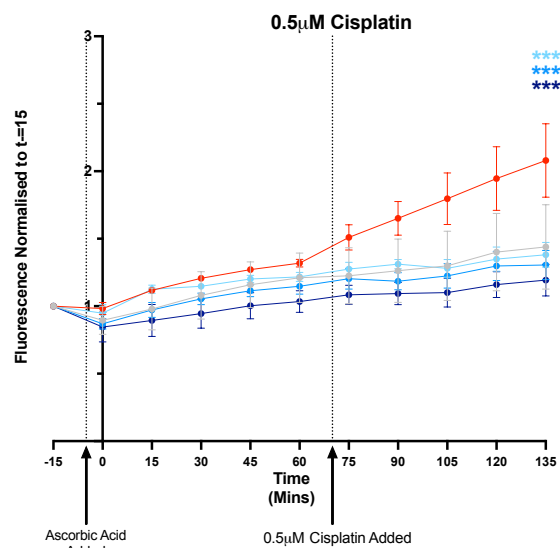
Figure 4.5 Pre-treatment with ascorbic acid dampens ROS levels following cisplatin treatment. The changes in fluorescence across 1hr treatments with ascorbic acid followed by cisplatin in DAOY and ONS-76 spheroids, at the concentrations 0.5uM, 1uM and 5uM cisplatin. A media control background fluorescence was subtracted at each time-point and values then normalised to the fluorescence value t=-15. At t=-5 ascorbic acid conditions are added to the wells (first dotted line) and at t=70 cisplatin conditions are added to the wells (second dotted line). Error bars represent the mean +/- SEM; n=3 with 3 internal replicates. Untreated control - grey; Cisplatin only – red; with 100μM ascorbic acid - pale blue; with 1mM ascorbic acid - blue; with 2.5mM ascorbic acid - midnight blue. The results of the two-way ANOVA and multiple comparisons test between AA co-treated and cisplatin only ROS levels at t=-135 are symbolised by ***** in the corresponding colour key. * $p<0.05$ ** $p<0.01$ *** $p<0.001$.

4.3.2. High-dose ascorbic acid potentially exacerbates oxidative stress in pre-stressed DAOY spheroids

Given the previous findings, we re-evaluated the experimental setup and reversed the treatment order, first treating with cisplatin and then AA. This was designed to test whether a pre-stressed environment would alter AA's role, potentially shifting 2.5mM AA to exerting pro-oxidant effects and increasing ROS production. Considering time constraints, this was purely exploratory, and the results shown in Figure 4.6 represent an n=1 in DAOY spheroids.
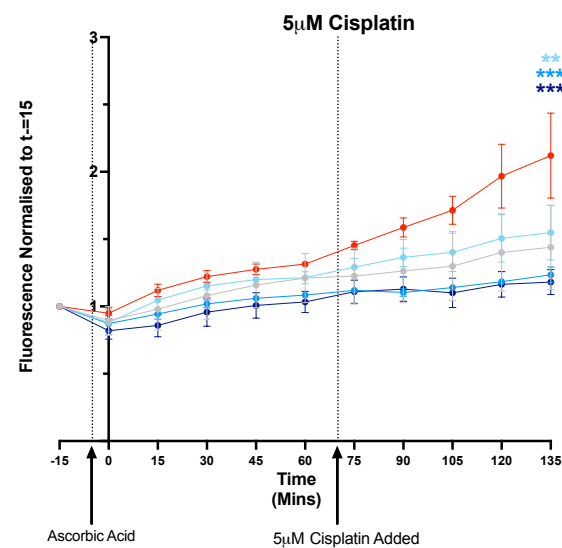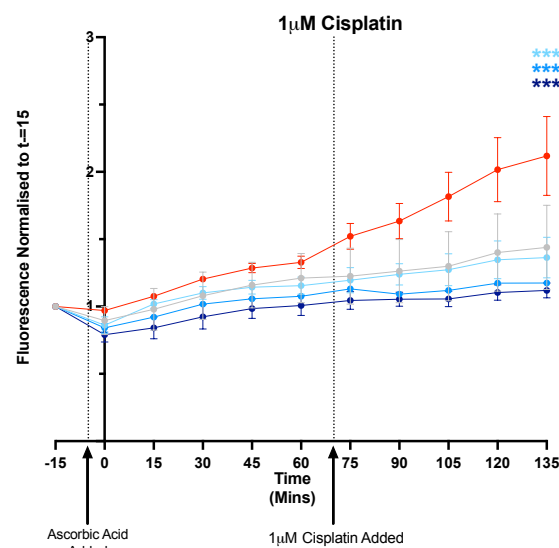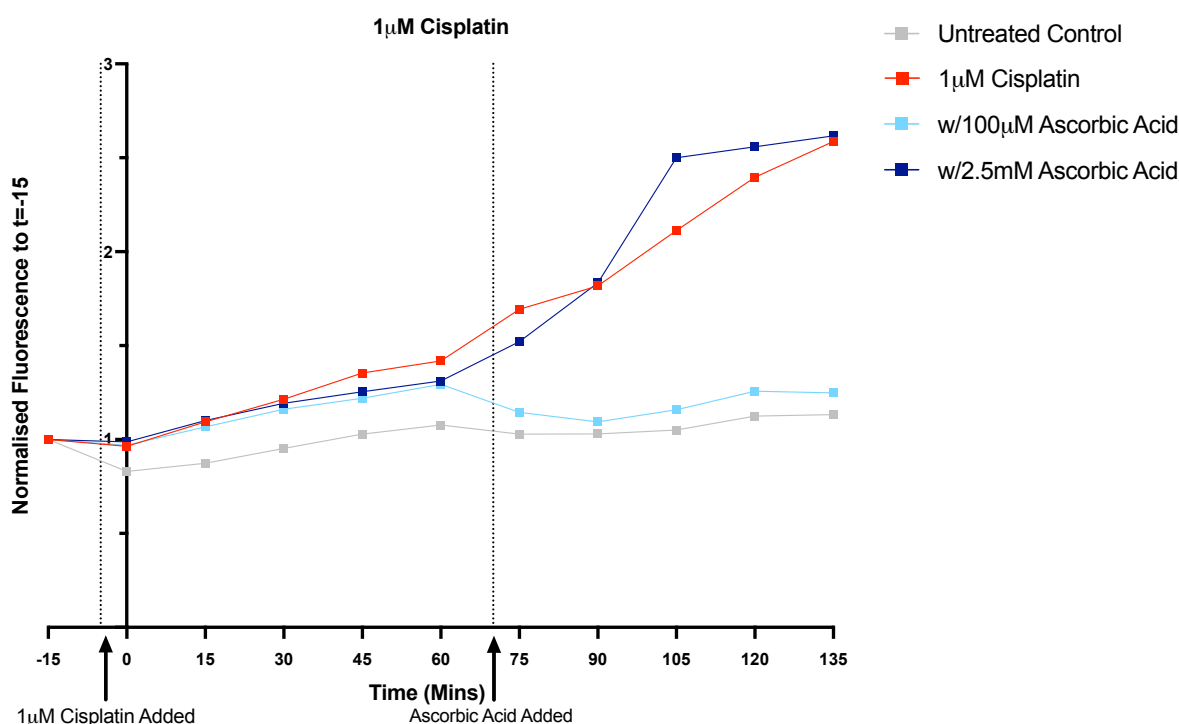

Figure 4.6 Pre-treatment with ascorbic acid dampens ROS levels following cisplatin treatment. The changes in fluorescence across 1hr treatments with ascorbic acid followed by cisplatin in DAOY and ONS-76 spheroids, at the concentrations 0.5μM, 1μM and 5μM cisplatin. A media control background fluorescence was subtracted at each time-point and values then normalised to the fluorescence value t=-15. At t=-5 ascorbic acid conditions are added to the wells (first dotted line) and at t=70 cisplatin conditions are added to the wells (second dotted line). Error bars represent the mean +/- SEM; n=3 with 3 internal replicates. Untreated control - grey; Cisplatin only – red; with 100μM ascorbic acid - pale blue; with 1mM ascorbic acid - blue; with 2.5mM ascorbic acid - midnight blue.

Following the addition of 1µM cisplatin, ROS levels gradually increased in the DAOY spheroids. When 100µM AA was added, a suppression of ROS was observed, comparable to untreated controls. This aligns with previously collected data suggesting that physiological concentrations of AA may mitigate cisplatin-induced oxidative stress. In contrast, pre-stressed spheroids treated with 2.5mM AA exhibited a marked increase in ROS levels, particularly after 90 minutes. While this sharp rise in ROS suggests that, under conditions of pre-existing oxidative stress, high-dose AA may act as a pro-oxidant, further experiments are required to determine whether it directly amplifies ROS production or if other oxidative stress-related mechanisms are involved.

5. Discussion

Medulloblastoma is a highly malignant paediatric brain tumour with a 5-year event-free survival rate of 70% (Ramaswamy et al., 2016). The current standard treatment strategy includes surgical resection, craniospinal radiotherapy and high-dose chemotherapy (Millard and de Braganca, 2016). However, these aggressive treatments come with significant long-term side effects, particularly neurological impairments, which underscores the urgent need for alternative or adjuvant therapies that reduce the treatment burden on young patients.

There is a growing interest in high-dose AA as a potential adjuvant therapy for a range of cancers, this notably includes glioblastoma multiforme – a highly malignant adult brain tumour (Allen et al., 2019). High-dose AA induces oxidative stress specifically in cancer cells, and has been shown to synergise with chemotherapeutics, sensitise previously chemo-resistant cells, and protect non-tumour cells from treatment-induced damage (O'Leary et al., 2018; Schoenfeld et al., 2017; Böttger et al., 2021; Figure 1.12).

In this thesis, we were interested in the potential role of AA in two critical contexts of medulloblastoma. Firstly, with consideration of AA's involvement in collagen production, we explored if AA contributed to the formation of the dense collagen-rich outer shell characteristic of SHH medulloblastoma tumours (Linke et al., 2023). Secondly, we investigated if the anti-tumour effects of high-dose AA both as a standalone treatment and in combination with the chemotherapeutic agent cisplatin extended to medulloblastoma cells. Additionally, we aimed to assess whether AA/DHA transporters play a role in these processes to provide further insights into their potential impact on tumour behaviour and therapy response.

5.1 SVCT2 and GLUT10 identified as potential mediators of ascorbic acid transport in medulloblastoma

To explore potential mediators of AA uptake in medulloblastoma, we performed a bioinformatic analysis of AA and DHA transporter genes in genomic patient datasets (Cavalli et al., 2017; Chapter 3). This identified GLUT10 and SVCT2 as potential key players in medulloblastoma biology, with opposing expression patterns and prognostic associations in SHH tumours.

GLUT10 expression was significantly higher in SHH tumours compared to other subgroups and correlated strongly with DHA recycling genes and collagen-related genes, particularly those forming the ECM-rich shell of SHH tumours. This link between GLUT10 and collagen metabolism aligns with previous findings in arterial tortuosity syndrome (ATS), a disorder caused by GLUT10 loss-of-function mutations that result in severe ECM disorganisation and collagen abnormalities (Coucke et al., 2006; Callewaert et al., 2008; Zoppi et al., 2015; Figure 5.1).
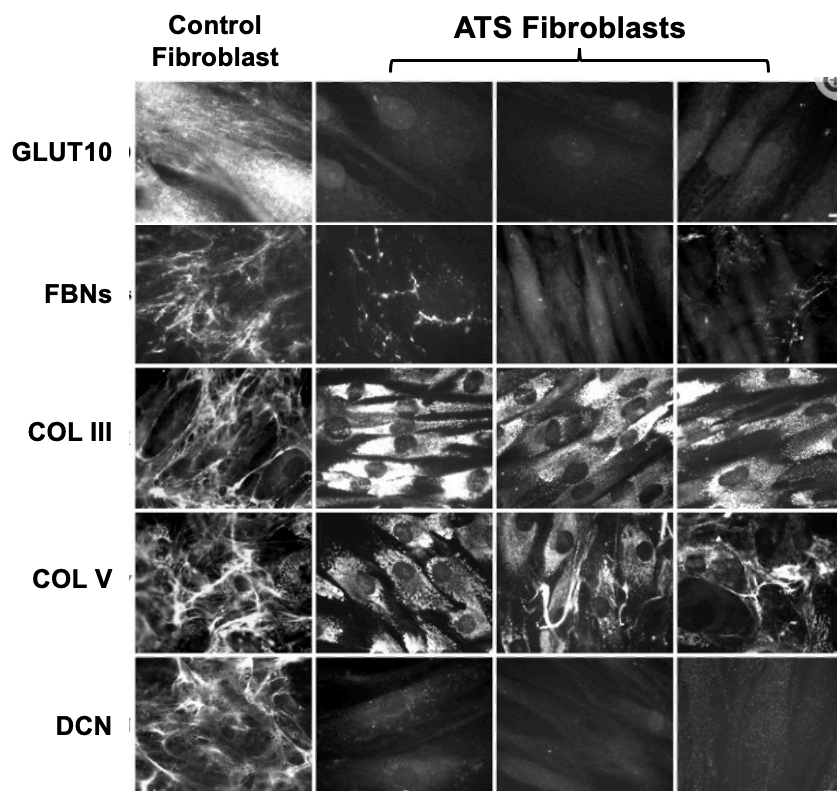
Figure 5.1. Immunofluorescence analysis visualising the impact of loss of function GLUT10 on extracellular matrix organisation in fibroblasts. In control fibroblasts the extracellular matrix is organised into an extensive network of fibronectins, collagens and decorin. In arterial tortuosity syndrome fibroblasts – loss of GLUT10 – collagen III and V are intracellularly retained and fibronectins and decorin are not present in the extracellular matrix. FBNs, fibronectin; DCN, decorin. *Figure adapted from Zoppi et al., 2015.*

SVCT2, in contrast, was also enriched in SHH tumours but was associated with worse survival outcomes. It showed an inverse correlation with DHA recycling genes and key antioxidant enzymes, suggesting a distinct role in redox regulation. Since high-dose AA uptake and efficacy have been shown to depend on SVCT2 expression in various cancer types (Wohlrab et al., 2017; Hong et al., 2012; Cho et al., 2018; Wang et al., 2017), its negative correlation with catalase (*CAT*) in medulloblastoma tumours is particularly interesting. As catalase reduces H_2O_2 cytotoxicity (Klingelhoeffer et al., 2012), lower catalase expression in SVCT2-high tumours could indicate an increased reliance on direct AA uptake while heightening oxidative stress susceptibility.

However, the most intriguing aspect of these findings is the inverse relationship between GLUT10 and SVCT2 across multiple levels, including patient prognosis, correlation with key genes and their expression relationship in SHH tumours. This suggests they may serve opposing roles in SHH medulloblastoma biology. GLUT10's association with collagen genes may support the integrity of the prognostically beneficial ECM shell, contributing to better survival outcomes. Conversely, SVCT2's inverse correlation with antioxidant genes, particularly catalase, could reflect a reliance on SVCT2 activity in response to heightened oxidative burden, potentially making these tumours more aggressive yet more sensitive to oxidative stress-based therapies.

One possible mechanism for this inverse relationship is that GLUT10-expressing tumours depend on DHA recycling for intracellular AA supply, while SVCT2-expressing tumours rely on direct AA uptake. This difference in AA handling could significantly influence redox balance, antioxidant capacity and tumour response to treatment. The association of SVCT2 with poorer prognosis suggests that tumours with high SVCT2 expression might exhibit a more unstable redox environment, potentially driving oxidative stress-mediated tumour progression. Future functional studies will be critical to determining whether this inverse expression pattern actively drives tumour behaviour or is a compensatory adaptation to metabolic pressures in SHH tumours.

5.2. Investigating the hypothesis 'ascorbic acid supports the production of collagen in SHH medulloblastoma'

Collagen plays a complex role in tumour biology (as discussed in section 1.4), and while collagen and it's modifying enzymes, such as MMPs and LOXs, have been studied in various cancers, the potential contribution of AA to collagen production in cancer remains unexplored (Huang et al., 2021). This gap is intriguing given AA not only serves as a co-factor for collagen synthesis but also exhibits broader roles in collagen production. These include increasing collagen mRNA expression, stimulating fibroblast proliferation and their secretion of ECM components including collagens, and inhibiting MMP activity (Pinell et al., 1987; Grinell et al., 1989; Chen et al., 2011). *In vivo* studies have indirectly supported a connection between AA and collagen in cancers through observations of increased collagen expression and clearer tumour boundaries in AA-treated mice models (Polireddy et al., 2017; Cha et al., 2013). However, these studies lack direct mechanistic insights into how AA influences collagen.

In the context of medulloblastoma, increased collagen and ECM deposition was observed around SHH tumours and associated with better patient survival outcomes (Linke et al., 2023). The collagen shell could act as a protective physical barrier to limit tumour spread thereby enhancing prognosis. Consequently, in this thesis we aimed to investigate whether AA contributes to collagen production in SHH medulloblastoma.

5.2.1.   Ascorbic acid increased the size of SHH spheroids

Based upon previous monotherapy studies, we hypothesised that treating spheroids with physiological concentrations of AA would lead to an increase in growth, whereas higher concentrations would induce a ROS-driven reduction in growth (Tronci et al., 2021; Chen et al., 2019; Takemura et al., 2010; Du et al., 2012). However, contrary to this expectation, all tested AA concentrations significantly increased DAOY spheroid growth, while ONS-76 spheroids exhibited a delayed significant growth response.

Based on previous monotherapy studies, we hypothesised that treating spheroids with physiological concentrations of AA would promote growth via collagen deposition, whereas higher concentrations would induce a ROS-driven reduction in growth (Tronci et al., 2021; Chen et al., 2019; Takemura et al., 2010; Du et al., 2012). However, contrary to this expectation, all tested AA concentrations significantly increased DAOY spheroid growth, while ONS-76 spheroids exhibited a delayed but ultimately significant growth response.

A key observation was the accompanying structural changes, including cell dissociation and protrusion formation. The peripheral dissociation could potentially be attributed to increased mechanical force from increased collagen deposition, as ECM stiffening has been shown to promote EMT (Fang et al., 2012). Alternatively, the protrusions suggest that AA treatment appeared to have an effect on the cytoskeleton. However, the irregular morphology of ONS-76 spheroids complicates this interpretation, as their shape variations may be independent of treatment effects.

The differences in DAOY and ONS-76 spheroid response could be influenced by their SHH-α and SHH-β subgroup identities (Table 2.4). While DAOY spheroids exhibited a rapid growth response, with significant increases as early as 24 hours post-treatment, ONS-76 spheroids responded more gradually, with significant changes only appearing at 72 hours post-treatment. This could suggest that DAOY spheroids are more sensitive to AA's growth-promoting effects, though their larger and more spherical initial morphology compared to the smaller and more irregular ONS-76 spheroids introduces confounding variables.

The interpretation of these results was limited by the set time point approach. Typically, spheroids are grown over the entire growth cycle to generate a sigmoidal growth curve, enabling assessment of parameters such as doubling time. The current analysis only compared growth at single time points, making it difficult to determine where each spheroid type sat within its growth phase. Future studies should assess full growth curves in the presence of AA to better characterise its effects on specific growth dynamics.

Finally, to investigate whether the AA-induced growth effects were mediated by increased collagen-deposition, as hypothesised, we attempted immunohistochemistry (IHC) on Day 7 AA-treated spheroids. However, technical challenges with paraffin-embedded HistoGel sectioning precluded analysis, despite multiple protocol optimisations. Future approaches could explore alternative ECM visualisation methods, such as immunofluorescence imaging or directly measuring collagen by hydroxyproline quantification. Given the observed growth-promoting effects of AA, this analysis would have been critical in distinguishing whether AA enhances spheroid expansion via ECM remodelling or alternative pathways. The inability to confirm collagen deposition leaves open the possibility that AA-mediated growth effects were driven by alternative mechanisms, such as modulation of redox balance or increased metabolite availability supporting cellular proliferation.

5.3. Investigating the hypothesis 'Ascorbic acid at supraphysiological concentrations is a pro-oxidant with anti-tumour roles in medulloblastoma'

ROS plays a complex role in cancer biology; as a by-product of the increased metabolic activity of cancer cells, ROS can drive carcinogenesis through promoting proliferation, survival, and metastatic potential (Figure 1.11; Nakamura et al., 2012). However, an excessive production of ROS induces chronic oxidative damage culminating in programmed cell death (Nakamura et al., 2012). Harnessing this redox vulnerability is the basis of numerous cancer therapies, including GSH recycling inhibitors which aim to deplete cancer cell's antioxidant defence as well as tyrosine kinase inhibitors which upregulate NADPH oxidase – an ROS producing enzyme – to exacerbate ROS production (Ju et al., 2015; Huang et al., 2021). These therapies when given in combination with standard therapies, are cytotoxic to cancer cells, and even could sensitise a previously chemo-resistant pancreatic cancer cell line (Ju et al., 2015).

AA acts as a pro-oxidant at high concentrations in the presence of transition metals such as Fe^{3+} and generates large amounts of ROS (Buettner et al., 1996). At these high concentrations (>1mM) AA can selectively induce cell death in a range of cancer cell lines when given alone (Tronci et al., 2021; Chen et al., 2019; Du et al., 2012) and in combination with standard treatments (O'Leary et al., 2018; Schoenfeld et al., 2017). In combination with standard treatment, the pro-oxidant effects of high-dose AA can amplify the oxidative stress induced by these treatments and improve their efficacy. These promising *in vitro* and *in vivo* studies have led to early-phase clinical trials of high-dose AA in combination with radiotherapy and/or chemotherapy in pancreatic cancer, ovarian cancer and glioblastoma multiforme (Bruckner et al., 2017; Ma et al., 2014; Allen et al., 2019). These trials have reported reduced toxicity and general trends towards an improved progression-free survival.

In this thesis, we aimed to explore whether the pro-oxidant and anti-tumour properties of high-dose AA extended to SHH medulloblastoma. We hypothesised that AA at 2.5mM would increase ROS production and exhibit anti-tumour effects in SHH medulloblastoma spheroids. Additionally, combining 2.5mM AA with cisplatin would exacerbate oxidative stress and enhance cisplatin's cytotoxicity. This study addresses a gap in medulloblastoma research by evaluating AA's role at potentially pharmacological doses, aiming to assess its potential as an adjuvant therapy alongside standard treatments such as cisplatin.

5.3.1. High-dose ascorbic acid enhances cisplatin-induced cytotoxicity specifically in DAOY spheroids

We investigated whether co-treatment of AA with cisplatin in SHH spheroids, a standard chemotherapeutic for medulloblastoma, would reveal differential concentration-dependent effects of AA. Given that high-dose AA has shown synergy with cisplatin in cancer cell lines (Ghavami et al., 2020), we hypothesised that cisplatin's transition metal content could enhance high-dose AA's pro-oxidant effects and thus spheroids treated with this combination would significantly decrease in growth (Marullo et al., 2013). However, SHH spheroids exhibited complex, context-dependent responses to AA and cisplatin.

At physiological concentrations, AA appeared to partially counteract cisplatin-induced cytotoxicity in both DAOY and ONS-76 spheroids, suggesting an antioxidant-mediated protective effect. This aligns with previous findings that physiological AA can neutralise ROS and mitigate chemotherapy-induced oxidative stress (Marullo et al., 2013).

In contrast, at 2.5mM AA, cisplatin-induced cytotoxicity was exacerbated in DAOY spheroids, leading to increased cell shedding by Day 7. Yet, in ONS-76 spheroids, 2.5mM AA reduced cisplatin cytotoxicity, with these spheroids retaining their size more effectively than those treated with cisplatin alone. The contrasting responses suggest that factors beyond baseline cisplatin sensitivity influence treatment outcomes, particularly spheroid morphology and intrinsic biological differences. DAOY spheroids were larger and more spherical, while ONS-76 spheroids are smaller and irregular, which could affect nutrient diffusion, drug penetration and oxidative stress susceptibility. However, if these differences persist under controlled morphology conditions, it would indicate that intrinsic biological differences drive their divergent responses.

A potential determinant could be their SHH subtype identity, as DAOY spheroids align with SHH-α tumours and ONS-76 with SHH-β tumours (Table 2.4). This is particularly relevant in the context of TP53 mutational status, as SHH-α tumours frequently harbour TP53 mutations, which influence redox regulation, apoptosis and chemotherapy resistance. Additionally, differences in AA and DHA transporter expression between these cell lines may alter AA uptake, metabolism and downstream effects on oxidative stress or collagen remodelling. These molecular differences may fundamentally shape their response to high-dose AA and cisplatin.

The additive cytotoxic effect of high-dose AA in DAOY spheroids may be attributed to its pro-oxidant properties, where excessive ROS production overwhelms cellular antioxidant defences, ultimately promoting oxidative damage and cell death. However, interpreting these results was complicated by the analysis method. Total spheroid volume, while providing an estimate of treatment effects, did not fully capture cell viability or structural changes. Notably, at high-dose cisplatin, spheroids exhibited a darkened appearance, characteristic of widespread cell death, yet this did not translate into complete spheroid disintegration. As a result, high-dose AA and cisplatin's cytotoxic effects may have been underestimated. A more precise assessment of AA's impact on cell survival would require complementary viability assays, such as live/dead staining, ATP-based metabolic assays, or caspase activity measurements. Limited by the timeframe, we decided to investigate this observation by measuring the acute ROS production of SHH spheroids in response to treatment.

5.3.2. Is the anti-tumour effect of high-dose ascorbic acid with cisplatin dependent on increased ROS?

Based on both the results of the previous analysis and extensive literature outlining high-dose AA as a pro-oxidant, we hypothesised that the addition of 2.5 mM AA would exacerbate ROS production in DAOY spheroids when combined with cisplatin. However, our ROS measurements using DCFH-DA revealed a surprising result: all AA concentrations, including 2.5 mM, significantly suppressed ROS production in the presence of cisplatin. This finding contradicted our hypothesis and suggested that AA does not act as a pro-oxidant under these conditions.

These results prompted us to reconsider the experimental design. In particular, we conducted a single trial that involved pre-treating DAOY spheroids with cisplatin prior to AA treatments. In this context, addition of high-dose 2.5mM AA did not suppress ROS production but retained ROS production compared to cisplatin controls. This could suggest a pre-stressed environment is needed for high-dose AA to act as a pro-oxidant.

However, further investigation into the interaction between DCFH-DA and AA suggested a potential methodological limitation. As AA is a potent electron donor, it can reduce the DCFH intermediate, thus interfering with the oxidation process and preventing the formation of the fluorescent product DCF. This interaction could have led to a significant underestimation of ROS levels in the presence of AA, thereby confounding the data and hindering our ability to interpret the true effects of AA on ROS production.

These insights underscore the importance of carefully considering the methodological limitations when using fluorescent probes like DCFH-DA in the presence of reactive compounds like AA. Future experiments should explore alternative ROS detection methods, such as more specific probes or direct assays of oxidative damage, to obtain a more accurate assessment of AA's role in modulating chemotherapy-induced oxidative stress.

5.4. Other future work

Throughout this discussion, several future experiments have been discussed, each stemming from the insights garnered in this study. For example, one key direction involves investigating the mechanism behind AA-mediated growth in SHH spheroids, specifically whether collagen deposition plays a pivotal role. Alternatively, exploring the synergistic effects of AA and cisplatin in SHH spheroids warrants further investigation, as it could offer a deeper understanding of how AA might enhance or modulate chemotherapy responses in this subgroup.

Additionally, expanding this research to other medulloblastoma subgroups would be valuable. For example, Group 3 and 4 do not deposit an ECM outer-shell so it could be interesting to observe if this inducible through AA treatment. Exploring whether high-dose AA all exerts potential anti-tumour effects in these subgroups could reveal further therapeutic potential of high-dose AA as an adjuvant therapy in medulloblastoma. Another potential expansion of this data would be by increasing tested AA concentrations above 2.5mM, as clinical trials have reported as high as 20mM plasma concentrations achieved.

5.5. Concluding statements

The data obtained from this thesis opens several promising avenues for future research and establishes key hypotheses of a role of AA in SHH medulloblastoma biology as well as a therapeutic potential. Increasing concentration of AA led to increased size of SHH spheroids. We hypothesised this to be a result of increased collagen deposition at the spheroid boundary, a process which has observed prognostic benefits in SHH patients. Physiological concentrations of AA partially mitigated the cytotoxic effect of cisplatin on SHH spheroid growth and ROS production. Whereas high concentrations of AA enhanced the cytotoxic effect of cisplatin on DAOY spheroid growth, which we hypothesised to be due to AA's role as a pro-oxidant at these concentrations exacerbating ROS to induce programmed cell death. These findings indicate a burgeoning therapeutic potential of high-dose AA in combination with current treatments, such as cisplatin, in medulloblastoma.

Bibliography

Adamson, D. C., Shi, Q., Wortham, M., Northcott, P. A., Di, C., Duncan, C. G., Li, J., McLendon, R. E., Bigner, D. D., Taylor, M. D., & Yan, H. (2010). OTX2 is critical for the maintenance and progression of Shh-independent medulloblastomas. Cancer Research, 70(1), 181–191.

Allen, B. G., Bodeker, K. L., Smith, M. C., Monga, V., Sandhu, S., Hohl, R., et al. (2019). First-in-human phase I clinical trial of pharmacologic ascorbate combined with radiation and temozolomide for newly diagnosed glioblastoma. Clinical Cancer Research, 25(22), 6590–6597.

Angelow S, Haselbach M, Galla HJ. (2003) Functional characterisation of the active ascorbic acid transport into cerebrospinal fluid using primary cultured choroid plexus cells. *Brain Research,* 988:105–113.

Bardyn M, Allard J, Crettaz D, et al. (2021) Image- and Fluorescence-Based Test Shows Oxidant-Dependent Damages in Red Blood Cells and Enables Screening of Potential Protective Molecules. *International Journal of Molecular Sciences*.;22(8):4293.

Barrera, G., Daga, M., Cucci, A. M., & Pizzimenti, S. (2017). The potential therapeutic target Nrf2 in childhood brain tumors. *Journal of Pediatric Oncology*, 5, 11–17.

Bigner, S., Friedman, H., Vogelstein, B., Oakes, VV. J., & Bigner, D. (1990). Amplification of the c-myc gene in human medulloblastoma cell lines and xenografts. *Cancer Research*.

Böttger, F., Vallés-Martí, A., Cahn, L., et al. (2021). High-dose intravenous vitamin C, a promising multi-targeting agent in the treatment of cancer. Journal of Experimental & Clinical Cancer Research, 40, 343.

Brett EA, Sauter MA, Machens HG, Duscher D. (2020) Tumor-associated collagen signatures: pushing tumor boundaries. *Cancer Metabolism,* 2020;8:14.

Brubaker, R. F., Bourne, W. M., Bachman, L. A., & McLaren, J. W. (2000). Ascorbic acid content of human corneal epithelium. *Investigative ophthalmology & visual science*, *41*(7), 1681–1683.

Bruckner, H., Hirschfeld, A., Gurell, D., & Lee, K. (2017). Broad safety impact of high-dose ascorbic acid and induction chemotherapy for high-risk pancreatic cancer. Journal of Clinical Oncology, 35(15)

Buettner, G. R., & Jurkiewicz, B. A. (1996). Catalytic metals, ascorbate and free radicals: Combinations to avoid. Radiation Research, 145, 532–541.

Burgess, E. R., Crake, R. L. I., Phillips, E., Morrin, H. R., Royds, J. A., Slatter, T. L., et al. (2022). Increased ascorbate content of glioblastoma is associated with a suppressed hypoxic response and improved patient survival. Frontiers in Oncology.

Callewaert, B. L., Willaert, A., Kerstjens-Frederikse, W. S., et al. (2008). Arterial tortuosity syndrome: Clinical and molecular findings in 12 newly identified families. Human Mutation, 29(1), 150-158.

Carr, A., & Frei, B. (1999). Does vitamin C act as a pro-oxidant under physiological conditions? FASEB Journal, 13(9), 1007-1024.

Cavalli, F. M. G., Remke, M., Rampasek, L., Peacock, J., Shih, D. J. H., Luu, B., Garzia, L., Torchia, J., Nor, C., Morrissy, A. S., Agnihotri, S., Thompson, Y. Y., Kuzan-Fischer, C. M., Farooq, H., Isaev, K., Daniels, C., Cho, B. K., Kim, S. K., Wang, K. C., … Taylor, M. D. (2017) 'Intertumoral Heterogeneity within Medulloblastoma Subgroups', Cancer Cell, 31(6), pp. 737-754.e6.

Cha J, Roomi MW, Ivanov V, Kalinovsky T, Niedzwiecki A, Rath M. (2013) Ascorbate supplementation inhibits growth and metastasis of B16FO melanoma and 4T1 breast cancer cells in vitamin C-deficient mice. *International Journal of Oncology*, 3;42(1):55-64.

Chen MF, Yang CM, Su CM, Liao JW, Hu ML. (2011) Inhibitory effect of vitamin C in combination with vitamin K3 on tumor growth and metastasis of Lewis lung carcinoma xenografted in C57BL/6 mice. *Nutrition and Cancer,* **63**(7):1036–1043.

Chen, L. H., & Thacker, R. R. (1984). An increase in glutathione peroxidase activity induced by high supplementation of vitamin C in rats. Nutrition Research, 4, 657-664.

Chen, Q., Espey, M. G., Krishna, M. C., et al. (2005). Pharmacologic ascorbic acid concentrations selectively kill cancer cells: Action as a pro-drug to deliver hydrogen peroxide to tissues. Proceedings of the National Academy of Sciences, 102(38), 13604–13609.

Chen, X. Y., Chen, Y., Qu, C. J., Pan, Z. H., Qin, Y., Zhang, X., et al. (2019). Vitamin C induces human melanoma A375 cell apoptosis via Bax- and Bcl-2-mediated mitochondrial pathways. Oncology Letters, 18, 3880–3886.

Chen, Z., Huang, Y., Cao, D., et al. (2022). Vitamin C intake and cancers: An umbrella review. Frontiers in Nutrition, 8, 812394.

Chevignard, M., Câmara-Costa, H., Doz, F., & Dellatolas, G. (2017) 'Core deficits and quality of survival after childhood medulloblastoma: a review', Neuro-Oncology Practice, 4(2), pp. 82.

Cho, S., Chae, J. S., Shin, H., Shin, Y., Song, H., Kim, Y., et al. (2018). Hormetic dose response to L-ascorbic acid as an anti-cancer drug in colorectal cancer cell lines according to SVCT-2 expression. Scientific Reports, 8, 11372.

Coucke, P. J., Willaert, A., Wessels, M. W., Callewaert, B., Zoppi, N., De Backer, J., et al. (2006). Mutations in the facilitative glucose transporter GLUT10 alter angiogenesis and cause arterial tortuosity syndrome. Nature Genetics, 38, 452–457.

Deng, D., Xu, C., Sun, P. *et al.* (2014) Crystal structure of the human glucose transporter GLUT1. *Nature* **510**, 121–125.

Devasagayam, T. P., Sundquist, A. R., Di Mascio, P., Kaiser, S., & Sies, H. (1991). Activity of thiols as singlet molecular oxygen quenchers. *Journal of photochemistry and photobiology. B, Biology*, *9*(1),

Doseděl, M., Jirkovský, E., Macáková, K., et al. (2021). Vitamin C - Sources, physiological role, kinetics, deficiency, use, toxicity, and determination. Nutrients, 13(2), 615.
Doskey, C. M., Buranasudja, V., Wagner, B. A., et al. (2016). Tumor cells have decreased ability to metabolize H2O2: Implications for pharmacological ascorbate in cancer therapy. Redox Biology, 10, 274–284.

Du, J., Cullen, J. J., & Buettner, G. R. (2012). Ascorbic acid: Chemistry, biology and the treatment of cancer. Biochimica et Biophysica Acta (BBA) - Reviews on Cancer, 1826(2), 443-457.

Du, J., Wagner, B. A., Buettner, G. R., & Cullen, J. J. (2015). Role of labile iron in the toxicity of pharmacological ascorbate. Free Radical Biology and Medicine, 84, 289-295.

Fang M, Yuan J, Peng C, Li Y. (2014)Collagen as a double-edged sword in tumor progression. *Tumour Biol*ogy,35(4):2871-2882.

Fiaschi, A., et al. (2005). Glutathione, ascorbic acid, and antioxidant enzymes in the tumor tissue and blood of patients with oral squamous cell carcinoma. European Review for Medical and Pharmacological Sciences, 9, 361–367.

Frei, B., England, L., & Ames, B. N. (1989). Ascorbate is an outstanding antioxidant in human blood plasma. *Proceedings of the National Academy of Sciences of the United States of America*, *86*(16), 6377–6381.

Gajjar, A. J., & Robinson, G. W. (2014). Medulloblastoma - Translating discoveries from the bench to the bedside. Nature Reviews Clinical Oncology, 11(12), 714–722. Nature Publishing Group.

Geesin, J. C., Darr, D., Kaufman, R., Murad, S., & Pinnell, S. R. (1988). Ascorbic acid specifically increases type I and type III procollagen messenger RNA levels in human skin fibroblast. Journal of Investigative Dermatology, 90(4), 420-424.

Gęgotek, A., & Skrzydlewska, E. (2022). Antioxidative and anti-inflammatory activity of ascorbic acid. Antioxidants, 11(10), 1993.

Ghavami G, Sardari S. (2020) Synergistic Effect of Vitamin C with Cisplatin for Inhibiting Proliferation of Gastric Cancer Cells. *Iranian Biomedical Journal*;24(2):119-127

Gibson, P., Tong, Y., Robinson, G., Thompson, M. C., Currle, D. S., Eden, C., Kranenburg, T. A., Hogg, T., Poppleton, H., Martin, J., Finkelstein, D., Pounds, S., Weiss, A., Patay, Z., Scoggins, M., Ogg, R., Pei, Y., Yang, Z. J., Brun, S., … Gilbertson, R. J. (2010) 'Subtypes of medulloblastoma have distinct developmental origins', Nature, 468(7327), pp. 1095–1099.

González, M. J., Berdiel, M. J., Miranda-Massari, J. R., López, D., Duconge, J., Rodriguez, J. L., et al. (2016). High dose intravenous vitamin C and metastatic pancreatic cancer: Two cases. Integrative Cancer Science and Therapy, 3(6), 1–2.

Grill, J., Sainte-Rose, C., Jouvet, A., Gentet, J. C., Lejars, O., Frappaz, D., Doz, F., Rialland, X., Pichon, F., Bertozzi, A. I., Chastagner, P., Couanet, D., Habrand, J. L., Raquin, M. A., Le Deley, M. C., & Kalifa, C. (2005) 'Treatment of medulloblastoma with postoperative chemotherapy alone: An SFOP prospective trial in young children', Lancet Oncology, 6(8), pp. 573–580.

Grinnell, F., Fukamizu, H., Pawelek, P., & Nakagawa, S. (1989). Collagen processing, crosslinking, and fibril bundle assembly in matrix produced by fibroblasts in long-term cultures supplemented with ascorbic acid. Experimental Cell Research, 181(2), 483-491.

Hoffer LJ, Robitaille L, Zakarian R, Melnychuk D, Kavan P, Agulnik J, et al. (2015) High-Dose Intravenous Vitamin C Combined with Cytotoxic Chemotherapy in Patients with Advanced Cancer: A Phase I-II Clinical Trial. Hills RK, editor. *Public Library of Science One.*;**10**(4):e0120228.

Hong, S.-W., Lee, S.-H., Moon, J.-H., Hwang, J. J., Kim, D. E., Ko, E., et al. (2012). SVCT-2 in breast cancer acts as an indicator for L-ascorbate treatment. Oncogene, 32, 1508–1517.

Huang WZ, Liu TM, Liu ST, Chen SY, Huang SM, Chen GS. (2023) Oxidative Status Determines the Cytotoxicity of Ascorbic Acid in Human Oral Normal and Cancer Cells. *International Journal of Molecular Science.* ;24(5):4851.

Huang, Z. et al. (2021) Suppressed mitochondrial respiration via NOX5-mediated redox imbalance contributes to the antitumor activity of anlotinib in oral squamous cell carcinoma. *Journal of Genetic Medicine* **48**, 582–594

Huijskens, M. J., Wodzig, W. K., Walczak, M., Germeraad, W. T., & Bos, G. M. (2016). Ascorbic acid serum levels are reduced in patients with hematological malignancies. Results in Immunology, 6, 8–10.

Jacobsen PF, Jenkyn DJ, Papadimitriou JM. (1985) Establishment of a human medulloblastoma cell line and its heterotransplantation into nude mice. *Journal of Neuropathology and Experimental Neurology.*;44(5):472-485.

Jafari, E., Alavi, M. & Zal, F. (2018) The evaluation of protective and mitigating effects of vitamin C against side effects induced by radioiodine therapy. *Radiation and Environmental Biophysics* **57**, 233–240

Johnson, J. E. C. (2022). Investigating the role of tumour-deposited extracellular matrix in medulloblastoma progression [Doctoral thesis, University of Nottingham].

Jones, D. T. W., Jäger, N., Kool, M., Zichner, T., Hutter, B., Sultan, M., Cho, Y. J., Pugh, T. J., Hovestadt, V., Stütz, A. M., Rausch, T., Warnatz, H. J., Ryzhova, M., Bender, S., Sturm, D., Pleier, S., Cin, H., Pfaff, E., Sieber, L., … Lichter, P. (2012). Dissecting the genomic complexity underlying medulloblastoma. Nature, 488(7409), 100–105.

Joost, H. G., Bell, G. I., Best, J. D., Birnbaum, M. J., Charron, M. J., Chen, Y. T., et al. (2002). Nomenclature of the GLUT/SLC2A family of sugar/polyol transport facilitators. American Journal of Physiology-Endocrinology and Metabolism, 282(4), E974–E976.

Ju, H. Q. et al. (2015) Mechanisms of overcoming intrinsic resistance to gemcitabine in pancreatic ductal adenocarcinoma through the redox modulation. *Molecular Cancer Therapeutics* **14**, 788–798

Kaźmierczak-Barańska, J., Boguszewska, K., Adamus-Grabicka, A., & Karwowski, B. T. (2020). Two faces of vitamin C: Antioxidative and pro-oxidative agent. Nutrients, 12(5), 1501.

Kerleroux, B., Cottier, J. P., Janot, K., Listrat, A., Sirinelli, D., & Morel, B. (2020). Posterior fossa tumors in children: Radiological tips & tricks in the age of genomic tumor classification and advance MR technology. Journal of Neuroradiology, 47, 46–53.

Khanzode, S. S., Muddeshwar, M. G., Khanzode, S. D., & Dakhale, G. N. (2004). Antioxidant enzymes and lipid peroxidation in different stages of breast cancer. Free Radical Research, 38(1), 81–85.

Kim, B., Choi, K. M., Yim, H. S., & Lee, M. G. (2013). Ascorbic acid enhances adipogenesis of 3T3-L1 murine preadipocyte through differential expression of collagens. Lipids in Health and Disease, 12(1), 182.

Klingelhoeffer, C., Kämmerer, U., Koospal, M., et al. (2012). Natural resistance to ascorbic acid-induced oxidative stress is mainly mediated by catalase activity in human cancer cells, and catalase-silencing sensitizes to oxidative stress. BMC Complementary and Alternative Medicine, 12(1), 61.

Kobayashi, T.A., Shimada, H., Sano, F.K. *et al.* (2024) Dimeric transport mechanism of human vitamin C transporter SVCT1. *Nature Communications* **15**, 5569

Koczkodaj, D., Muzyka-Kasietczuk, J., Chocholska, S., & Podhorecka, M. (2021). Prognostic significance of isochromosome 17q in hematologic malignancies. Oncotarget, 12(7), 708.

Kool, M., Jones, D. T. W., Jäger, N., Northcott, P. A., Pugh, T. J., Hovestadt, V., Piro, R. M., Esparza, L. A., Markant, S. L., Remke, M., Milde, T., Bourdeaut, F., Ryzhova, M., Sturm, D., Pfaff, E., Stark, S., Hutter, S., Sxeker-Cin, H., Johann, P., … Pfister, S. M. (2014) 'Genome sequencing of SHH medulloblastoma predicts genotype-related response to smoothened inhibition', Cancer Cell, 25(3), pp. 393–405.

Kool, M., Korshunov, A., Remke, M., Jones, D. T. W., Schlanstein, M., Northcott, P. A., Cho, Y.-J., Koster, J., Schouten-van Meeteren, A., van Vuurden, D., Clifford, S. C., Pietsch, T., von Bueren, A. O., Rutkowski, S., McCabe, M., Collins, V. P., Bäcklund, M. L., Haberler, C., Bourdeaut, F., … Pfister, S. M. (2012) 'Molecular subgroups of medulloblastoma: an international meta-analysis of transcriptome, genetic aberrations, and clinical data of WNT, SHH, Group 3, and Group 4 medulloblastomas', Acta Neuropathologica, 123(4), pp. 473–484.

Krejbich, P., & Birringer, M. (2020). Vitamin C as a modifier of the cancer epigenome. Frontiers in Nutrition, 7, 173.

Lee, B., Oh, S. W., & Myung, S. K. (2015). Efficacy of vitamin C supplements in prevention of cancer: A meta-analysis of randomized controlled trials. Korean Journal of Family Medicine, 36(6), 278–285.

Li X, Jin Y, Xue J. (2024) Unveiling Collagen's Role in Breast Cancer: Insights into Expression Patterns, Functions and Clinical Implications. *International Journal of General Medicine*.;17:1773-1787.

Li, S., Chen, J., Fan, Y., et al. (2022). Liposomal honokiol induces ROS-mediated apoptosis via regulation of ERK/p38-MAPK signaling and autophagic inhibition in human medulloblastoma. Signal Transduction and Targeted Therapy, 7, 49.

Li, Y., Goodwin, R., Sang, Y., Rosen, E. M., Laterra, J., & Xia, S. (2009). Camptothecin and Fas receptor agonists synergistically induce medulloblastoma cell death: ROS-dependent mechanisms. Anti-Cancer Drugs, 20(9), 770–778.

Liebes, L., Krigel, R., Kuo, S., Nevrla, D., Pelle, E., & Silber, R. (1981). Increased ascorbic acid content in chronic lymphocytic leukemia B lymphocytes. Proceedings of the National Academy of Sciences, 78(10).

Linke, F., Johnson, J. E. C., Kern, S., et al. (2023). Identifying new biomarkers of aggressive group 3 and SHH medulloblastoma using 3D hydrogel models, single cell RNA sequencing and 3D OrbiSIMS imaging. Acta Neuropathologica Communications, 11(1), 6.

Long, W., & Cheeseman, C. (2015). Structure of, and functional insight into the GLUT family of membrane transporters. Cell Health and Cytoskeleton, 7, 167-183.

Lőrincz, T., Holczer, M., Kapuy, O., & Szarka, A. (2019). The Interrelationship of Pharmacologic Ascorbate Induced Cell Death and Ferroptosis. *Pathology oncology research* , *25*(2), 669–679.

Louis, D. N. et al. (2007) 'The 2007 WHO classification of tumours of the central nervous system', Acta Neuropathologica.

Louis, D. N. et al. (2016) 'The 2016 World Health Organization Classification of Tumors of the Central Nervous System: a summary', Acta Neuropathologica, 131(6), pp. 803–820.

M. Uhlén, L. Fagerberg, B.M. Hallström, C. Lindskog, P. Oksvold, A. Mardinoglu, *et al.* (2015) Proteomics. Tissue-based map of the human proteome Science, 347 Article 1260419

Ma, Y., Chapman, J., Levine, M., Polireddy, K., Drisko, J., & Chen, Q. (2014). High-dose parenteral ascorbate enhanced chemosensitivity of ovarian cancer and reduced toxicity of chemotherapy. Science Translational Medicine, 6(222), 222ra18.

Marullo R, Werner E, Degtyareva N, Moore B, Altavilla G, Ramalingam SS, et al. (2013) Cisplatin Induces a Mitochondrial-ROS Response That Contributes to Cytotoxicity Depending on Mitochondrial Redox Status and Bioenergetic Functions.

Massimino, M., Biassoni, V., Gandola, L., Garrè, M. L., Gatta, G., Giangaspero, F., Poggi, G., & Rutkowski, S. (2016) 'Childhood medulloblastoma', Critical Reviews in Oncology/Hematology, 105, pp. 35–51.

May, J. M., Mendiratta, S., Hill, K. E., & Burk, R. F. (1997). Reduction of dehydroascorbate to ascorbate by the selenoenzyme thioredoxin reductase. Journal of Biological Chemistry, 272, 22607–22610.

May, J. M., Qu, Z., & Cobb, C. E. (2001). Recycling of the ascorbate free radical by human erythrocyte membranes. Free Radical Biology and Medicine, 31(1), 117–124.

McCormick, W. J. (1959). Cancer: A collagen disease, secondary to a nutritional deficiency. Archives of Pediatrics, 76, 166–171.

Michalski, J.M.; Janss, A.J.; Vezina, L.G.; Smith, K.S.; Billups, C.A.; Burger, P.C.; Embry, L.M.; Cullen, P.L.; Hardy, K.K.; Pomeroy, S.L.; et al. Children's oncology group phase III Trial of reduced-dose and reduced-volume radiotherapy with chemotherapy for newly diagnosed average-risk medulloblastoma. J. Clin. Oncol. 2021, 39, 2685–2697.

Milde, T., Lodrini, M., Savelyeva, L., Korshunov, A., Kool, M., Brueckner, L. M., Antunes, A. S. L. M., Oehme, I., Pekrun, A., Pfister, S. M., Kulozik, A. E., Witt, O., & Deubzer, H. E. (2012). HD-MB03 is a novel Group 3 medulloblastoma model demonstrating sensitivity to histone deacetylase inhibitor treatment. *Journal of Neuro-Oncology*, *110*(3), 335–348 Millard, N. E., & De Braganca, K. C. (2016) 'Medulloblastoma', Journal of Child Neurology, 31(12), pp. 1341–1353.

Montel-Hagen, A., Kinet, S., Manel, N., Mongellaz, C., Prohaska, R., Battini, J. L., Delaunay, J., Sitbon, M., & Taylor, N. (2008). Erythrocyte GLUT1 triggers dehydroascorbic acid uptake in mammals unable to synthesize vitamin C. Cell, 132(6), 1039–1048.

Moriarly, M. J., Mulgrew, S., Malone, J. R., et al. (1977). Results and analysis of tumor levels of ascorbic acid. Irish Journal of Medical Science, 146, 74–78.

Murad, S., Grove, D., & Lindberg, K. (1981). Regulation of collagen synthesis by ascorbic acid. Proceedings of the National Academy of Sciences, 78(5), 2879-2882.

Nakamura H, Takada K. (2021) Reactive oxygen species in cancer: Current findings and future directions. *Cancer Scientific*;112(10):3945-3952.
Nielsen, T. K., Højgaard, M., Andersen, J. T., Jørgensen, N. R., Zerahn, B., Kristensen, B., et al. (2017). Weekly ascorbic acid infusion in castration-resistant prostate cancer patients: A single-arm phase II trial. Translational Andrology and Urology, 6(3), 517–528.

Nigar, T., Goodman, A., & Pervin, S. (2021). Total antioxidant capacity and lipid peroxidation status in cervical cancer patients compared with women without cervical cancer in Bangladesh. Indian Journal of Gynecological Oncology, 19, 60.

Niki, E. (1987). Interaction of ascorbate and alpha-tocopherol. Annals of the New York Academy of Sciences, 498, 186-199.

Njus, D., Kelley, P. M., Tu, Y. J., & Schlegel, H. B. (2020). Ascorbic acid: The chemistry underlying its antioxidant properties. Free Radical Biology and Medicine, 159, 37-43.

Northcott, P. A., Buchhalter, I., Morrissy, A. S., et al. (2017). The whole-genome landscape of medulloblastoma subtypes. Nature, 547(7663), 311-317.

Northcott, P. A., Dubuc, A. M., Pfister, S., & Taylor, M. D. (2012) 'Molecular subgroups of medulloblastoma', Expert Review of Neurotherapeutics, 12(7), pp. 871–884.

Northcott, P. A., Robinson, G. W., Kratz, C. P., Mabbott, D. J., Pomeroy, S. L., Clifford, S. C., Rutkowski, S., Ellison, D. W., Malkin, D., Taylor, M. D., Gajjar, A., & Pfister, S. M. (2019) 'Medulloblastoma', Nature Reviews Disease Primers, 5(1).

O'Leary, B. R., Houwen, F. K., Johnson, C. L., Allen, B. G., Mezhir, J. J., Berg, D. J., et al. (2018). Pharmacological ascorbate as an adjuvant for enhancing radiation-chemotherapy responses in gastric adenocarcinoma. Radiation Research, 189(5), 456.

Oh S, Kim YJ, Lee EK, Park SW, Yu HG. (2020)Antioxidative Effects of Ascorbic Acid and Astaxanthin on ARPE-19 Cells in an Oxidative Stress Model. *Antioxidants (Basel)*, 9(9):833.

Ohshima-Hosoyama, S., Davare, M. A., Hosoyama, T., et al. (2011). Bortezomib stabilizes NOXA and triggers ROS-associated apoptosis in medulloblastoma. Journal of Neuro-Oncology, 105, 475–483.

Olney KE, Du J, van 't Erve TJ, et al. (2013) Inhibitors of hydroperoxide metabolism enhance ascorbate-induced cytotoxicity. *Free Radical Research*;47(3):154-163.

Orr, B. A. (2020). Pathology, diagnostics, and classification of medulloblastoma. Brain Pathology, 30(3), 664-678.

Padayatty, S. J., Sun, H., Wang, Y., et al. (2004). Vitamin C pharmacokinetics: Implications for oral and intravenous use. Annals of Internal Medicine, 140, 533-537.

Pei, J., Pan, X., Wei, G., & Hua, Y. (2023). Research progress of glutathione peroxidase family (GPX) in redoxidation. Frontiers in Pharmacology, 14, 1147414.

Phillips, C. L., Combs, S. B., & Pinnell, S. R. (1994). Effects of ascorbic acid on proliferation and collagen synthesis in relation to the donor age of human dermal fibroblasts. Journal of Investigative Dermatology, 103(2), 228-232.

Pinnell, S. R., Murad, S., & Darr, D. (1987). Induction of collagen synthesis by ascorbic acid: A possible mechanism. Archives of Dermatology, 123(12), 1684–1686.

Pizer, B. L., & Clifford, S. C. (2009) 'The potential impact of tumour biology on improved clinical practice for medulloblastoma: Progress towards biologically driven clinical trials', British Journal of Neurosurgery, 23(4), pp. 364–375.

Polkinghorn, W. R., & Tarbell, N. J. (2007) 'Medulloblastoma: tumorigenesis, current clinical paradigm, and efforts to improve risk stratification', Nature Clinical Practice Oncology, 4(5).

Preston-Martin, S., Pogoda, J. M., Mueller, B. A., Lubin, F., Holly, E. A., Filippini, G., et al. (1998). Prenatal vitamin supplementation and risk of childhood brain tumors. International Journal of Cancer, 78, 17–22.

Ramaswamy, V., Remke, M., Bouffet, E., Bailey, S., Clifford, S. C., Doz, F., Kool, M., Dufour, C., Vassal, G., Milde, T., Witt, O., von Hoff, K., Pietsch, T., Northcott, P. A., Gajjar, A., Robinson, G. W., Padovani, L., André, N., Massimino, M., … Pomeroy, S. L. (2016) 'Risk stratification of childhood medulloblastoma in the molecular era: the current consensus', Acta Neuropathologica, 131(6), pp. 821–831.

Ricard-Blum, S. (2011). The collagen family. Cold Spring Harbor Perspectives in Biology, 3(1)

Riordan, H. D., Casciari, J. J., González, M. J., Riordan, N. H., Miranda-Massari, J. R., Taylor, P., et al. (2005). A pilot clinical study of continuous intravenous ascorbate in terminal cancer patients. P R Health Sciences Journal, 24(4), 269–276.

Robert L. Saylors, David Sidransky, Henry S. Friedman, Sandra H. Bigner, Darell D. Bigner, Bert Vogelstein, Garrett M. Brodeur (1991) Infrequent *p53* Gene Mutations in Medulloblastomas[1]. *Cancer Research*; 51 (17): 4721–4723.

Rumsey, S. C., Daruwala, R., Al-Hasani, H., Zarnowski, M. J., Simpson, I. A., & Levine, M. (2000). Dehydroascorbic acid transport by GLUT4 in Xenopus oocytes and isolated rat adipocytes. Journal of Biological Chemistry, 275(37), 28246–28253.

Rumsey, S. C., Kwon, O., Xu, G. W., Burant, C. F., Simpson, I., & Levine, M. (1997). Glucose transporter isoforms GLUT1 and GLUT3 transport dehydroascorbic acid. Journal of Biological Chemistry, 272(30), 18982–18989.

Salo, A. M., & Myllyharju, J. (2021). Prolyl and lysyl hydroxylases in collagen synthesis. Experimental Dermatology, 30, 38–49.

Schober P, Boer C, Schwarte LA. (2018) Correlation Coefficients: Appropriate Use and Interpretation. *Anaesthesia and Analgesia*, 126(5):1763-1768.

Schoenfeld, J. D., Sibenaller, Z. A., Mapuskar, K. A., Wagner, B. A., Cramer-Morales, K. L., Furqan, M., et al. (2017). $O_2^{\cdot-}$ and H_2O_2-mediated disruption of Fe metabolism causes the differential susceptibility of NSCLC and GBM cancer cells to pharmacological ascorbate. Cancer Cell, 31(4), 487–500.e8.

Seo, M.-S., Kim, J.-K., & Shim, J.-Y. (2015). High-dose vitamin C promotes regression of multiple pulmonary metastases originating from hepatocellular carcinoma. Yonsei Medical Journal, 56(5), 1449.

Shamberger, R. J., Corlett, C. L., Beaman, K. D., & Kasten, B. L. (1979). Antioxidants reduce the mutagenic effect of malonaldehyde and P-propiolactone. Mutation Research, 66, 349–355.

Sharma, T., Schwalbe, E. C., Williamson, D., Sill, M., Hovestadt, V., Mynarek, M., Rutkowski, S., Robinson, G. W., Gajjar, A., Cavalli, F., Ramaswamy, V., Taylor, M. D., Lindsey, J. C., Hill, R. M., Jäger, N., Korshunov, A., Hicks, D., Bailey, S., Kool, M., … Clifford, S. C. (2019). Second-generation molecular subgrouping of medulloblastoma: An international meta-analysis of Group 3 and Group 4 subtypes. Acta Neuropathologica, 138(2), 309–326.

Sies, H., Belousov, V. V., Chandel, N. S., et al. (2022). Defining roles of specific reactive oxygen species (ROS) in cell biology and physiology. Nature Reviews Molecular Cell Biology, 23, 499–515.

Sipilä L, Ruotsalainen H, Sormunen R, et al. (2007) Secretion and assembly of type IV and VI collagens depend on glycosylation of hydroxylysines. *Journal of Biological Chemi*stry, 282(46):33381-33388.

Slaga, T. J., & Bracken, W. M. (1977). The effects of antioxidants on skin tumor initiation and aryl hydrocarbon hydroxylase. Cancer Research, 37, 1631–1635.

Stephenson, C. M., Levin, R. D., Spector, T., & Lis, C. G. (2013). Phase I clinical trial to evaluate the safety, tolerability, and pharmacokinetics of high-dose intravenous ascorbic acid in patients with advanced cancer. Cancer Chemotherapy and Pharmacology, 72(1), 139–146.

Sun, L., Moritake, T., Ito, K., Matsumoto, Y., Yasui, H., Nakagawa, H., et al. (2017). Metabolic analysis of radioresistant medulloblastoma stem-like clones and potential therapeutic targets. PLoS ONE, 12, e01761622.

Tajima, S., & Pinnell, S. R. (1996). Ascorbic acid preferentially enhances type I and III collagen gene transcription in human skin fibroblasts. Journal of Dermatological Science, 11(3), 250-253.

Takemura, Y., Satoh, M., Satoh, K., Hamada, H., Sekido, Y., & Kubota, S. (2010). High dose of ascorbic acid induces cell death in mesothelioma cells. Biochemical and Biophysical Research Communications, 394, 249–253.

Tang, L., Deng, Y., Gao, M., Lin, X., Zhu, J., & Li, Y. (2017). Nrf-2 and HO-1 expression in medulloblastoma: A clinicopathological analysis. Journal of Biosciences and Medicine (Irvine), 5, 142–147.

Taylor, M. D., Northcott, P. A., Korshunov, A., Remke, M., Cho, Y. J., Clifford, S. C., Eberhart, C. G., Parsons, D. W., Rutkowski, S., Gajjar, A., Ellison, D. W., Lichter, P., Gilbertson, R. J., Pomeroy, S. L., Kool, M., & Pfister, S. M. (2012) 'Molecular subgroups of medulloblastoma: The current consensus', Acta Neuropathologica, 123(4), pp. 465–472. Thomas, A., & Noel, G. (2019) 'Medulloblastoma: optimizing care with a multidisciplinary approach', Journal of Multidisciplinary Healthcare, 12, pp. 335–347.

Thompson, M. C., Fuller, C., Hogg, T. L., Dalton, J., Finkelstein, D., Lau, C. C., Chintagumpala, M., Adesina, A., Ashley, D. M., Kellie, S. J., Taylor, M. D., Curran, T., Gajjar, A., & Gilbertson, R. J. (2006) 'Genomics identifies medulloblastoma subgroups that are enriched for specific genetic alterations', Journal of Clinical Oncology, 24(12), pp. 1924–1931.

Torti, S. V., & Torti, F. M. (2013). Iron and cancer: More ore to be mined. Nature Reviews Cancer, 13(5), 342–355.

Torzilli PA, Bourne JW, Cigler T, Vincent CT (2012) A new paradigm for mechanobiological mechanisms in tumor metastasis. *Seminars in Cancer Biology,* 22:385–95

Towbin H, Staehelin T, Gordon J. (1979) Electrophoretic transfer of proteins from polyacrylamide gels to nitrocellulose sheets: procedure and some applications. *Proceedings of the National Academy of Sciences U S A*, 76(9):4350-4354.

Trombetta-Lima, M., Rosa-Fernandes, L., Angeli, C. B., et al. (2021). Extracellular matrix proteome remodeling in human glioblastoma and medulloblastoma. Journal of Proteome Research, 20(10), 4693–4707.

Tronci, L., Serreli, G., Piras, C., et al. (2021). Vitamin C cytotoxicity and its effects in redox homeostasis and energetic metabolism in papillary thyroid carcinoma cell lines. Antioxidants (Basel), 10(5), 809.

Wang, C., Lv, H., Yang, W., Li, T., Fang, T., Lv, G., et al. (2017). SVCT-2 determines the sensitivity to ascorbate-induced cell death in cholangiocarcinoma cell lines and patient derived xenografts. Cancer Letters, 398, 1–11.

Wang, M., He, J., Li, S. *et al.* (2023) Structural basis of vitamin C recognition and transport by mammalian SVCT1 transporter. *Nature Communications* **14**, 1361

Wells, W. W., Xu, D. P., Yang, Y. F., & Rocque, P. A. (1990). Mammalian thioltransferase (glutaredoxin) and protein disulfide isomerase have dehydroascorbate reductase activity. Journal of Biological Chemistry, 265(25), 15361–15364.

Wilson, J. X. (2005). Regulation of vitamin C transport. Annual Review of Nutrition, 25, 105–125.

Winkler, J., Abisoye-Ogunniyan, A., Metcalf, K.J. *et al.* (2020) Concepts of extracellular matrix remodelling in tumour progression and metastasis. *Nature Communications* **11**, 5120

Wohlrab C, Phillips E, Dachs GU. (2017). Vitamin C Transporters in Cancer: Current Understanding and Gaps in Knowledge. *Frontiers in Oncology*, 7:74.

Xu, R., Greening, D. W., Rai, A., Ji, H., & Simpson, R. J. (2015). Highly purified exosomes and shed microvesicles isolated from the human colon cancer cell line LIM1863 by sequential centrifugal ultrafiltration are biochemically and functionally distinct. *Methods*, *87*, 11–25.

Yamada M, Shimizu K, Tamura K, et al. (1989) [Establishment and biological characterization of human medulloblastoma cell lines]. No to Shinkei = Brain and Nerve.;41(7):695-702.

Ye, M., Song, Y., Pan, S., Chu, M., Wang, Z.-W., & Zhu, X. (2020). Evolving roles of lysyl oxidase family in tumorigenesis and cancer therapy. Pharmacology & Therapeutics, 215, 107633.

Yun, J., Mullarky, E., Lu, C., et al. (2015). Vitamin C selectively kills KRAS and BRAF mutant colorectal cancer cells by targeting GAPDH. Science, 350(6266), 1391–1396.

Zhang S, Chang W, Wu H, Wang YH, Gong YW, Zhao YL, et al. (2020) Pan-Cancer Analysis of Iron Metabolic Landscape Across the Cancer Genome Atlas. *Journal of Cellular Physiology* ,235(2):1013–24.

Zhitkovich A. (2020) Nuclear and Cytoplasmic Functions of Vitamin C. *Chemical Research in Toxicology.* 19;33(10):2515-2526